UNIVERSITY OF ZAGREB
FACULTY OF MECHANICAL ENGINEERING AND NAVAL ARCHITECTURE

MASTER'S THESIS

Robert Keser

Zagreb, 2016.

UNIVERSITY OF ZAGREB
FACULTY OF MECHANICAL ENGINEERING AND NAVAL ARCHITECTURE

MASTER'S THESIS

Supervisor: Student:

Prof. dr. sc. Hrvoje Jasak   Robert Keser

Zagreb, 2016.

SVEUČILIŠTE U ZAGREBU
FAKULTET STROJARSTVA I BRODOGRADNJE
Središnje povjerenstvo za završne i diplomske ispite
Povjerenstvo za diplomske ispite studija strojarstva za smjerove:
procesno-energetski, konstrukcijski, brodostrojarski i inženjersko modeliranje i računalne simulacije

Sveučilište u Zagrebu	
Fakultet strojarstva i brodogradnje	
Datum	Prilog
Klasa:	
Ur.broj:	

DIPLOMSKI ZADATAK

Student: **Robert Keser**   Mat. br.: 0035177233

Naslov rada na
hrvatskom jeziku: **Blok-spregnuti algoritam za dvo-jednadžbene modele turbulencije**

Naslov rada na
engleskom jeziku: **Block-Coupled Solution Algorithms for 2-equation Turbulence Models**

Opis zadatka:

Korištenje spregnutih rješavača za povezivanje brzine i tlaka u simulaciji strujanja proračunskom mehanikom fluida dovelo je do znatno brže konvergencije sistema jednadžbi brzine i tlaka u usporedbi s tradicionalnim odvojenim rješavačima tipa SIMPLE ili PISO. Kod simulacije turbulentnih strujanja spregnutim rješavačima često se događa da konvergenciju usporava upravo rješenje jednadžbi modela turbulencije.

Po prirodi, jednadžbe modela turbulencije baziranih na ideji turbulentne viskoznosti s dvije jednadžbe su dobar primjer gdje je moguće analizirati vezu između jednadžbi i predložiti alternativne forme linearizacije koje bi mogle dovesti do ubrzanja konvergencije.

Kandidat će izvršiti sljedeće zadatke tokom izrade rada:

- izvršiti pregled literature vezane uz formulaciju i linearizaciju dvo-jednadžbenih modela turbulencije baziranih na ideji turbulentne viskoznosti. Posebnu pažnju potrebno je obratiti na modele k-epsilon i k-omega SST (engl. Shear Stress Transport);
- predložiti razne forme linearizacije veznih članova između jednadžbe kinetičke energije turbulencije i jednadžbe prostorne ili vremenske skale. Opisati kakve se posljedice na stabilnost modela i ograničenost rješenja očekuju u raznim formama linearizacije;
- predložiti forme linearizacije modela funkcija zida u spregnutom rješavaču;
- izvršiti implementaciju blok-spregnutog algoritma rješenja za modele turbulencije uz odgovarajuću linearizaciju u softverskom paketu OpenFOAM;
- izvršiti verifikaciju točnosti modela i usporediti karakteristike spregnutog i odvojenog rješenja na kanoničkim primjerima strujanja;
- opisati implementaciju i ostvarene rezultate u diplomskom radu.

U radu navesti korištenu literaturu i eventualno dobivenu pomoć.

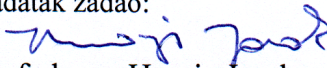Zadatak zadan: Rok predaje rada: Predviđeni datumi obrane:

14. siječnja 2016.   17. ožujka 2016.   23., 24. i 25. ožujka 2016.

Zadatak zadao: Predsjednica Povjerenstva:

Prof. dr. sc. Hrvoje Jasak   Prof. dr. sc. Tanja Jurčević Lulić

Contents

i

List of Figures

List of Tables

Nomenclature

Latin Characters

a_1	-	Closure coefficient
$a_{i,j}$	-	Matrix element
a_{k_i,k_j}	-	Matrix entry which models the coupling between k in cell i with k in cell j
a_{k_i,ε_j}	-	Matrix entry which models the coupling between k in cell i with ε in cell j
a_{ε_i,k_j}	-	Matrix entry which models the coupling between ε in cell i with k in cell j
$a_{\varepsilon_i,\varepsilon_j}$	-	Matrix entry which models the coupling between ε in cell i with ε in cell j
arg_1	-	Argument for function F_1
arg_2	-	Argument for function F_2
arg_3	-	Argument for function F_3
b_1	-	Closure coefficient
c	m	Airfoil chord length
c_1	-	Closure coefficient
C_1	-	Closure coefficient
C_2	-	Closure coefficient
C_μ	-	Closure coefficient
C_d	-	Drag coefficient
C_f	-	Skin friction coefficient
C_l	-	Lift coefficient
C_p	-	Pressure coefficient
$CD_{k\omega}$	-	Cross-diffusion in ω equation
$CD_{k\omega+}$	-	Positive portion of the cross-diffusion in ω equation
E	-	Constant
F_1	-	Blending function
F_2	-	Blending function

F_{23}	-	Blending function
F_3	-	Optional term for rough wall flows
G	m²/s³	Production of k
H	m	Step height
$\mathbf{I}$	-	Identity tensor
k	m²/s²	Turbulent kinetic energy
Re_c	-	Reynolds number per airfoil chord c
Re_H	-	Reynolds number per step height H
S	-	Net source term
S_2	1/s²	Modulus of the mean strain rate tensor to the second power
p	m²/s²	Instantaneous kinematic pressure
$\overline{p}$	m²/s²	Mean kinematic pressure
p'	m²/s²	Fluctuating kinematic pressure
P	Pa	Pressure
p_{inf}	m²/s²	Freestream kinematic pressure
p_{ref}	m²/s²	Kinematic pressure at the experimental reference location
u, v	m/s	Mean velocity components in x (chordwise), y (crossflow) directions
$\mathbf{u}$	m/s	Instantaneous velocity in vector notation
$\overline{\mathbf{u}}$	m/s	Mean velocity in vector notation
$\mathbf{u}'$	m/s	Fluctuating velocity in vector notation
$\overline{\mathbf{u}'\mathbf{u}'}$	m²/s²	Temporal average of fluctuating velocities
U	m/s	Mean velocity magnitude
U_{inf}	m/s	Freestream velocity value
U_{ref}	m/s	Velocity value at the experimental reference location
U^+	-	Dimensionless velocity
x, y, z	m	Rectangular Cartesian coordinates
y	m	Wall distance
y^+	-	Normalised distance to the wall
y^+_{lam}	-	Interface of the viscous and inertial sublayer

Greek Characters

α	°	Angle of incidence
α_{k_1}	-	Closure coefficient
α_{k_2}	-	Closure coefficient
α_k	-	Blended closure coefficient
α_{ω_1}	-	Closure coefficient
α_{ω_2}	-	Closure coefficient
α_ω	-	Blended closure coefficient
β	-	Blended closure coefficient
β_1	-	Closure coefficient
β_2	-	Closure coefficient
γ_1	-	Closure coefficient
γ_2	-	Closure coefficient
γ	-	Blended closure coefficient
β^*	-	Closure coefficient
Γ	m^2/s	Diffusivity
$\Gamma_{\varepsilon,eff}$	m^2/s	Effective diffusivity for ε
$\Gamma_{k,eff}$	m^2/s	Effective diffusivity for k
$\Gamma_{\omega,eff}$	m^2/s	Effective diffusivity for ω
ε	m^2/s^3	Dissipation per unit mass
ν	m^2/s	Kinematic molecular viscosity
ν_{eff}	m^2/s	Kinematic effective viscosity
ν_t	m^2/s	Kinematic eddy viscosity
ρ	kg/m^3	Density
σ_ε	-	Closure coefficient
τ_w	m^2/s^2	Wall shear stress
ϕ	-	Generic always-positive (scalar) dependent variable
ϕ_i	-	Field value
ω	1/s	Specific dissipation rate

Superscripts

q^T	Transpose
q'	Fluctuation around the mean value
$\bar{q}$	Mean (temporal average)
q^n	New time-level
q^o	Old time-level
q^+	Always positive part
q^-	Always negative part
q^*	Always positive part

Subscripts

$q_{i,j}$	Matrix element address
q_{inf}	Freestream values
q_{log}	Value in the log-layer (inertial sublayer)
q_{vis}	Value in the viscous sublayer

Abbreviations

BFS - Backward Facing Step

CFD - Computation Fluid Dynamics

CPU - Central processing unit

CV - Control Volume

DNS - Direct Numerical Simulation

FVM - Finite Volume Method

LES - Large Eddy Simulation

LHS - Left Hand Side

NACA - National Advisory Committee for Aeronautics

NASA - National Aeronautics and Space Administration

RANS - Reynolds-Averaged Navier-Stokes Equations

RHS - Right Hand Side

SST - Shear Stress Transport

Abstract

Modern implicitly coupled pressure–velocity algorithms introduced a considerable increase in the convergence rates when compared with segregated algorithms. Although, segregated treatment of turbulence model equations often limits such algorithms from reaching their full potential. Hence, implicit coupling of two-equation turbulence models is investigated.

In order to implement the implicitly coupled turbulence models in the block-matrix framework, it is necessary to linearise the non-linear source and sink terms. The linearised sources and sinks also need to undergo the stability and boundedness analysis. Linearisation and implementation of two-equation turbulence models, $k - \varepsilon$ and $k - \omega\,SST$, in foam-extend (the community-driven fork of the OpenFOAM) software is presented.

Validation of implemented turbulence models is performed. The two validation cases are: a separated flow past a NACA 4412 airfoil at maximum lift and an incompressible turbulent flow over a backward facing step. Validation of the implicitly coupled $k - \omega\,SST$ model is performed for both cases, whereas validation of the implicitly coupled $k - \varepsilon$ model is performed only for the backward facing step case.

Finally, performance of implemented turbulence models is compared with existing segregated models. Benchmarking is performed on the two validation cases. Similarly as for the validation, both implemented turbulence models are benchmarked on the backward facing step case and only the $k - \omega\,SST$ is benchmarked on the NACA 4412 case.

Key words: *CFD*, *OpenFOAM*, *foam-extend*, *turbulence modelling*, $k - \varepsilon$, $k - \omega\,SST$, *block-matrix*, *implicit coupling*, *linearisation*, *validation*, *benchmarking*.

Sažetak

Korištenje modernih implictno spregnutih algoritama za povezivanje jednadžbi brzine i tlaka dovelo je do znatno brže konvergencije rješenja u usporedbi s tradicionalnim odvojenim algoritmima. Prilikom simulacije turbulentnih strujanja spregnutim rješavačima brzine i tlaka konvergenciju rješenja često ograničava odvojeno rješavanje jednadžbi modela turbulencije, stoga se u ovom radu razmatra implicitno sprezanje dvojednadžbenih modela turbulencije.

Prije implementacije implicitno spregnutih dvojednadžbenih modela turbulencije, nužno je provesti linearizaciju nelinearnih izvorskih i ponorskih članova te analizu stabilnosti i pozitivnosti produkata linearizacije. Prikazuju se linearizacija i implementacija dvojednadžbenih modela turbulencije $k - \varepsilon$ i $k - \omega SST$ unutar foam-extend (OpenFOAM-ova inačica koju razvija zajednica) softverskog paketa.

Validacija implementiranih modela turbulencija provodi se na dva poznata slučaja strujanja za koja su dostupna eksperimentalna mjerenja: odvojeno nestlačivo strujanje oko NACA 4412 aeroprofila pri maksimalnom uzgonu te nestlačivo strujanje u kanalu s naglim proširenjem. Validacija $k - \omega SST$ modela turbulencije provodi se na oba slučaja strujanja, dok se $k - \varepsilon$ model validira samo na strujanju unutar kanala.

Također se uspoređuju performanse implementiranih implicitno spregnutih modela s odgovarajućim postojećim odvojenim inačicama modela turbulencija. Slično kao i prilikom validacije, usporeba $k - \omega SST$ modela provodi se na oba slučaja strujanja, dok se $k - \varepsilon$ model uspoređuje samo na slučaju strujanja unutar kanala.

Ključne riječi: *CFD*, *OpenFOAM*, *foam-extend*, *modeliranje turbulencije*, $k - \varepsilon$, $k - \omega SST$, *blok-matrica*, *implicitno sprezanje*, *linearizacija*, *validacija*, *mjerenje performansi*.

Prošireni sažetak

Korištenje modernih implicitno spregnutih algoritama za povezivanje jednadžbi brzine i tlaka dovelo je do znatno brže konvergencije rješenja u usporedbi s tradicionalnim odvojenim algoritmima. Prilikom simulacije turbulentnih strujanja spregnutim rješavačima konvergenciju rješenja često ograničava odvojeno rješavanje jednadžbi modela turbulencije, stoga se u ovom radu razmatra implicitno sprezanje dvojednadžbenih modela turbulencije $k - \varepsilon$ i $k - \omega\, SST$ unutar foam-extend (OpenFOAM-ova inačica koju razvija zajednica) softverskog paketa.

Nestlačivi $k - \varepsilon$ model turbulencije

Jednadžba turbulentne kinetičke energije unutar $k - \varepsilon$ modela turbulencije glasi:

$$\frac{\partial k}{\partial t} + \nabla_\bullet(\overline{\mathbf{u}}k) - k\nabla_\bullet\overline{\mathbf{u}} - \nabla_\bullet(\Gamma_{k,eff}\nabla k) = G - \varepsilon, \tag{1}$$

gdje k označava turbulentnu kinetičku energiju, $\overline{\mathbf{u}}$ vremenski osrednjenu brzinu, $\Gamma_{k,eff}$ efektivnu difuziju za polje k, G izvorski član (stvaranje turbulentne kinetičke energije), a ε je ponorski član, odnosno disipacija turbulentne kinetičke energije. Jednadžba disipacije turbulentne kinetičke energije glasi:

$$\frac{\partial \varepsilon}{\partial t} + \nabla_\bullet(\overline{\mathbf{u}}\varepsilon) - \varepsilon\nabla_\bullet\overline{\mathbf{u}} - \nabla_\bullet(\Gamma_{\varepsilon,eff}\nabla\varepsilon) = C_1\frac{\varepsilon}{k}G - C_2\frac{\varepsilon^2}{k}, \tag{2}$$

gdje $\Gamma_{\varepsilon,eff}$ označava efektivnu difuziju za polje ε, a C_1 i C_2 su konstantne modela.

Nestlačivi $k - \omega\, SST$ model turbulencije

Jednadžba turbulentne kinetičke energije unutar $k - \omega\, SST$ modela turbulencije glasi:

$$\frac{\partial k}{\partial t} + \nabla_\bullet(\overline{\mathbf{u}}k) - k\nabla_\bullet\overline{\mathbf{u}} - \nabla_\bullet(\Gamma_{k,eff}\nabla k) = \min(G, c_1\beta^* k\omega) - \beta^* k\omega, \tag{3}$$

gdje c_1 i β^* označavaju konstante modela. Jednadžba specifične disipacije turbulentne kinetičke energije glasi:

$$\begin{aligned}
\frac{\partial \omega}{\partial t} + \nabla_\bullet(\overline{\mathbf{u}}\omega) - \omega\nabla_\bullet\overline{\mathbf{u}} - \nabla_\bullet(\Gamma_{\omega,eff}\nabla\omega) = \\
\gamma\min\left[S_2, \frac{c_1}{a_1}\beta^*\omega\max\left(a_1\omega, b_1 F_{23}\sqrt{S_2}\right)\right] \\
-\beta\omega^2 + (1 - F_1)CD_{k\omega},
\end{aligned} \tag{4}$$

gdje $\Gamma_{\omega,eff}$ označava efektivnu difuziju za polje ω, S_2 kvadrat simetričnog dijela tenzora gradijenta brzine, F_1 funkciju miješanja, $CD_{k\omega}$ međudifuziju, dok su a_1, β i c_1 konstante modela.

Struktura blok-sustava

Većina CFD algoritama koristi odvojene algoritme, koji rješavaju svaku jednadžbu zasebno, jednu nakon druge. Nedostatak takvih algoritama je u eksplicitnom sprezanju jednadžbi, tj. rješenja jednadžbi se moraju znatno podrelaksirati radi osiguravanja numeričke stablinosti te konvergencije rješenja. Prilikom implicitnog sprezanja, jednadžbe se rješavaju simultano, unutar blok-matrice, što rezultira većim linearnim sustavom, ali smanjenjem potrebe za podrelaksiranjem te ubrzavanjem procesa konvergencije rješenja.

Prostornom diskretizacijom domene (koristeći metodu konačnih volumena) dobivamo linearni sustav jednadžbi:

$$\begin{pmatrix} a_{1,1} & a_{1,2} & \cdots & a_{1,N} \\ a_{2,1} & a_{2,2} & \cdots & a_{2,N} \\ \vdots & \vdots & \ddots & \vdots \\ a_{N,1} & a_{N,2} & \cdots & a_{N,N} \end{pmatrix} \begin{pmatrix} \phi_1 \\ \phi_2 \\ \vdots \\ \phi_N \end{pmatrix} = \begin{pmatrix} b_1 \\ b_2 \\ \vdots \\ b_N \end{pmatrix}, \tag{5}$$

gdje N označava broj kontrolnih volumena, $a_{i,j}$ član matrice, ϕ_i vrijednost polja u ćeliji i za koju se rješava sustav, dok b_i označava desnu stranu jednadžbe za ćeliju i.

Kod odvojenih algoritama, članovi matrica $a_{i,j}$, vrijednosti polja ϕ_i i b_i su skalari jer se svaka jednadžba rješava zasebno. Prilikom implicitnog sprezanja jednadžbi, odnosno kod blok-matrica, $a_{i,j}$ je tenzor dimenzija $n \times n$ gdje je n broj implicitno spregnutih jednadžbi, u skladu s tim ϕ_i i b_i postaju vektori dimenzija n.

U ovom se radu razmatraju dvojednadžbeni modeli turbulencija, stoga radi jednostavnijeg i preglednijeg prikaza uvode se dvije generičke, uvijek pozitivne, varijable ϕ_A i ϕ_B te pripadajuće generičke skalarne transportne jednadnžbe:

$$\frac{\partial \phi_A}{\partial t} + \nabla_\bullet(\overline{\mathbf{u}}\phi_A) - \phi_A\nabla_\bullet\overline{\mathbf{u}} - \nabla_\bullet(\Gamma_A\nabla\phi_A) = S_A, \tag{6}$$

$$\frac{\partial \phi_B}{\partial t} + \nabla_\bullet(\overline{\mathbf{u}}\phi_B) - \phi_B\nabla_\bullet\overline{\mathbf{u}} - \nabla_\bullet(\Gamma_B\nabla\phi_B) = S_B, \tag{7}$$

gdje su S_A i S_B neto izvorski članovi, koji u sebi uključuju sve izvorske i ponorske članove jednadžbe, stoga mogu poprimiti i pozitivnu i negativnu vrijednost. U slučaju implicitnog

sprezanja jednadžbi (6) i (7), ϕ_i postaje vektor:

$$\phi_i = \begin{pmatrix} \phi_{Ai} \\ \phi_{Bi} \end{pmatrix}, \tag{8}$$

a član matrice $a_{i,j}$ tenzor:

$$a_{i,j} = \left(\begin{array}{c|c} a_{\phi_{Ai},\phi_{Aj}} & a_{\phi_{Ai},\phi_{Bj}} \\ \hline a_{\phi_{Bi},\phi_{Aj}} & a_{\phi_{Bi},\phi_{Bj}} \end{array} \right). \tag{9}$$

Linearizacija

Prije umetanja jednadžbi u blok-matricu, neto izvorski članovi moraju biti linearizirani po svim varijablama koje se tretiraju implicitno:

$$S_A^n \approx S_A^o + \left(\frac{\partial S_A}{\partial \phi_A} \right)^o (\phi_A^n - \phi_A^o) + \left(\frac{\partial S_A}{\partial \phi_B} \right)^o (\phi_B^n - \phi_B^o), \tag{10}$$

$$S_B^n \approx S_B^o + \left(\frac{\partial S_B}{\partial \phi_A} \right)^o (\phi_A^n - \phi_A^o) + \left(\frac{\partial S_B}{\partial \phi_B} \right)^o (\phi_B^n - \phi_B^o), \tag{11}$$

gdje eksponent $\cdot^n$ označava implicitno tretirani član, a $\cdot^o$ označava eksplicitno tretirani član. Nakon linearizacije dobiveni članovi se analiziraju te razvrstavaju u odgovarajuće grupe:

$$S_A^n = S_A^+ + S_A^* \phi_B^n + S_A^- \phi_A^n, \tag{12}$$

$$S_B^n = S_B^+ + S_B^* \phi_A^n + S_B^- \phi_B^n, \tag{13}$$

gdje su S^+ eksplicitni (uvijek pozitivni) izvori, S^* (uvijek pozitivni) izvori koji implicitno sprežu jednadžbe, a S^- implicitni (uvijek negativni) ponori. Analiza i preraspodjela produkata linearizacija nužna je radi očuvanja pozitivnosti rješenja jednadžbi. Varijable koje se javljaju unutar modela turbulencije (npr. k, ε, ω itd.) su po definiciji uvijek pozitivne vrijednosti te u slučaju pojavljivanja negativnog rješenja u procesu rješavanja sustava jednadžbi, često uzrokuju destabilizaciju i neželjene učinke na ostatak proračuna. Implicitno tretiranje ponora pridonosi dijagonalnoj dominantnosti matrice što povoljno utječe na linearne rješavače. Izvori koji implicitno sprežu jednadžbe nalaze se izvan dijagonale člana matrice (9), stoga njihov predznak mora biti suprotan od onih na dijagonali kako ne bi negativno utjecao na dijagonalnu dominantnost, isto se pravilo primjenjuje i za eksplicitne izvore jer desna strana jednadnžbe, kod uvijek pozitivnih varijabli, mora biti suprotnog predznaka od dijagonale da bi se osigurala pozitivna
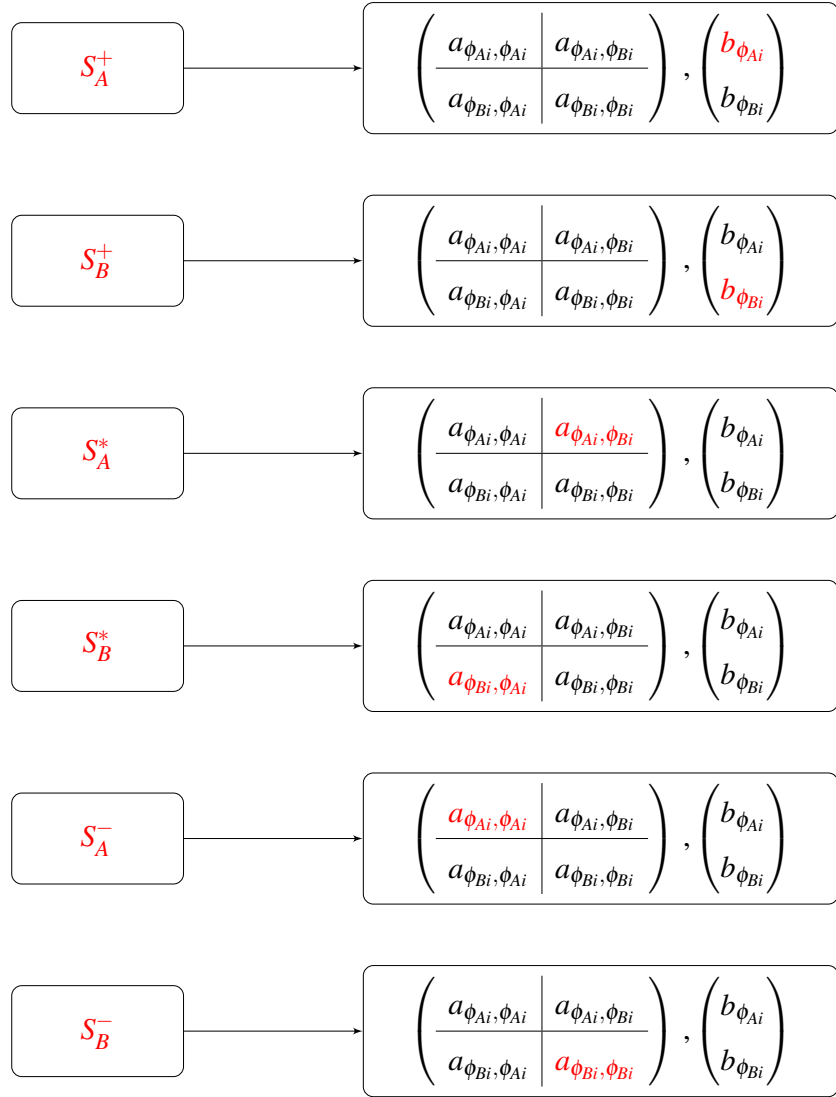
Slika 1: Doprinos pojedinih produkata linearizacije blok-sustavu.

ograničenost rješenja. Doprinos pojedinih članova jednadžbi (12) i (13) blok-sustavu prikazan je na slici 1.

Implementacija implicitno spregnutog $k - \varepsilon$ modela turbulencije

Nakon manipulacije ponora unutar jednadžbe (1), nakon provedene linearizacije te analize članova, implicitno spregnuti $k - \varepsilon$ model turbulencije implementiran je u sljedećoj formi:

$$\frac{\partial k}{\partial t} + \nabla_\bullet(\overline{\mathbf{u}}k) - k\nabla_\bullet\overline{\mathbf{u}} - \nabla_\bullet(\Gamma_{k,eff}\nabla k) = G + C_\mu \frac{(k^o)^2}{\nu_t} - 2C_\mu \frac{k^o}{\nu_t}k^n, \tag{14}$$

$$\frac{\partial \varepsilon}{\partial t} + \nabla_\bullet(\overline{\mathbf{u}}\varepsilon) - \varepsilon\nabla_\bullet\overline{\mathbf{u}} - \nabla_\bullet(\Gamma_{\varepsilon,eff}\nabla\varepsilon) = C_1\frac{\varepsilon^o}{k^o}G + C_2\left(\frac{\varepsilon^o}{k^o}\right)^2 k^n - 2C_2\frac{\varepsilon^o}{k^o}\varepsilon^n, \tag{15}$$

gdje su članovi označeni plavom bojom izvori koji implicitno sprežu jednandžbe, a članovi označeni crvenom bojom implicitni ponori.

Implementacija implicitno spregnutog $k - \omega\, SST$ modela turbulencije

Nakon linearizacije te analize članova jednadžbi (3) i (4), implicitno spregnuti $k - \omega\, SST$ model turbulencije implementiran je u sljedećoj formi:

$$\frac{\partial k}{\partial t} + \nabla_\bullet(\overline{\mathbf{u}}k) - k\nabla_\bullet\overline{\mathbf{u}} - \nabla_\bullet(\Gamma_{k,eff}\nabla k) = \min\left(G, c_1\beta^*k^o\omega^n\right) - \beta^*\omega^o k^n, \tag{16}$$

$$\frac{\partial \omega}{\partial t} + \nabla_\bullet(\overline{\mathbf{u}}\omega) - \omega\nabla_\bullet\overline{\mathbf{u}} - \nabla_\bullet(\Gamma_{\omega,eff}\nabla\omega) =$$
$$\gamma\min\left[S_2, \frac{c_1}{a_1}\beta^*\omega^o\max\left(a_1\omega^o, b_1F_{23}\sqrt{S_2}\right)\right] \tag{17}$$
$$+ \beta\left(\omega^o\right)^2 - 2\beta\omega^o\omega^n + (1-F_1)CD_{k\omega},$$

gdje su članovi označeni plavom bojom izvori koji implicitno sprežu jednadžbe, članovi označeni crvenom bojom implicitni ponori, a član $(1-F_1)CD_{k\omega}$ definiran je izrazom:

$$(1-F_1)CD_{k\omega} = \begin{cases} (1-F_1)CD_{k\omega} = \frac{(1-F_1)CD_{k\omega}}{k^o}k^n & CD_{k\omega} > 0, \\ (1-F_1)CD_{k\omega} = \frac{(1-F_1)CD_{k\omega}}{\omega^o}\omega^n & CD_{k\omega} < 0. \end{cases} \tag{18}$$

Primjeri validacije implementiranih modela turbulencije

Validacija implementiranih modela turbulencija se provodi na dva poznata slučaja strujanja za koja su dostupna eksperimentalna mjerenja: odvojeno nestlačivo strujanje oko NACA 4412 aeroprofila pri maksimalnom uzgonu te nestlačivo strujanje u kanalu s naglim proširenjem. Validacija $k - \omega\, SST$ modela turbulencije provodi se na oba slučaja strujanja, dok se $k - \varepsilon$ model validira samo na strujanju unutar kanala.

Slika 2 prikazuje usporedbu površinske raspodjele koeficijenta tlaka po aeroprofilu. Iz nje je vidljivo da rezultati dobiveni implicitno spregnutim $k - \omega\, SST$ modelom turbulencije dobro opisuju trendove eksperimentalnih podataka.

Slika 3 prikazuje položaj šest linija duž kojih su dostupni eksperimentalni podaci normalizirane brzine u smjeru profila, dok slika 4 prikazuje usporedbu dobivenih rezultata s eksperimentalnim podacima iz koje je vidljivo da se numerički rezultati poklapaju s eksperimentalnima.

NACA 4412
Surface Pressure Coefficient
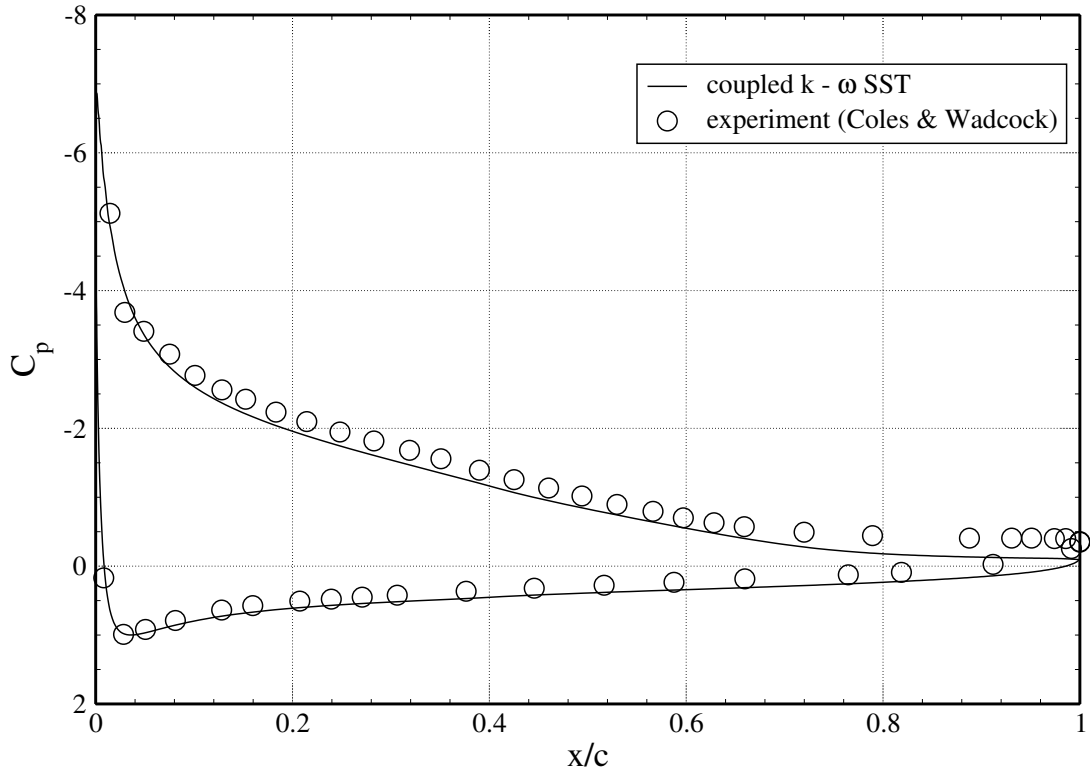
Slika 2: NACA 4412: Usporedba površinske raspodjele koeficijenta tlaka.
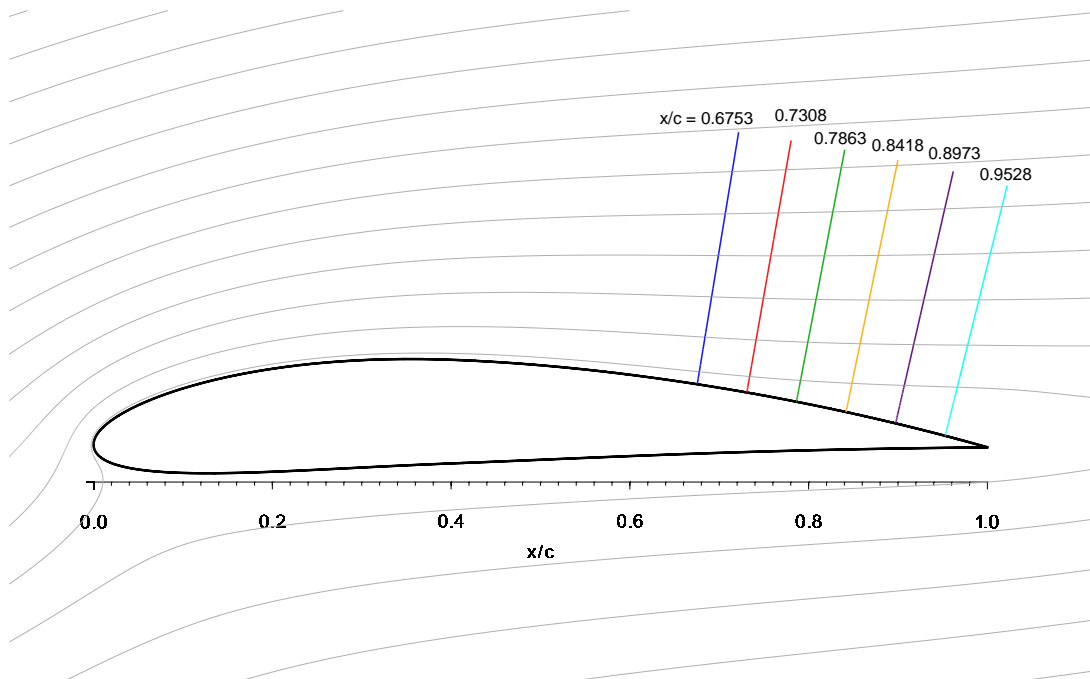
Slika 3: NACA 4412: Položaj linija duž kojih su dostupni eksperimentalni podaci.
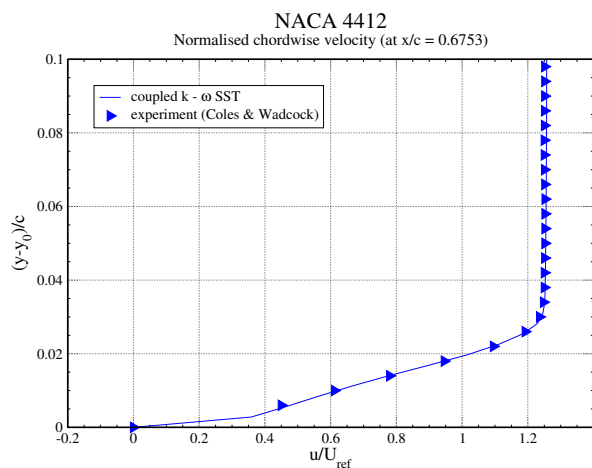
(a) x/c = 0.6753,
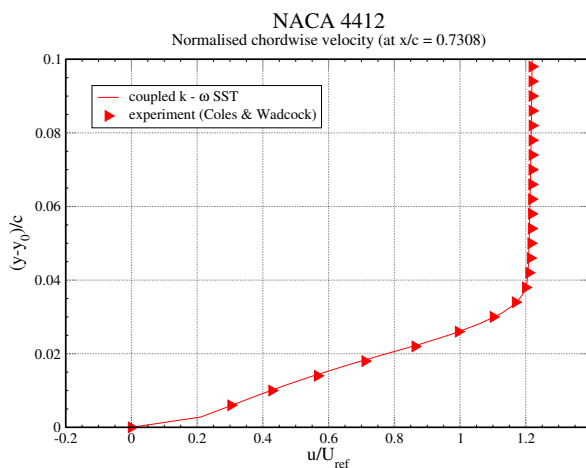
(b) x/c = 0.7308,
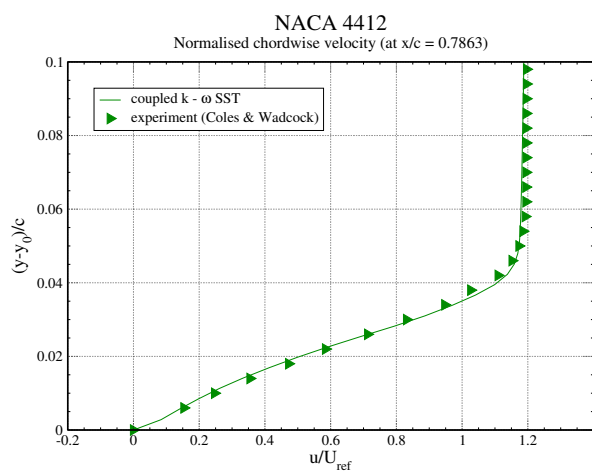
(c) x/c = 0.7863,
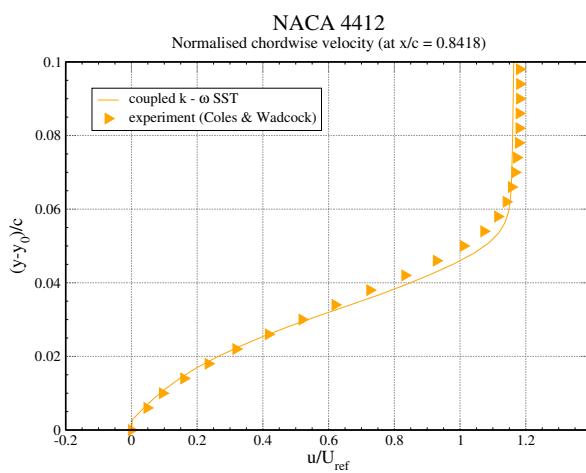
(d) x/c = 0.8418,
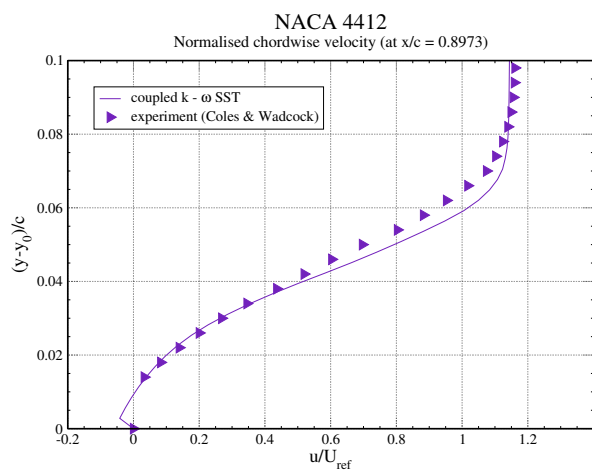
(e) x/c = 0.8973,
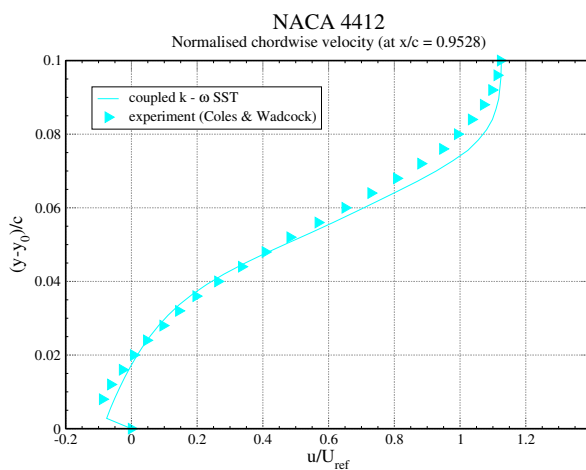
(f) x/c = 0.9528.

Slika 4: NACA 4412: Usporedba normaliziranih profila brzine u smjeru aeroprofila.

Slika 5 prikazuje usporedbu površinske raspodjele koeficijenta tlaka po donjem zidu kanala, a slika 6 usporedbu površinske raspodjele koeficijenta trenja po donjem zidu kanala. Iz njih je vidljivo da rezultati dobiveni obama implicitno spregnutim modelima turbulencije dobro opisuju trendove eksperimentalnih podataka.

BFS
Wall Pressure Coefficient (along the LowerWall)
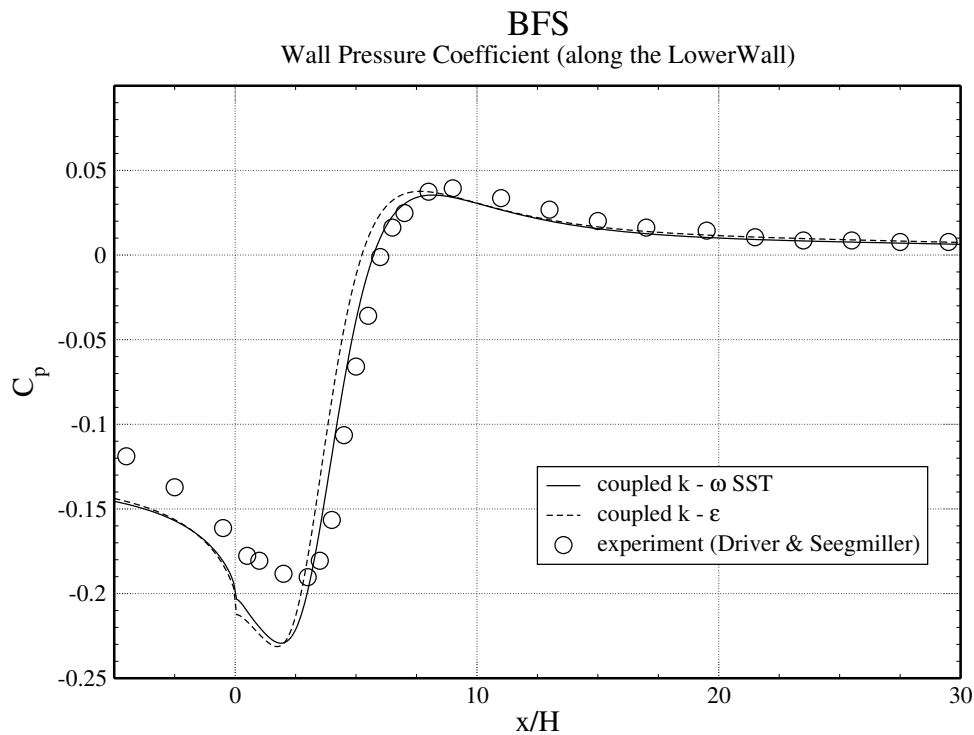
Slika 5: BFS: Usporedba raspodjele koeficijenta tlaka duž donjeg zida.

Slika 7 prikazuje položaj pet linija duž kojih su dostupni eksperimentalni podaci normalizirane brzine u *x* smjeru, dok slika 8 prikazuje usporedbu dobivenih rezultata s eksperimentalnim podacima iz koje je vidljivo da se numerički rezultati dobiveni obama implementiranim modelima poklapaju s eksperimentalnima.

BFS
Wall Skin Friction Coefficient (along the LowerWall)
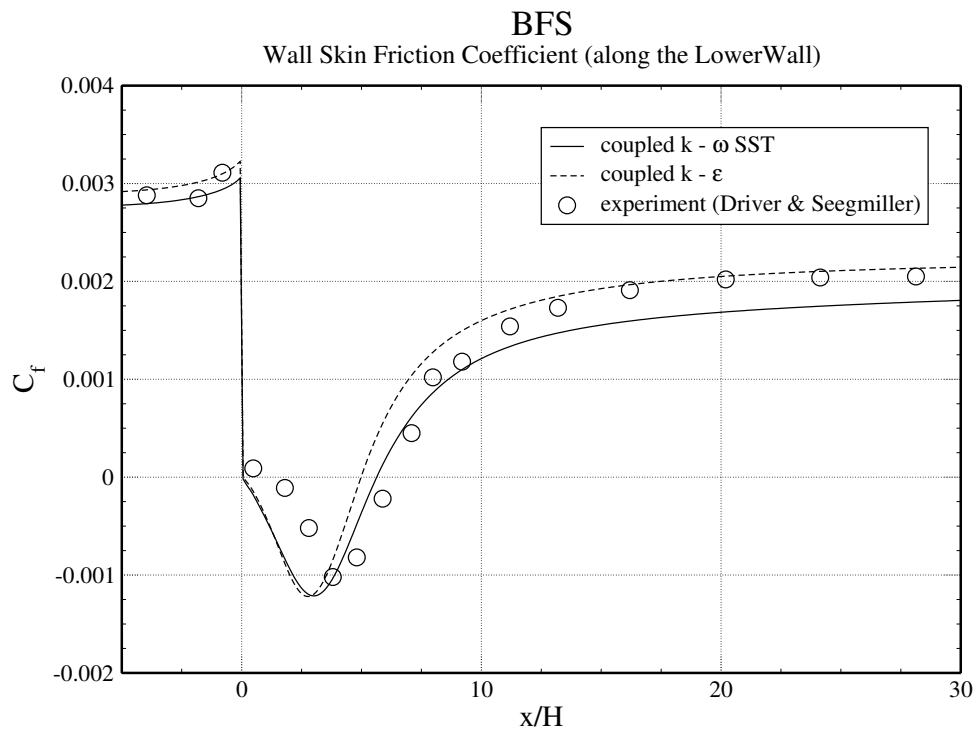
Slika 6: BFS: Usporedba raspodjele koeficijena trenja duž donjeg zida.
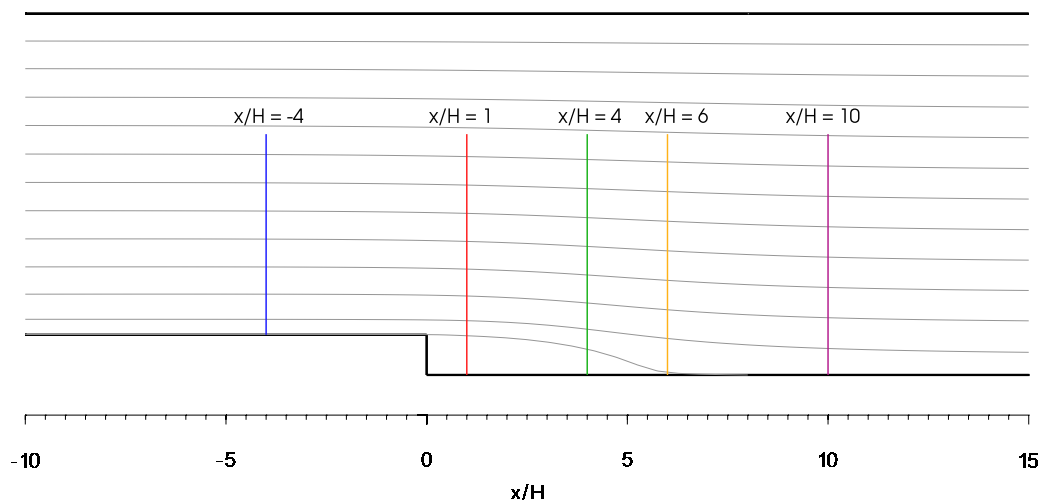
Slika 7: BFS: Položaj linija duž kojih su dostupni eksperimentalni podaci.

(a) x/H = -4,

(b) x/H = 1,

(c) x/H = 4,

(d) x/H = 6,

(e) x/H = 10.
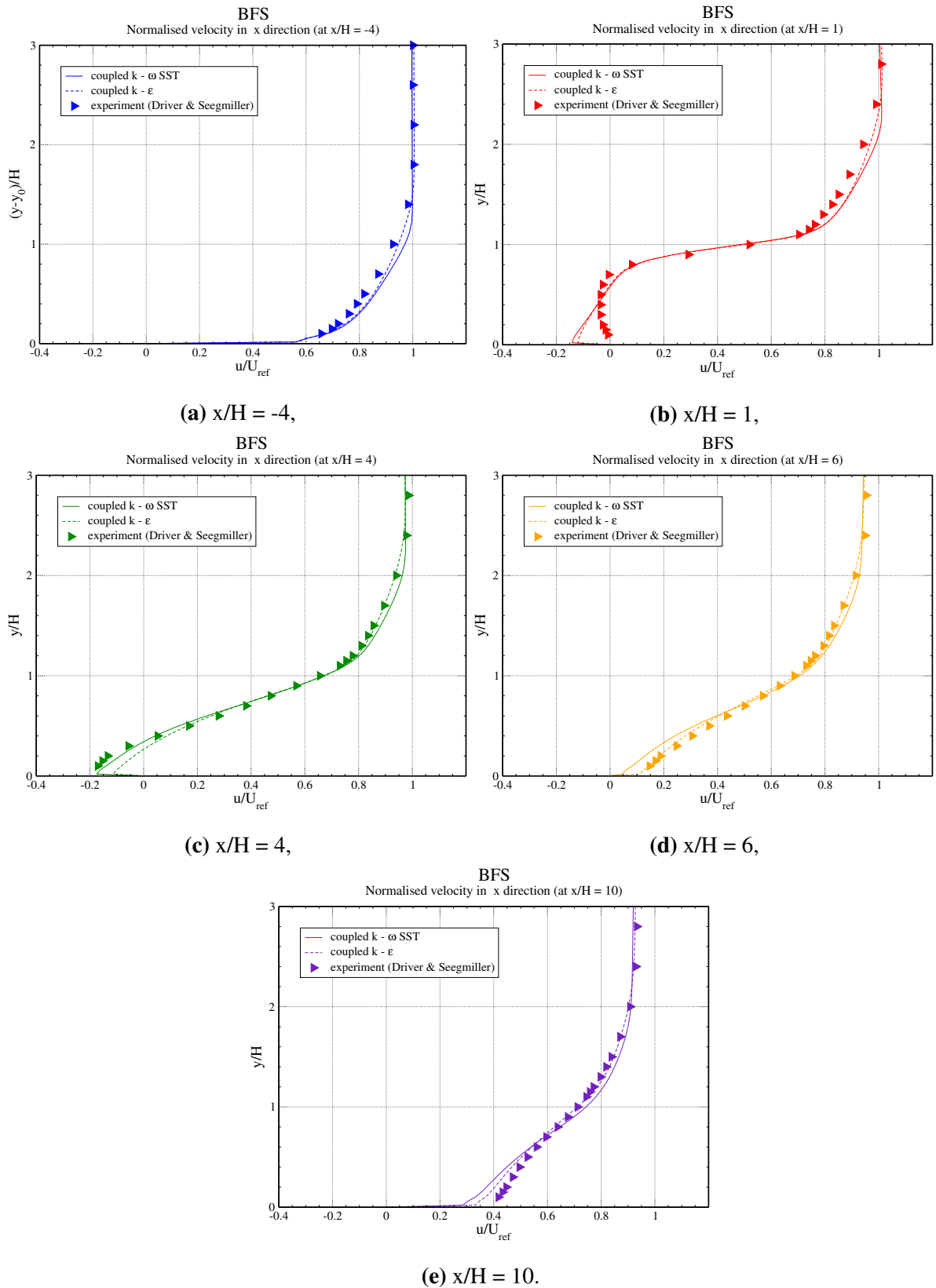
Slika 8: BFS: Usporedba normaliziranih profila brzine u x smjeru.

Usporedba performansi implementiranih implicitno spregnutih modela s odvojenim modelima turbulencije

Provodi se i usporedba performansi implementiranih implicitno spregnutih modela s odgovarajućim postojećim odvojenim inačicama modela turbulencija. Slično kao i prilikom validacije, usporeba $k - \omega\,SST$ modela provodi se na oba slučaja strujanja, dok se $k - \varepsilon$ model uspoređuje samo na slučaju strujanja unutar kanala.

Slika 9 prikazuje položaj triju sondi pomoću kojih su praćene vrijednosti polja kroz iteracije. Slike 10 i 11 prikazuju usporedbu konvergencije vrijednosti polja implicitno spregnutog i odvojenog $k - \varepsilon$ modela te spregnutog i odvojenog $k - \omega\,SST$ modela turbulencije.
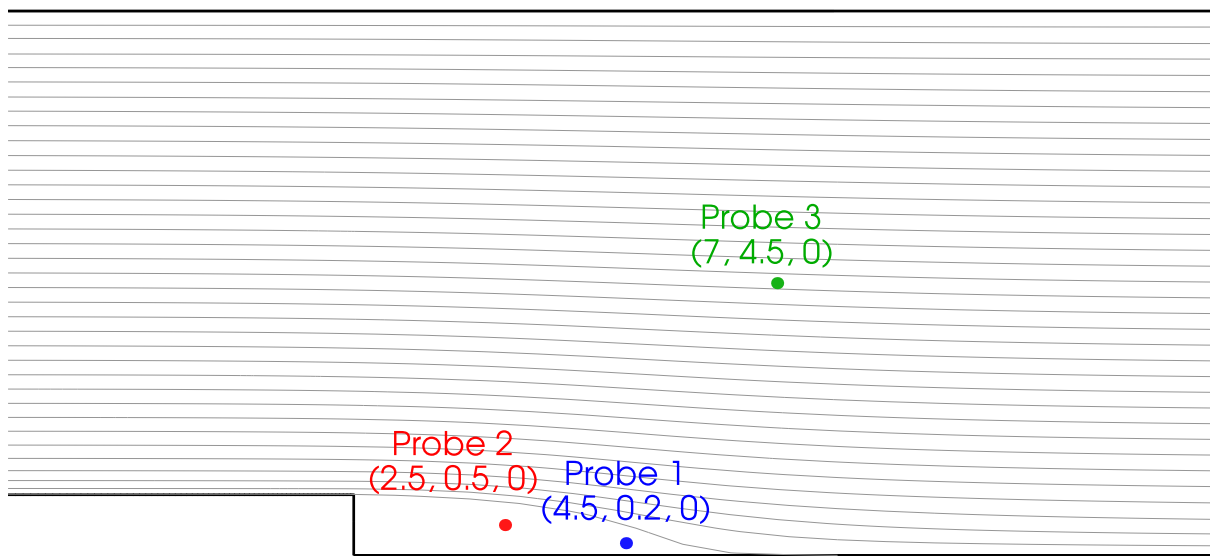
Slika 9: BFS: Položaj sondi.

(a) U_x,

(b) U_y,

(c) p,

(d) v_t.
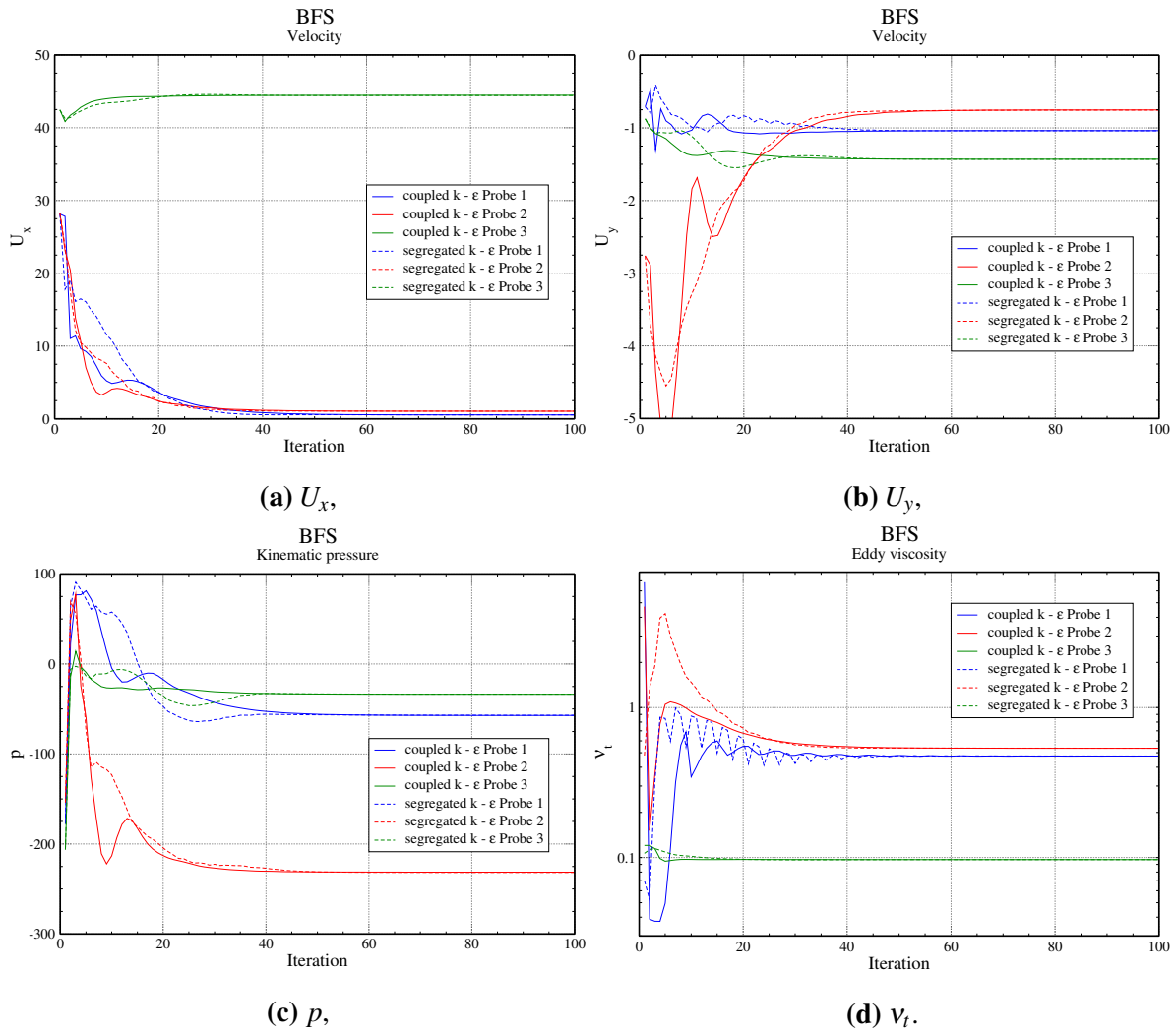
Slika 10: BFS: Usporedba konvergencije vrijednosti polja implicitno spregnutog i odvojenog $k - \varepsilon$ modela turbulencije.

(a) U_x,

(b) U_y,

(c) p,

(d) ν_t.
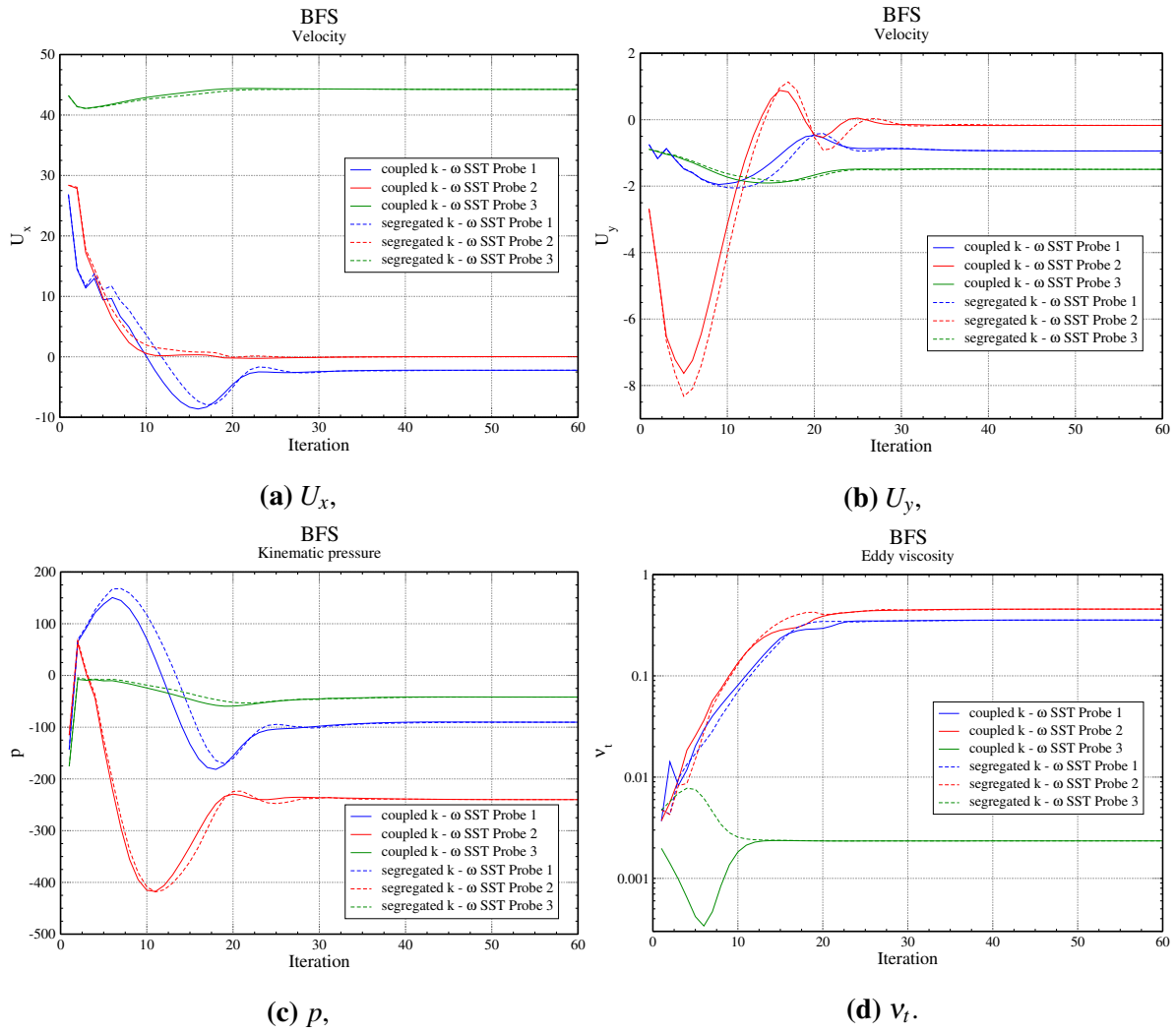
Slika 11: BFS: Usporedba konvergencije vrijednosti polja implicitno spregnutog i odvojenog $k - \omega\,SST$ modela turbulencije.

Slika 12 prikazuje konvergenciju minimalnih i maksimalnih vrijednosti polja po iteracijama za oba implementirana modela te pripadajuće odvojene inačice.

(a) max(U),

(b) max(p),
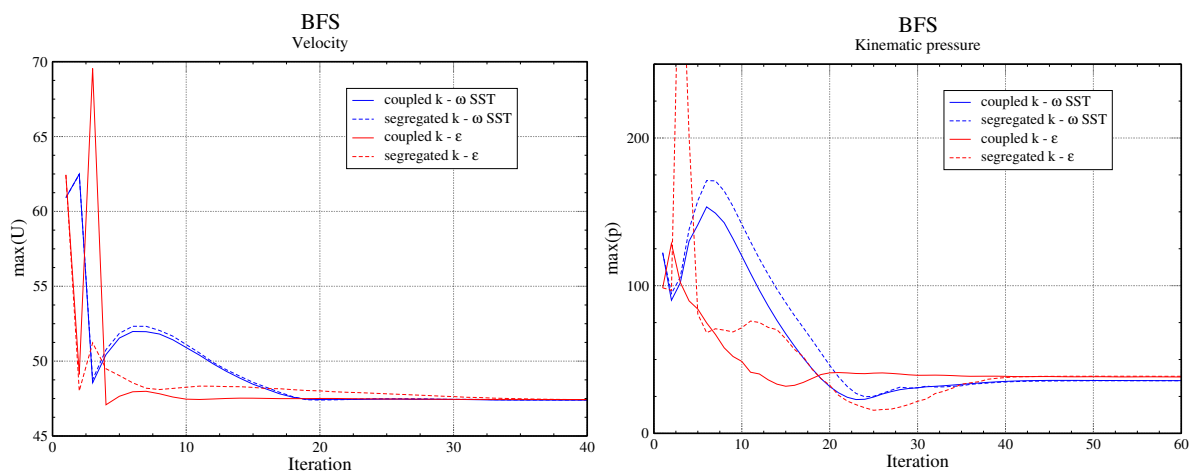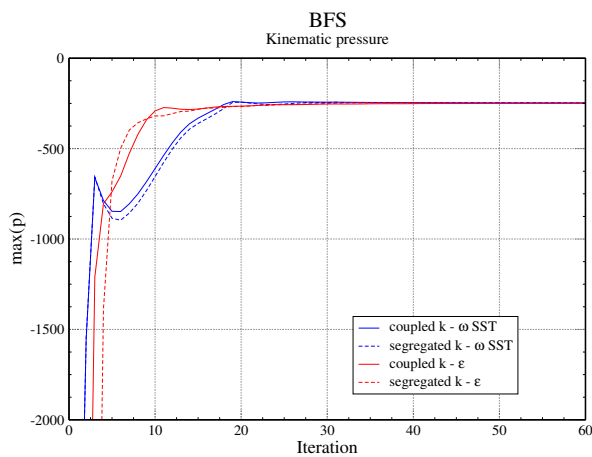
(c) min(p).

Slika 12: BFS: Usporedba konvergencije minimalnih i maksimalnih vrijednosti polja.

Slika 13 prikazuje konvergenciju koeficijenata sile po iteracijama dobivenih implicitno spregnutim te odvojenim $k - \omega SST$ modelom turbulencije na slučaju opstrujavanja NACA 4412 aeroprofila.
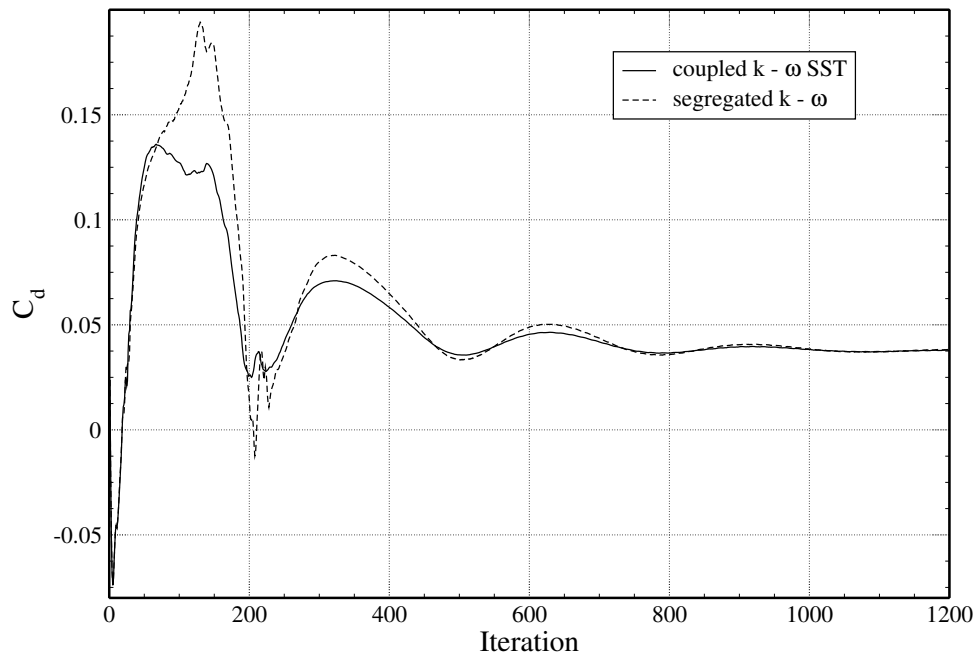
(a) Koeficijent otpora.
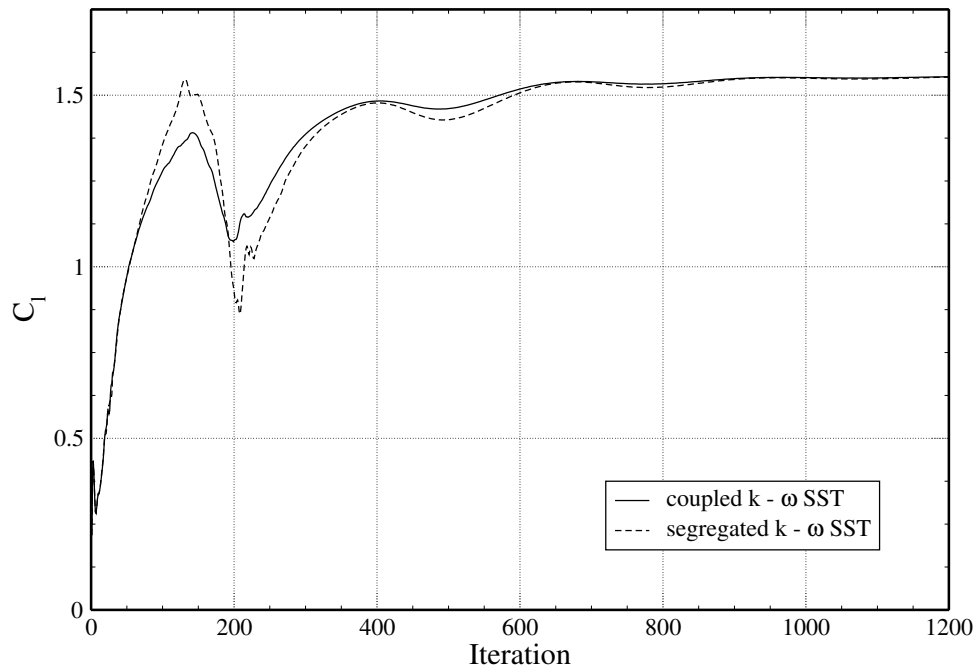
(b) Koeficijent uzgona.

Slika 13: NACA: Konvergencija koeficijenata sile po iteracijama.

Slika 14 prikazuje konvergenciju minimalnih i maksimalnih vrijednosti polja po iteracijama za implicitno spregnuti te odvojeni $k - \omega\,SST$ model turbulencije.
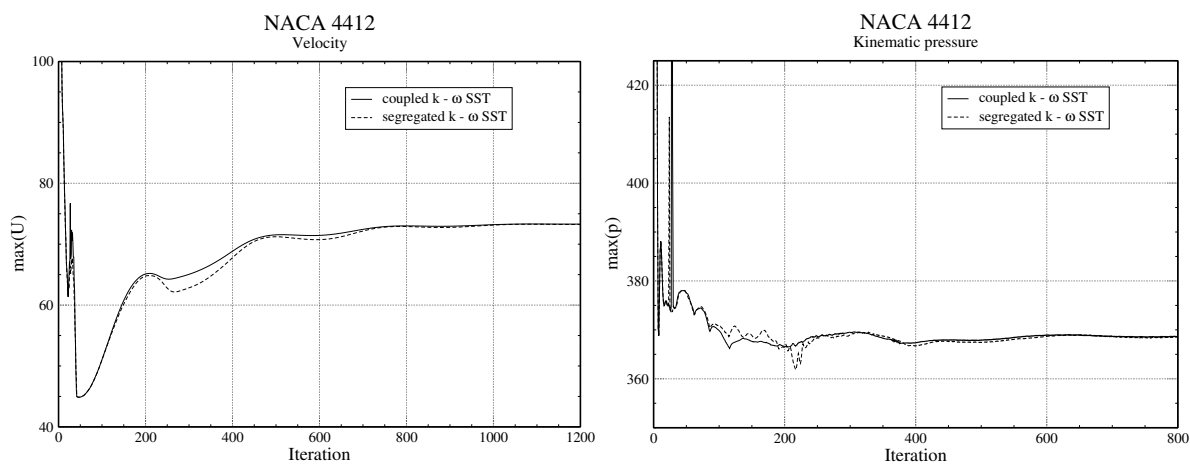
(a) $\max(U)$,

(b) $\max(p)$,
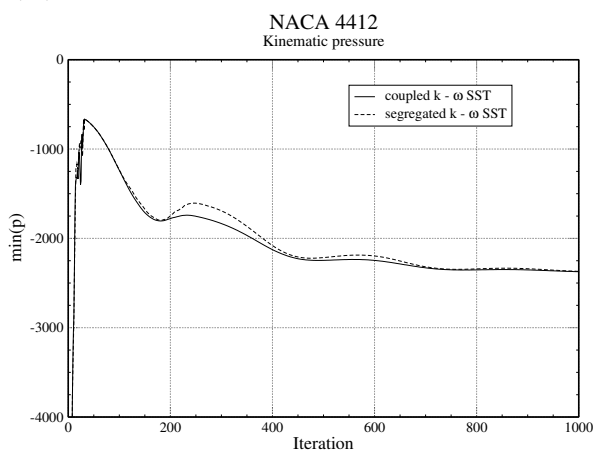
(c) $\min(p)$.

Slika 14: NACA: Usporedba konvergencije minimalnih i maksimalnih vrijednosti polja.

Slika 15 prikazuje konvergenciju koeficijenata sile kao funkciju procesorskog vremena, za implicitno spregnuti te odvojeni $k - \omega\,SST$ model turbulencije.
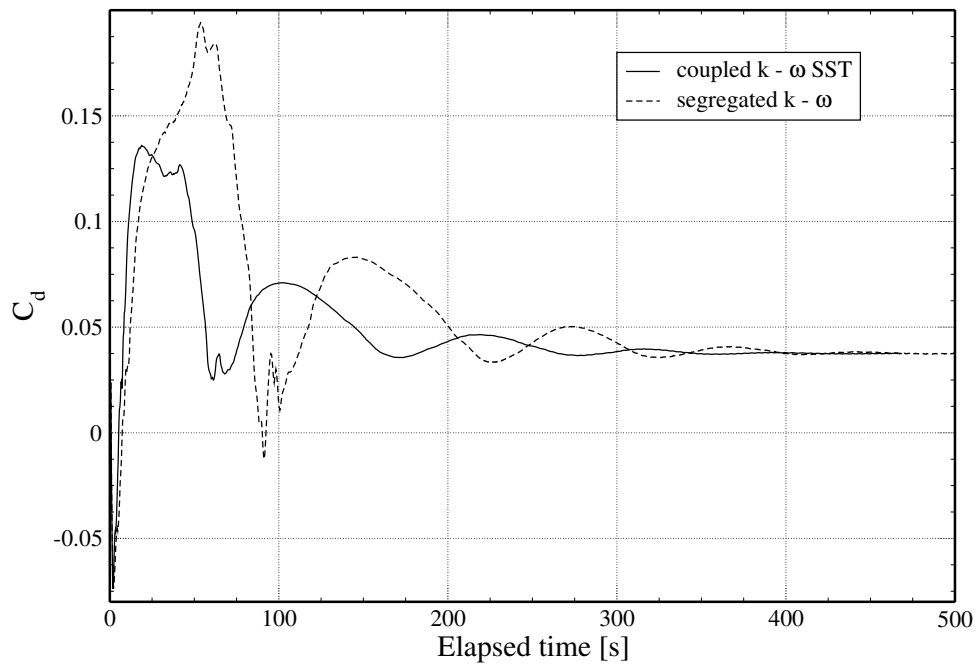
(a) Koeficijent otpora,
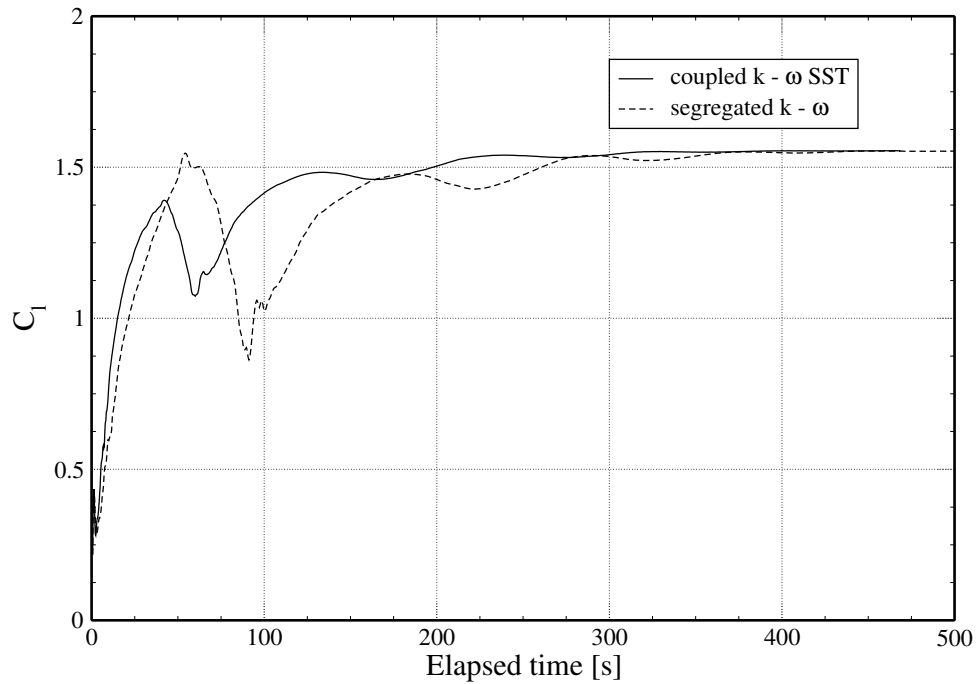
(b) Koeficijent uzgona.

Slika 15: NACA: Konvergencija koeficijenata sile kroz procesorsko vrijeme.

Iz prethodno prikazanih slika vidljivo je da implicitno sprezanje jednadžbi modela turbulencije pospješuje mirniju i bržu konvergenciju rješenja (ne samo turbulentnih varijabli već i tlaka i brzine), često sprječava premašivanje vrijednosti u procesu računanja te ubrzava konvergenciju minimalnih i maksimalnih vrijednosti polja u proračunskoj domeni. Implicitno spregnuti modeli dosljedniji su u očuvanju pozitivnosti varijabli te u kontekstu procesorskog vremena skraćuju vrijeme trajanja proračuna. U slučaju proračuna koeficijenata sile uzgona i otpora za NACA 4412 aeroprofil, ubrzanje je otprilike 20%.

Chapter 1

Introduction

1.1 Background

Development and implementation of implicitly coupled pressure–velocity algorithms for incompressible flows in Computational Fluid Dynamics (CFD) introduced a substantial increase in the convergence rates for the velocity and pressure equations, compared with corresponding segregated algorithms (e.g. SIMPLE or PISO) [1]. When implicitly coupled solvers are used for turbulent flow simulations, convergence rates are often controlled by segregated treatment of turbulence model equations. Therefore, implicit coupling of two-equation eddy viscosity (incompressible) turbulence models, $k - \varepsilon$ and $k - \omega \, SST$, shall be presented in this thesis.

1.2 Previous and Related Studies

Two-equation turbulence models include two extra transport equations for representation of the turbulent flow properties, which are by definition positive quantities. Despite their relatively simple mathematical representation, turbulence model equations present serious numerical difficulties, among which are non-linear coupling, convergence and positivity preserving difficulties. The inter-equation coupling is usually strongly non-linear, leading to added numerical stiffness which usually results in slower convergence. Furthermore, in the process of convergence, non-physical solutions, namely negative values of the turbulence quantities may appear even if the equation set analytically guarantees to remain positive [2]. Therefore, stability and boundedness of the implemented turbulence models is becoming an active and challenging field

for research.

Ilinca et al. [3, 4] propose a substitution of dependent variables that guarantees positivity of turbulence variables in numerical simulation algorithms. The approach solves for the natural logarithm of the turbulence variables which are known to be strictly positive.

Du and Wu [5] prove that the mixed (analytical/numerical) method based on operator splitting, which is extended to the $k - \varepsilon$ turbulence model, does not converge to a stable steady state solution. Therefore, an unsplit mixed method with implicit treatment of the source term is proposed.

Wasserman et al. [6] present a robust multigrid method for the solution of Reynolds-Averaged Navier-Stokes (RANS) equations with two-equation turbulence models. The method employs a basic relaxation scheme (alternating line Gauss-Siedel) where mean-flow and turbulence model equations are marched in time in a loosely-coupled manner. The proposed multigrid method uses an extended version of the unconditionally positive-convergent scheme for two-equation turbulence models (adapted for use in multigrid) and a strongly coupled multigrid cycling strategy.

Moryossef and Levy [7, 8] propose an unconditionally positive-convergent implicit procedure for two-equation turbulence models. The implicit procedure is based on designing the implicit Jacobian to be an M-matrix. The suggested M-matrix design should guarantee the positivity of the turbulence equation dependent variables for any time step, without the use of any a posteriori artificial numerical bounding.

In this thesis we shall explore options for accelerated convergence of the two-equation eddy viscosity turbulence equations by means of block-solution. Here, equations of the turbulence model are solved together using a block-matrix and a single call of the (iterative) linear equation solver. This allows us to consider various forms of linearised implicit inter-equation coupling, with a view of accelerated convergence.

1.3   Thesis Outline

Chapter 2 introduces the basic governing equations in fluid dynamics and gives a brief overview of turbulence modelling for CFD, with a focus on the (incompressible) $k - \varepsilon$ and $k - \omega SST$ turbulence models and the corresponding wall functions.

Chapter 3 describes the block-system structure which is used to achieve inter-equation coupling. Linearisation procedure for the non-linear source terms is described. Analysis of stability and boundedness of the linearised model is examined. Furthermore, linearisation and implementation of $k - \varepsilon$ and $k - \omega\, SST$ turbulence models in the block-matrix framework is summarised.

Chapter 4 presents validation of the implemented turbulence models. Two validation cases are examined, a separated flow past a NACA 4412 airfoil at maximum lift and an incompressible turbulent flow over a backward facing step.

Chapter 5 presents the performance benchmark tests of implemented turbulence models on both validation cases. The implemented models are compared with the corresponding segregated versions.

Chapter 6 summarises the Thesis and gives a comprehensive conclusion.

Chapter 2

Turbulent Flow Modelling

Majority of flows encountered in engineering practice are turbulent by nature, therefore the ability to appropriately model turbulent phenomena is essential. As Wilcox [9] suggests, an ideal turbulence model should introduce minimal amount of complexity while capturing the essence of the relevant physics. Main properties of turbulent flows are:

- High unsteadiness,

- Three-dimensionality,

- Vorticity,

- High diffusivity (turbulent diffusion),

- Dissipation,

- Coherent structures,

- Fluctuations on broad ranges of length and time scales. [10]

Time-dependent, three-dimensional Navier-Stokes equations describe all the physics of turbulent flow. However, due to the non-linearity of the convection term, resolving the whole range of spatial and temporal scales of turbulence is prohibitively expensive for most engineering applications [9, 11]. The goal of turbulence modelling is to find approximate solutions for the Navier-Stokes equations in a manner that they either describe the turbulence in terms of mean properties or limit the spatial/temporal resolution requirements associated with the full model [11].

2.1 Incompressible Navier–Stokes Equation

The Navier-Stokes or the momentum equation, is the basic governing equation which describes the motion of viscous fluids and belongs to the class of vector convection-diffusion equations.The momentum equation is accompanied by the continuity (mass conservation) and the energy conservation equation. This thesis does not deal with heat transfer, therefore the energy equation is neglected.

The momentum and the continuity equation for the incompressible flow read:

$$\frac{\partial \mathbf{u}}{\partial t} + \nabla \boldsymbol{\cdot} (\mathbf{u}\mathbf{u}) - \nabla \boldsymbol{\cdot} (\nu \nabla \mathbf{u}) = -\nabla p, \tag{2.1.1}$$

$$\nabla \boldsymbol{\cdot} \mathbf{u} = 0, \tag{2.1.2}$$

where $\mathbf{u}$ is the instantaneous velocity field, ν is the kinematic molecular viscosity and p is the kinematic pressure defined as $p = P/\rho$, where P is the pressure and ρ is the density.

2.2 Overview of Turbulence Modelling for CFD

There are three basic approaches for predicting turbulent flows in CFD [9]:

- Direct Numerical Simulation (DNS), solves the Navier-Stokes equations for all scales without turbulence modelling. Sufficient temporal and spatial resolution is required.

- Large Eddy Simulation (LES), solves filtered Navier-Stokes equations, where large scale turbulence and coherent structures are simulated, but filtered small scale eddies are modelled.

- Reynolds-Averaged Navier-Stokes equations (RANS), solves the averaged Navier-Stokes equations, where turbulent fluctuations are appropriately modelled. Consequently, a coarser spatial and temporal resolution is sufficient and it is possible to introduce a convent of solutions which are steady or two-dimensional in the mean, compared to the intrinsically three-dimensional and unsteady nature of turbulent flows. Additional closure correlations are required.

In this thesis, only the RANS approach will be considered in a more detailed manner.

2.2.1 Reynolds Temporal Averaging of Navier-Stokes Equations

If the objective of the simulations is to obtain the mean properties of the flow without considering the details of turbulent fluctuations, Reynolds averaging is the most appropriate choice.

Following the Reynolds decomposition of $\mathbf{u}$ and p, instantaneous fields are decomposed into a mean and fluctuating part:

$$\mathbf{u} = \overline{\mathbf{u}} + \mathbf{u}', \tag{2.2.1}$$

$$p = \overline{p} + p', \tag{2.2.2}$$

where $\overline{\cdot}$ denotes the mean and $\cdot'$ denotes the fluctuating part.

Time averaging of Equations (2.1.1) and (2.1.2) yields the Reynolds-Averaged Navier-Stokes Equations and the time-averaged continuity equation:

$$\frac{\partial \overline{\mathbf{u}}}{\partial t} + \nabla_\bullet (\overline{\mathbf{u}}\,\overline{\mathbf{u}}) - \nabla_\bullet (\nu \nabla \overline{\mathbf{u}}) = -\nabla \overline{p} - \nabla_\bullet \left(\overline{\mathbf{u}'\mathbf{u}'}\right), \tag{2.2.3}$$

$$\nabla_\bullet \overline{\mathbf{u}} = 0. \tag{2.2.4}$$

Equation (2.2.4) is identical to (2.1.2), with the mean velocity replacing the instantaneous velocity. The only difference between the time-averaged Equation (2.2.3) and instantaneous momentum Equation (2.1.1) is the appearance of the correlation $-\overline{\mathbf{u}'\mathbf{u}'}$, which is commonly known as the Reynolds-stress tensor [9]. As Equations (2.2.3) and (2.2.4) do not form a closed set, a turbulence model is introduced to model the Reynolds-stress tensor. The most common types of turbulence models are the eddy viscosity models in which the Reynolds-stress tensor is modelled with:

$$-\overline{\mathbf{u}'\mathbf{u}'} = \nu_t \left(\nabla \overline{\mathbf{u}} + (\nabla \overline{\mathbf{u}})^T\right) - \frac{2}{3}\mathbf{I}k, \tag{2.2.5}$$

where ν_t is the kinematic eddy viscosity, $\mathbf{I}$ is the identity tensor (Kronecker delta) and k is the turbulent kinetic energy.

Following [10], the molecular viscosity ν is replaced with the effective viscosity ν_{eff} which is equal to the sum of the molecular and eddy viscosity (turbulent viscosity) $\nu_{eff} = \nu + \nu_t$. The Reynolds-averaged momentum equation with an eddy-viscosity turbulence model has the following form:

$$\frac{\partial \overline{\mathbf{u}}}{\partial t} + \nabla_\bullet (\overline{\mathbf{u}}\,\overline{\mathbf{u}}) - \nabla_\bullet \left(\nu_{eff} \nabla \overline{\mathbf{u}}\right) = -\nabla \overline{p}, \tag{2.2.6}$$

and the continuity equation remains the same, Equation (2.2.4).

Eddy viscosity models are often divided into [9]:

- Algebraic models,

- One-equation models,

- Two-equation models.

Only the two-equation models are covered in scope of this thesis, more information about remaining models can be found in [9].

2.3   Two-Equation Turbulence Models

The two-equation models are the work-horse of engineering simulations today. Therefore, two extensively used two-equation turbulence models $k - \varepsilon$ and $k - \omega SST$ will be analysed in this thesis. [12, 11]

In most of the two-equation models, the first equation is the turbulent kinetic energy k equation which determines the velocity scale, and the second equation is the turbulent dissipation ε equation which determines the length scale of the turbulence. Instead of ε, the inverse time scale ω (specific turbulence dissipation or eddy turnover time) can also be used as the second equation.

At this point, it is useful to emphasize that the complexity of turbulence phenomena makes it unlikely that any single Reynolds-averaged model will be able to represent all turbulent flows. Hence, turbulence models should be regarded as engineering approximations rather than scientific laws [10].

Equations described in the following sections represent the implementation of the incompressible $k - \varepsilon$ and $k - \omega SST$ models in OpenFOAM [13], more precisely in the community-driven fork of the OpenFOAM, i.e. the OpenFOAM Extend-Project [14] (hereinafter referred to as foam-extend).

2.3.1   Incompressible $k - \varepsilon$ Turbulence Model

In foam-extend, $k - \varepsilon$ turbulence model (`kEpsilon`) is implemented according to Jones and Launder [15] and is often referred to as the standard $k - \varepsilon$ turbulence model. In the standard

$k - \varepsilon$ model the turbulent kinetic energy equation reads:

$$\frac{\partial k}{\partial t} + \nabla\bullet(\overline{\mathbf{u}}k) - k\nabla\bullet\overline{\mathbf{u}} - \nabla\bullet(\Gamma_{k,eff}\nabla k) = G - \varepsilon, \tag{2.3.1}$$

Despite the fact that the flow is assumed to be incompressible, the $-k\nabla\bullet\overline{\mathbf{u}}$ term is implemented, because it enhances the conservativeness of the solution during the calculation.

$$\Gamma_{k,eff} = \nu + \nu_t. \tag{2.3.2}$$

Dissipation of turbulence kinetic energy equation reads:

$$\frac{\partial \varepsilon}{\partial t} + \nabla\bullet(\overline{\mathbf{u}}\varepsilon) - \varepsilon\nabla\bullet\overline{\mathbf{u}} - \nabla\bullet(\Gamma_{\varepsilon,eff}\nabla\varepsilon) = C_1\frac{\varepsilon}{k}G - C_2\frac{\varepsilon^2}{k}, \tag{2.3.3}$$

$$\Gamma_{\varepsilon,eff} = \nu + \frac{\nu_t}{\sigma_\varepsilon}. \tag{2.3.4}$$

The eddy viscosity is defined as:

$$\nu_t = C_\mu \frac{k^2}{\varepsilon}, \tag{2.3.5}$$

and the production of turbulent kinetic energy:

$$G = 2\nu_t \left| \frac{1}{2}\left(\nabla\overline{\mathbf{u}} + (\nabla\overline{\mathbf{u}})^T\right) \right|^2. \tag{2.3.6}$$

Closure coefficients have the following values: $C_\mu = 0.09$, $C_1 = 1.44$, $C_2 = 1.92$, $\sigma_\varepsilon = 1.3$.

2.3.2 Incompressible $k - \omega SST$ Turbulence model

In foam-extend, $k - \omega SST$ turbulence model (`kOmegaSST`) is implemented according to the model described by Menter and Esch [16] with updated coefficients from [12], but with the consistent production according to *NASA Turbulence Modeling Resource* web-page [17]. Optional F_3 term for rough walls is added according to Hellsten [18]. In the $k - \omega SST$ model turbulent kinetic energy equation reads:

$$\frac{\partial k}{\partial t} + \nabla\bullet(\overline{\mathbf{u}}k) - k\nabla\bullet\overline{\mathbf{u}} - \nabla\bullet(\Gamma_{k,eff}\nabla k) = \min\left(G, c_1\beta^*k\omega\right) - \beta^*k\omega, \tag{2.3.7}$$

$$\Gamma_{k,eff} = \alpha_k\nu_t + \nu. \tag{2.3.8}$$

Specific dissipation rate equation reads:

$$\frac{\partial \omega}{\partial t} + \nabla\bullet(\overline{\mathbf{u}}\omega) - \omega\nabla\bullet\overline{\mathbf{u}} - \nabla\bullet(\Gamma_{\omega,eff}\nabla\omega) =$$

$$\gamma\min\left[S_2, \frac{c_1}{a_1}\beta^*\omega\max\left(a_1\omega, b_1F_{23}\sqrt{S_2}\right)\right] \tag{2.3.9}$$

$$- \beta\omega^2 + (1 - F_1)CD_{k\omega},$$

$$\Gamma_{\omega,eff} = \alpha_\omega \nu_t + \nu. \tag{2.3.10}$$

The eddy viscosity is calculated as:

$$\nu_t = \frac{a_1 k}{\max\left[a_1 \omega, b_1 F_{23}\sqrt{2}\left|\frac{1}{2}\left(\nabla\mathbf{\bar{u}} + (\nabla\mathbf{\bar{u}})^T\right)\right|\right]} \tag{2.3.11}$$

and the production of turbulent kinetic energy reads:

$$G = \nu_t S_2, \tag{2.3.12}$$

$$S_2 = 2\left|\frac{1}{2}\left(\nabla\mathbf{\bar{u}} + (\nabla\mathbf{\bar{u}})^T\right)\right|^2. \tag{2.3.13}$$

The $k - \omega\, SST$ formulation combines the best properties of $k - \omega$ and $k - \varepsilon$ turbulence models. The use of $k - \varepsilon$ in the free-stream removes the the sensitivity of the original $k - \omega$ to the inlet free-stream turbulence properties. The use of $k - \omega$ in the inner parts of the boundary layer makes the model usable close to the wall without damping functions. Thus, each of the constants represents a blend of constants from set $_1$ $(k - \omega)$ and set $_2$ $(k - \varepsilon)$:

$$\alpha_k = F_1\left(\alpha_{k_1} - \alpha_{k_2}\right) + \alpha_{k_2}, \tag{2.3.14}$$

$$\alpha_\omega = F_1\left(\alpha_{\omega_1} - \alpha_{\omega_2}\right) + \alpha_{\omega_2}, \tag{2.3.15}$$

$$\beta = F_1\left(\beta_1 - \beta_2\right) + \beta_2, \tag{2.3.16}$$

$$\gamma = F_1\left(\gamma_1 - \gamma_2\right) + \gamma_2, \tag{2.3.17}$$

where the blending is performed via blending functions, F_1 is a function that is one in the sublayer and logarithmic region of the boundary layer and gradually switches to zero in the wake region [19]:

$$F_1 = \tanh\left[(arg_1)^4\right], \tag{2.3.18}$$

$$arg_1 = \min\left\{\min\left[\max\left(\frac{\sqrt{k}}{\beta^*\omega y}, \frac{500\nu}{y^2\omega}\right), \frac{4\alpha_{\omega 2}k}{CD_{k\omega+}y^2}\right], 10\right\}, \tag{2.3.19}$$

F_2 is a function that is one for boundary-layer flows and zero for free shear layers [19]:

$$F_2 = \tanh\left[(arg_2)^2\right], \tag{2.3.20}$$

$$arg_2 = \min\left[\max\left(\frac{2\sqrt{k}}{\beta^*\omega y}, \frac{500\nu}{y^2\omega}\right), 100\right]. \tag{2.3.21}$$

Hellsten [18] introduced the implementation of function F_3 designed to prevent the SST limitation from being activated in the roughness layer in rough-wall flows, i.e. the layer very close to the rough wall:

$$F_3 = 1 - \tanh\left[(arg_3)^4\right], \tag{2.3.22}$$

$$arg_3 = \min\left(\frac{150\nu}{y^2\omega}, 10\right). \tag{2.3.23}$$

Blending function F_{23} is by default equal to F_2, but if the optional F_3 function is activated, F_{23} becomes equal to the product of both F_2 and F_3.

$$F_{23} = \begin{cases} F_{23} = F_2 & \text{default setting,} \\ F_{23} = F_2 F_3 & \text{optional term for rough-wall flows.} \end{cases} \tag{2.3.24}$$

Positive portion of the cross-diffusion term is introduced for numerical stability:

$$CD_{k\omega+} = \max\left(CD_{k\omega}, 10^{-10}\right), \tag{2.3.25}$$

$$CD_{k\omega} = 2\alpha_{\omega2}\frac{\nabla k \cdot \nabla \omega}{\omega}. \tag{2.3.26}$$

Closure coefficients have the following values: $\alpha_{k_1} = 0.85$, $\alpha_{k_2} = 1$, $\alpha_{\omega_1} = 0.5$, $\alpha_{\omega_2} = 0.856$, $\beta_1 = 0.075$, $\beta_2 = 0.0828$, $\beta^* = 0.09$, $\gamma_1 = 5/9$, $\gamma_2 = 0.44$, $a_1 = 0.31$, $b_1 = 1$, $c_1 = 10$.

2.4   Near-Wall Treatment

When studying part of the wall bounded turbulent flows, the near-wall region is traditionally divided into the inner and outer turbulent boundary layer. In this thesis only the inner layer will be briefly investigated since all the important phenomena for near-wall flow modelling in CFD occur in this layer. Various regions of the turbulent boundary layer are shown in Figure 2.4.1.

Roughly speaking, the inner layer consists of: the viscous linear sublayer $(0 < y^+ < 5)$, the buffer sublayer $(5 < y^+ < 30)$ and the inertial sublayer $(30 < y^+ < 200 - 300)$ where y^+ is the normalised distance to the wall calculated as:

$$y^+ = \frac{C_\mu^{1/4} k^{1/2}}{\nu} y. \tag{2.4.1}$$
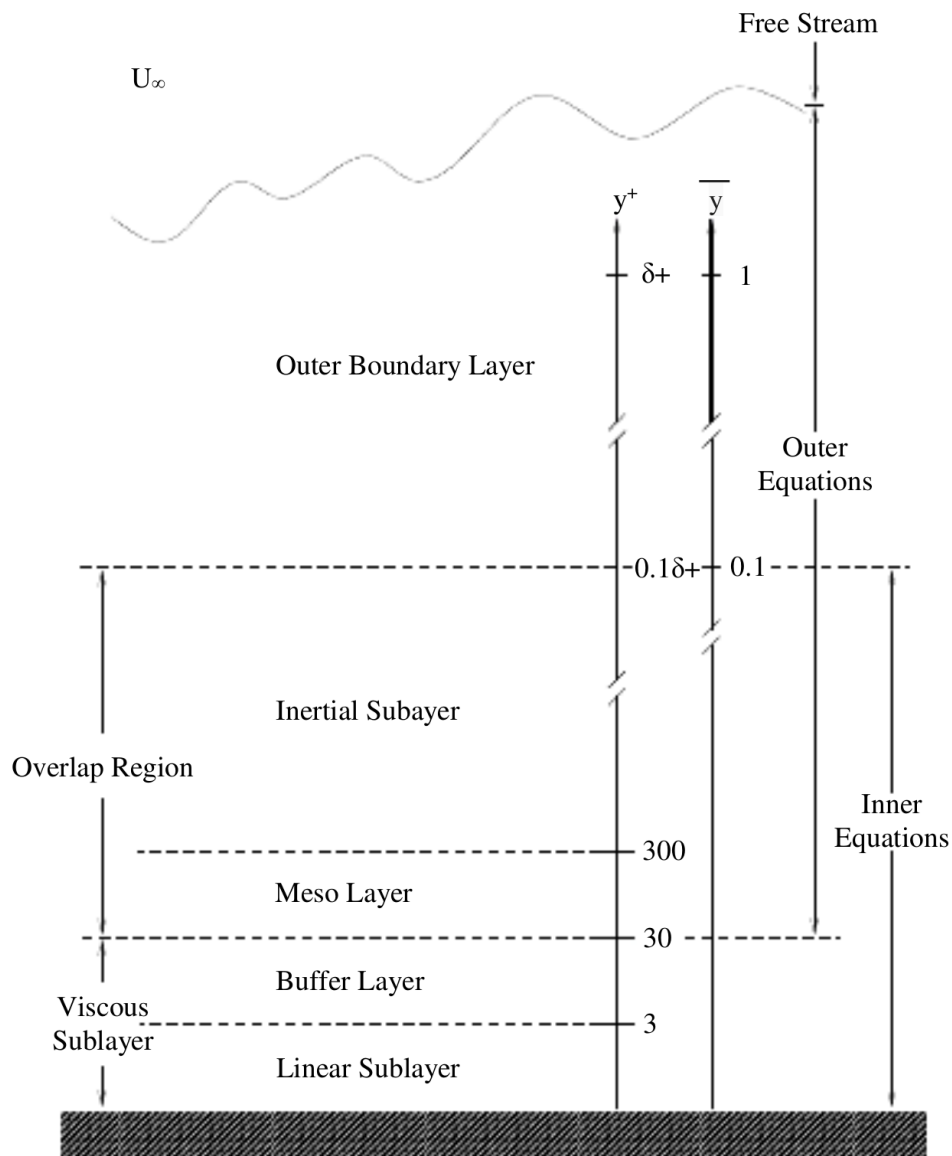
Figure 2.4.1: Regions of the turbulent boundary layer. [20]

In the viscous linear sublayer, molecular viscosity is dominant and the turbulence effects are negligible. In the inertial sublayer, turbulent viscosity is dominant, making the molecular viscosity unimportant. In the buffer sublayer both turbulent and molecular viscosities are equally important.

The presented assumptions allow implementation of simple expressions, which model behaviour of important variables in the near-wall region (as functions of wall distance). Figure 2.4.2 shows the dependency of dimensionless velocity U^+ with respect to y^+ (the red line

represents the experimental observations and the two blue lines represent the two derived profiles). The linear profile in the viscous sublayer and the logarithmic profile in the inertial sublayer fit the experimental observations, while the buffer sublayer can be viewed as a smooth transition between the two. Consequently, it is recommended to put the first cell centre either in the viscous linear sublayer or in the inertial sublayer. The buffer sublayer should be avoided, as it represents a transitional region from the linear to the log profile.
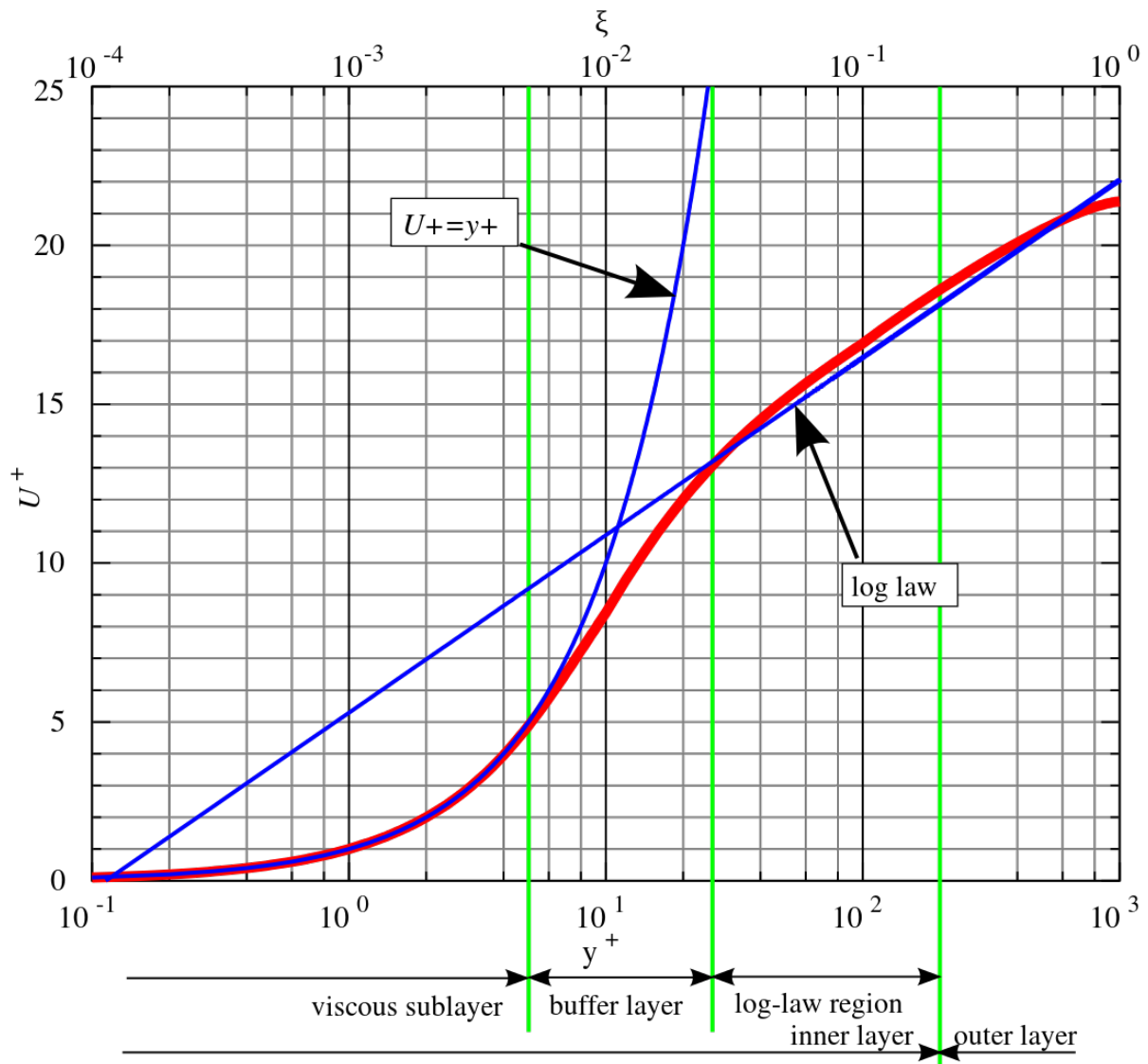
Figure 2.4.2: Law of the wall. [21]

Positioning the first cell in the linear sublayer is an attribute of low Reynolds turbulence modelling, while placing it in the inertial (log-layer) is a characteristic of high Reynolds mod-

elling.
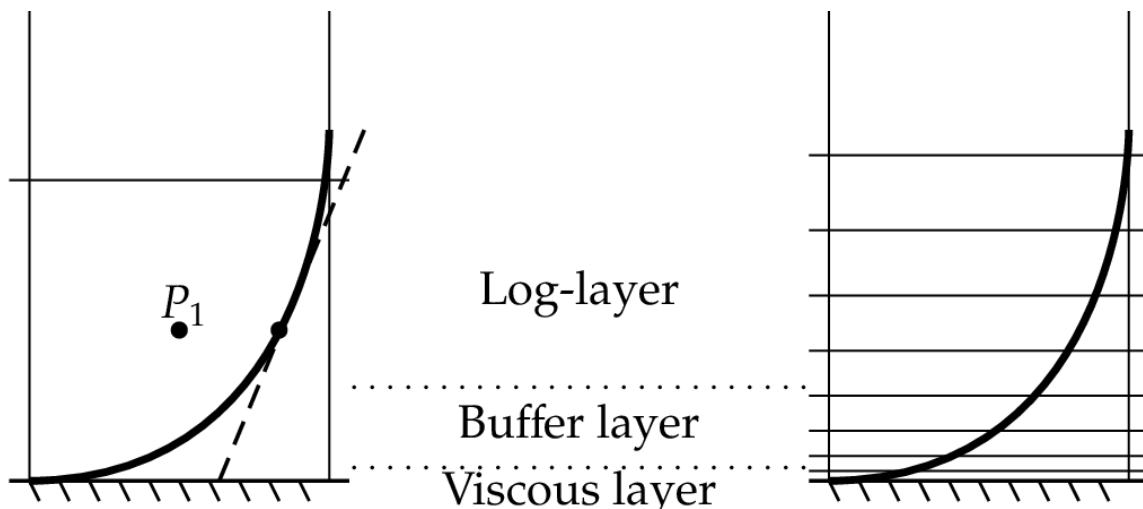
Figure 2.4.3: High Reynolds number vs. low Reynolds number approach. [22]

In CFD codes, the previously described correlations are implemented as wall functions. The focus of this thesis is the implicit coupling of two-equation incompressible $k - \omega \, SST$ and $k - \varepsilon$ turbulence models, therefore wall boundary conditions for k, ε and ω, and their implementation in foam-extend will be covered in detail.

In foam-extend wall function for field k is denoted with `kqRWallFunction`, for field ε `epsilonWallFunction`, for ω `omegaWallFunction` and the correction for ν_t is done in `nutWallFunction`.

2.4.1 Standard Wall Functions for $k - \varepsilon$ Turbulence Model

In foam-extend, $k - \varepsilon$ turbulence model is implemented only as a high Reynolds version and therefore uses standard wall functions, which avoid solving the flow inside the viscous sublayer by using empirical relations applicable in the inertial sublayer. Furthermore, in adjacent cells to the wall, Equation (2.3.3) for ε is not solved and an algebraic expression is used instead:

$$\varepsilon = \frac{C_\mu^{3/4} k^{3/2}}{\kappa y}, \tag{2.4.2}$$

where κ is the von Kármán constant with a default value of 0.41. The production term G in Equation (2.3.1) for k is calculated using the following expressions:

$$G = \begin{cases} G = G_{vis} & \text{for } y^+ \leq y^+_{lam}, \\ G = G_{log} & \text{for } y^+ > y^+_{lam}, \end{cases} \tag{2.4.3}$$

$$G_{vis} = 0, \tag{2.4.4}$$

$$G_{log} = \frac{\left((\nu_t + \nu)\,|\nabla\overline{\mathbf{u}}|\right)^2}{\kappa C_\mu^{1/4} k^{1/2} y}. \tag{2.4.5}$$

The k equation is still solved in cells adjacent to the wall. Equation (2.4.5) was altered in comparison with [23] for achieving consistency with ANSYS Fluent implementation [24]. Similarly as in [23] the normalised distance to the wall y^+ is calculated from Equation (2.4.1) and the interface between the viscous and the inertial sublayer (log-layer) y^+_{lam} is calculated with:

$$y^+_{lam} = \frac{\ln\left(\max\left(E\,y^+_{lam},\,1\right)\right)}{\kappa}, \tag{2.4.6}$$

where E is a dimensionless constant with a default value of 9.8. Equation (2.4.6) is solved iteratively in ten iterations.

2.4.2   Automatic Wall Treatment for $k - \omega\,SST$ Turbulence Model

In contrast to the $k - \varepsilon$, the $k - \omega\,SST$ (and $k - \omega$) turbulence model does not need extra damping functions to act as a low Reynolds model because the ω equation has a known solution in both viscous and inertial (log-layer) sublayer. Adopting this property, Menter [16] developed a blending technique which allows a smooth transition from high to low Reynolds formulation and vice versa. Despite the smooth shift, automatic wall treatment does not give a correct representation of the buffer layer. The blending is performed by:

$$\omega = \sqrt{\omega_{vis}^2 + \omega_{log}^2}, \tag{2.4.7}$$

where ω_{vis} and ω_{log} are defined as follows:

$$\omega_{vis} = \frac{6\nu}{\beta_1 y^2}, \tag{2.4.8}$$

$$\omega_{log} = \frac{k^{1/2}}{\kappa C_\mu^{1/4} y}. \tag{2.4.9}$$

Similarly as in the standard wall functions for $k - \varepsilon$, Equation (2.3.9) for ω is not solved for cells adjacent to the wall, rather, its value is obtained from Equation (2.4.7). In these cells the production term G in Equation (2.3.9) is modified according to:

$$G = \begin{cases} G = G_{vis} & \text{if } y^+ \leq y^+_{lam}, \\ G = G_{log} & \text{if } y^+ > y^+_{lam}. \end{cases} \tag{2.4.10}$$

$$G_{vis} = 0, \tag{2.4.11}$$

$$G_{log} = \frac{C_\mu^{1/4} k^{1/2} \left(\nu_t + \nu \right) |\nabla \overline{\mathbf{u}}|}{\kappa y}, \tag{2.4.12}$$

where y^+ and y^+_{lam} are calculated from Equation (2.4.1) and Equation (2.4.6).

Chapter 3

Implicit Coupling of Two-Equation Turbulence Models

In the previous chapter, a short theoretical overview of turbulence modelling in CFD was described and special attention was given on two-equation turbulence models ($k - \varepsilon$ and $k - \omega\,SST$) and their implementation in foam-extend. In this chapter, implementation of two-equation turbulence models ($k - \varepsilon$ and $k - \omega\,SST$) in the block-matrix framework is presented. Related problems regarding the linearisation, stability and boundedness of the models are also investigated.

3.1   Block-Coupling

Most CFD algorithms use segregated algorithms in order to solve two-equation turbulence models, where the turbulence equations are solved sequentially one after another. Bottleneck of segregated algorithms is the explicit coupling, where the solution variables need to be substantially under-relaxed to ensure numerical stability. On the other hand, segregated algorithms are memory-efficient because only one discretisation matrix at a time needs to be stored.

Implicit coupling introduces a simultaneous way of solving governing equations. All the equations are considered as part of a single system which has a block-banded structure [10], and all equations in the block are solved together. Implicit coupling should be able to improve convergence (under-relaxation factors can be considerably increased) but it leads to a substantially larger linear system and an increased memory usage [25].

3.2 Block-System Structure

The structure of the block-system can be represented by two levels: the first is bound to the calculated compact-stencil discretisation of the computational domain with control volumes (CV) and the second handles the format of the each matrix entry [25].

Spatial discretisation (via finite volume method) of the domain into N CVs, leads to a linear system of N unknowns:

$$
\begin{pmatrix}
a_{1,1} & a_{1,2} & \cdots & a_{1,N} \\
a_{2,1} & a_{2,2} & \cdots & a_{2,N} \\
\vdots & \vdots & \ddots & \vdots \\
a_{N,1} & a_{N,2} & \cdots & a_{N,N}
\end{pmatrix}
\begin{pmatrix}
\phi_1 \\
\phi_2 \\
\vdots \\
\phi_N
\end{pmatrix}
=
\begin{pmatrix}
b_1 \\
b_2 \\
\vdots \\
b_N
\end{pmatrix},
\tag{3.2.1}
$$

where $a_{i,j}$ is a matrix entry, ϕ_i is the field value to be solved in the cell i, and b_i is the right hand side (RHS) term for the cell i.

In the segregated approach, each matrix entry is a scalar, since every equation is solved sequentially. In the simultaneous implicitly coupled approach, each ϕ_i is a n-dimensional vector, where n is the number of the implicitly coupled equations. The same applies for the RHS vector b_i and each matrix entry $a_{i,j}$ is a $n \times n$ tensor, which models the coupling between the implicitly coupled equations.

If the two-equation turbulence models are used, two additional transport equations need to be solved, which are coupled through source and sink terms. Assume that the two transported variables are ϕ_A and ϕ_B (which are also positive-bounded) and that the transport equations have the following generic form:

$$
\frac{\partial \phi_A}{\partial t} + \nabla \bullet (\overline{\mathbf{u}} \phi_A) - \phi_A \nabla \bullet \overline{\mathbf{u}} - \nabla \bullet (\Gamma_A \nabla \phi_A) = S_A,
\tag{3.2.2}
$$

$$
\frac{\partial \phi_B}{\partial t} + \nabla \bullet (\overline{\mathbf{u}} \phi_B) - \phi_B \nabla \bullet \overline{\mathbf{u}} - \nabla \bullet (\Gamma_B \nabla \phi_B) = S_B,
\tag{3.2.3}
$$

where S_A and S_B are net source terms, which are both functions of ϕ_A and ϕ_B, i.e. $S_A = S_A(\phi_A, \phi_B)$ and $S_B = S_B(\phi_A, \phi_B)$. In case of implicit coupling of the two-equations, field value ϕ_i in the cell i is a two-dimensional vector:

$$
\phi_i = \begin{pmatrix} \phi_{Ai} \\ \phi_{Bi} \end{pmatrix},
\tag{3.2.4}
$$

and each matrix entry $a_{i,j}$ is a 2×2 tensor which models the coupling between the two-equations:

$$a_{i,j} = \left(\begin{array}{c|c} a_{\phi_{Ai},\phi_{Aj}} & a_{\phi_{Ai},\phi_{Bj}} \\ \hline a_{\phi_{Bi},\phi_{Aj}} & a_{\phi_{Bi},\phi_{Bj}} \end{array} \right), \qquad (3.2.5)$$

where $a_{\phi_{Ai},\phi_{Aj}}$ models the coupling between ϕ_A in cell i with ϕ_A in cell j, $a_{\phi_{Ai},\phi_{Bj}}$ models the coupling between ϕ_A in cell i with ϕ_B in cell j, $a_{\phi_{Bi},\phi_{Aj}}$ models the coupling between ϕ_B in cell i with ϕ_A in cell j and $a_{\phi_{Bi},\phi_{Bj}}$ models the coupling between ϕ_B in cell i with ϕ_B in cell j.

Here, it is important to emphasize that the turbulence equations are mainly coupled through their source terms, as shown in Chapter 2, therefore, cross-coupling terms $a_{\phi_{Ai},\phi_{Bj}}$ and $a_{\phi_{Bi},\phi_{Aj}}$ which are located on the off-diagonal of the matrix entry $a_{i,j}$ (3.2.5) have a nonzero value only on the diagonal of the linear system (3.2.1), i.e. when $i = j$.

Furthermore, the global sparseness pattern related to mesh connectivity can be preserved by choosing an appropriate form of the block-matrix layout.

3.3   Analysis of Stability and Boundedness of the Linearised Model

Turbulence variables, e.g. turbulent kinetic energy k, dissipation ε and specific dissipation ω belong to the group of positive-bounded variables, i.e. these variables are physically or by definition non-negative quantities, therefore their value should always remain positive during the calculation. If the negative values do occur, numerical instabilities are inevitable, which may have an undesirable effect on the rest of the calculation. [26]

If ϕ is a generic, positive-bounded scalar dependent variable and Equation (3.3.1) is the appropriate generic scalar transport equation:

$$\frac{\partial \phi}{\partial t} + \nabla \bullet (\overline{\mathbf{u}}\phi) - \phi \nabla \bullet \overline{\mathbf{u}} - \nabla \bullet (\Gamma \nabla \phi) = S, \qquad (3.3.1)$$

the net source term S in Equation (3.3.1), accounts for any sources or sinks that either create or destroy ϕ, therefore S can acquire both positive and negative values. If the net source term is not properly handled, the positive-bounded variable may acquire erroneous negative values. Hence, Patankar [26] suggests dividing the net source term into the source (which is always

positive) and sink (which is always negative) terms:

$$S = S^+ + S^- \phi \,, \tag{3.3.2}$$

where the sink term S^- is treated implicitly and the source term S^+ is treated explicitly. Implicit treatment of the sink term, increases the diagonal dominance of the matrix, which is conducive to convergence and explicit treatment of the source, enhances the boundedness and the stability of the solution.

In case of turbulence modelling, the source/sink terms are often non-linear functions of the dependent variable itself. Since the discretised equations are solved using linear algebraic solvers, the non-linear dependency needs to be linearised. In this thesis the Picard's method is adopted:

$$S^n \approx S^o + \left(\frac{\partial S}{\partial \phi} \right)^o (\phi^n - \phi^o) \,, \tag{3.3.3}$$

where the superscript $\cdot^n$ denotes the new time-level (implicit treatment) and the superscript $\cdot^o$ denotes the old time-level (explicit treatment).

After the linearisation, the source terms are converted into the explicit form and added into the S^+ term, while the sink terms are treated implicitly by combining them into S^-:

$$S^n = S^+ + S^- \phi^n \,. \tag{3.3.4}$$

If the two-equation turbulence model equations should be solved in an implicitly coupled manner, linearisation of the net source terms with respect to both variables is necessary. Again, the two generic transport equations (Equations (3.2.2) and (3.2.3)) are used as an example and the linearisation is performed according to the Taylor expansion:

$$S_A^n \approx S_A^o + \left(\frac{\partial S_A}{\partial \phi_A} \right)^o (\phi_A^n - \phi_A^o) + \left(\frac{\partial S_A}{\partial \phi_B} \right)^o (\phi_B^n - \phi_B^o) \,, \tag{3.3.5}$$

$$S_B^n \approx S_B^o + \left(\frac{\partial S_B}{\partial \phi_A} \right)^o (\phi_A^n - \phi_A^o) + \left(\frac{\partial S_B}{\partial \phi_B} \right)^o (\phi_B^n - \phi_B^o) \,. \tag{3.3.6}$$

Despite the fact that the equations are inserted into the block-system and that the system is solved in a simultaneous manner, proper net source term treatment is necessary, if the boundedness of the variables is to be preserved.

Applying the same reasoning for the net source term treatment as previously described in this section, products of linearisation are divided into three groups: the explicit sources S^+, the implicit cross-coupling sources S^* and the implicit sinks S^-:

$$S_A^n = S_A^+ + S_A^* \phi_B^n + S_A^- \phi_A^n,$$
(3.3.7)

$$S_B^n = S_B^+ + S_B^* \phi_A^n + S_B^- \phi_B^n.$$
(3.3.8)

The contribution of the individual terms from Equations (3.3.7) and (3.3.8) to the block-system is shown in Figure 3.3.1.
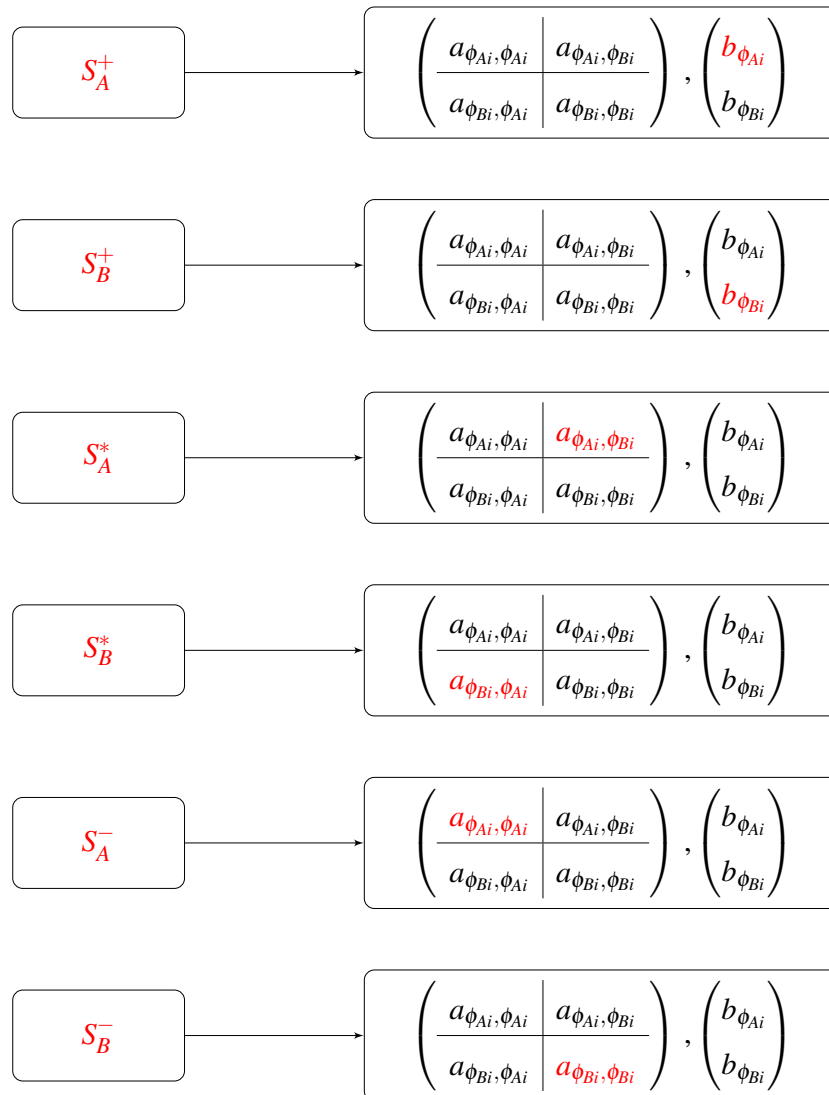
Figure 3.3.1: Contribution of the individual products of the linearisation to the block-system.

Regarding the division and treatment of the products of the linearisation, the only major difference between the segregated and the implicitly coupled approach lies in the S^* term, which models the implicit cross-coupling of the two-equations. Since this term lies on the off-diagonal of the matrix entry $a_{i,i}$, its sign needs to be opposite of that from S^-, in order to preserve the diagonal dominance of the block-matrix. If the same sign (negative on the RHS of the equation) is used, problems regarding the boundedness of the always positive variables emerge (which destabilises the convergence of the solution), hence lower under–relaxation factors need to be used which directly negates potential benefits of the implicit cross-coupling. Therefore, negative signs of the S^* term should be avoided at all cost.

3.4 Linearisation and Implementation of the Two-Equation Models

In this section the derived guidelines for the linearisation and proper net source treatment of implicitly coupled equations are carried out on the incompressible $k - \varepsilon$ and $k - \omega \, SST$ turbulence models. Furthermore, implementation of the implicitly coupled turbulence equations in the block-matrix framework is presented.

3.4.1 Linearisation and Implementation of the $k - \varepsilon$ Turbulence Model in the Block-Matrix Framework

Prior to the implementation of the $k - \varepsilon$ turbulence model in the block-matrix framework, some manipulations of Equations (2.3.1) and (2.3.1) and linearisation of the corresponding net source terms are necessary.

If S_k is the (net source term) RHS of Equation (2.3.1) for k, in the current formulation of the $k - \varepsilon$ turbulence model, S_k is equal to:

$$S_k = G - \varepsilon. \qquad (3.4.1)$$

The linearisation of the S_k with respect to both variables yields:

$$S_k^n \approx S_k^o + \left(\frac{\partial S_k}{\partial k} \right)^o (k^n - k^o) + \left(\frac{\partial S_k}{\partial \varepsilon} \right)^o (\varepsilon^n - \varepsilon^o). \qquad (3.4.2)$$

and division of the linearisation products in appropriate groups (see Section 3.3) is:

$$S_k^n = S_k^+ + S_k^* \varepsilon^n + S_k^- k^n. \tag{3.4.3}$$

This gives the corresponding terms: $S_k^* = 0$, $S_k^- = 0$ and $S_k^n = S_k^+$. Therefore, the current formulation of Equation (2.3.1) is not suitable for implicit coupling. In order to model the cross-coupling in a numerically beneficial way, the sink term is substituted with [27, 28, 29]:

$$-\varepsilon = -C_\mu \frac{k^2}{\nu_t}. \tag{3.4.4}$$

Also, the production term G is substituted with Equation (2.3.6) where ν_t is expressed as in Equation (2.3.5):

$$G = 2C_\mu \left| \frac{1}{2} \left(\nabla \overline{\mathbf{u}} + (\nabla \overline{\mathbf{u}})^T \right) \right|^2 \frac{k^2}{\varepsilon}. \tag{3.4.5}$$

After the substitutions, the new formulation of the k equation has the following form:

$$\frac{\partial k}{\partial t} + \nabla \cdot (\overline{\mathbf{u}} k) - k \nabla \cdot \overline{\mathbf{u}} - \nabla \cdot (\Gamma_{k,eff} \nabla k) = 2C_\mu \left| \frac{1}{2} \left(\nabla \overline{\mathbf{u}} + (\nabla \overline{\mathbf{u}})^T \right) \right|^2 \frac{k^2}{\varepsilon} - C_\mu \frac{k^2}{\nu_t}. \tag{3.4.6}$$

Once again, the linearisation of the new S_k (with respect to both variables) is performed. For clarity, the linearisation is performed one term at a time. Moreover the linearisation products which have a contribution to the implicit cross-coupling source S_k^* are coloured blue and products which have a contribution to the implicit sink S_k^- are coloured red:

$$C_\mu^* = 2C_\mu \left| \frac{1}{2} \left(\nabla \overline{\mathbf{u}} + (\nabla \overline{\mathbf{u}})^T \right) \right|^2, \tag{3.4.7}$$

$$\left(C_\mu^* \frac{k^2}{\varepsilon} \right)^n \approx \left(C_\mu^* \frac{k^2}{\varepsilon} \right)^o + \left(\frac{\partial \left(C_\mu^* \frac{k^2}{\varepsilon} \right)}{\partial k} \right)^o (k^n - k^o) + \left(\frac{\partial \left(C_\mu^* \frac{k^2}{\varepsilon} \right)}{\partial \varepsilon} \right)^o (\varepsilon^n - \varepsilon^o), \tag{3.4.8}$$

$$\begin{aligned} \left(C_\mu^* \frac{k^2}{\varepsilon} \right)^n &= C_\mu^* \frac{(k^o)^2}{\varepsilon^o} + 2C_\mu^* \frac{k^o}{\varepsilon^o} (k^n - k^o) - C_\mu^* \frac{(k^o)^2}{(\varepsilon^o)^2} (\varepsilon^n - \varepsilon^o), \\ &= 2C_\mu^* \frac{k^o}{\varepsilon^o} k^n - C_\mu^* \left(\frac{k^o}{\varepsilon^o} \right)^2 \varepsilon^n, \end{aligned} \tag{3.4.9}$$

$$\left(-C_\mu \frac{k^2}{\nu_t} \right)^n \approx \left(-C_\mu \frac{k^2}{\nu_t} \right)^o + \left(\frac{\partial \left(-C_\mu \frac{k^2}{\nu_t} \right)}{\partial k} \right)^o (k^n - k^o), \tag{3.4.10}$$

$$
\begin{aligned}
\left(-C_\mu \frac{k^2}{\nu_t}\right)^n &= -C_\mu \frac{(k^o)^2}{\nu_t} - 2C_\mu \frac{k^o}{\nu_t}(k^n - k^o), \\
&= C_\mu \frac{(k^o)^2}{\nu_t} - 2C_\mu \frac{k^o}{\nu_t} k^n, \\
&= C_\mu \frac{(k^o)^2}{\nu_t} - 2C_\mu \frac{k^o}{\nu_t} k^n.
\end{aligned}
\tag{3.4.11}
$$

Although, the substitutions do not give a suitable implicit cross-coupling term, an implicit sink term is provided:

$$
\begin{aligned}
\frac{\partial k}{\partial t} + \nabla \cdot (\overline{\mathbf{u}}k) - k\nabla \cdot \overline{\mathbf{u}} - \nabla \cdot (\Gamma_{k,eff} \nabla k) = \\
2C_k^* \frac{k^o}{\varepsilon^o} k^n - C_k^* \left(\frac{k^o}{\varepsilon^o}\right)^2 \varepsilon^n + C_\mu \frac{(k^o)^2}{\nu_t} - 2C_\mu \frac{k^o}{\nu_t} k^n.
\end{aligned}
\tag{3.4.12}
$$

The following form of the k equation for the $k - \varepsilon$ turbulence model is reformulated as follows:

$$
\frac{\partial k}{\partial t} + \nabla \cdot (\overline{\mathbf{u}}k) - k\nabla \cdot \overline{\mathbf{u}} - \nabla \cdot (\Gamma_{k,eff} \nabla k) = G + C_\mu \frac{(k^o)^2}{\nu_t} - 2C_\mu \frac{k^o}{\nu_t} k^n.
\tag{3.4.13}
$$

After the reformulation of the k equation, the ε equation is investigated. S_ε is the (net source term) RHS of Equation (2.3.3). Linearisation of the S_ε in respect with both variables is performed according to:

$$
S_\varepsilon^n \approx S_\varepsilon^o + \left(\frac{\partial S_\varepsilon}{\partial k}\right)^o (k^n - k^o) + \left(\frac{\partial S_\varepsilon}{\partial \varepsilon}\right)^o (\varepsilon^n - \varepsilon^o).
\tag{3.4.14}
$$

Again, the linearisation products are divided into appropriate groups (see Section 3.3):

$$
S_\varepsilon^n = S_\varepsilon^+ + S_\varepsilon^* k^n + S_\varepsilon^- \varepsilon^n.
\tag{3.4.15}
$$

The linearisation is performed one term at a time and the linearisation products which have a contribution to the implicit cross-coupling source S_ε^* are coloured blue and products which have a contribution to the implicit sink S_ε^- are coloured red:

$$
\left(C_1 \frac{\varepsilon}{k} G\right)^n \approx \left(C_1 \frac{\varepsilon}{k} G\right)^o + \left(\frac{\partial \left(C_1 \frac{\varepsilon}{k} G\right)}{\partial k}\right)^o (k^n - k^o) + \left(\frac{\partial \left(C_1 \frac{\varepsilon}{k} G\right)}{\partial \varepsilon}\right)^o (\varepsilon^n - \varepsilon^o), \tag{3.4.16}
$$

$$
\begin{aligned}
\left(C_1 \frac{\varepsilon}{k} G\right)^n &= C_1 \frac{\varepsilon^o}{k^o} G - C_1 \frac{\varepsilon^o}{(k^o)^2} G(k^n - k^o) + C_1 \frac{1}{k^o} G(\varepsilon^n - \varepsilon^o), \\
&= C_1 \frac{\varepsilon^o}{k^o} G - C_1 \frac{\varepsilon^o}{(k^o)^2} G k^n + C_1 \frac{1}{k^o} G \varepsilon^n,
\end{aligned}
\tag{3.4.17}
$$

$$\left(-C_2\frac{\varepsilon^2}{k}\right)^n \approx \left(-C_2\frac{\varepsilon^2}{k}\right)^o + \left(\frac{\partial\left(-C_2\frac{\varepsilon^2}{k}\right)}{\partial k}\right)^o (k^n - k^o) + \left(\frac{\partial\left(-C_2\frac{\varepsilon^2}{k}\right)}{\partial\varepsilon}\right)^o (\varepsilon^n - \varepsilon^o),$$

$$(3.4.18)$$

$$\left(-C_2\frac{\varepsilon^2}{k}\right)^n = -C_2\frac{(\varepsilon^o)^2}{k^o} + C_2\frac{(\varepsilon^o)^2}{(k^o)^2}(k^n - k^o) - 2C_2\frac{\varepsilon^o}{k^o}(\varepsilon^n - \varepsilon^o),$$

$$= C_2\left(\frac{\varepsilon^o}{k^o}\right)^2 k^n - 2C_2\frac{\varepsilon^o}{k^o}\varepsilon^n, \qquad (3.4.19)$$

$$= \textcolor{red}{C_2\left(\frac{\varepsilon^o}{k^o}\right)^2 k^n} \textcolor{blue}{-2C_2\frac{\varepsilon^o}{k^o}\varepsilon^n}.$$

After the linearisation and substitution, the ε equation has the following form:

$$\frac{\partial\varepsilon}{\partial t} + \nabla{\cdot}(\overline{\mathbf{u}}\varepsilon) - \varepsilon\nabla{\cdot}\overline{\mathbf{u}} - \nabla{\cdot}(\Gamma_{\varepsilon,eff}\nabla\varepsilon) =$$
$$C_1\frac{\varepsilon^o}{k^o}G - C_1\frac{\varepsilon^o}{(k^o)^2}Gk^n + C_1\frac{1}{k^o}G\varepsilon^n + \textcolor{red}{C_2\left(\frac{\varepsilon^o}{k^o}\right)^2 k^n} \textcolor{blue}{-2C_2\frac{\varepsilon^o}{k^o}\varepsilon^n}. \qquad (3.4.20)$$

The ε equation for the $k-\varepsilon$ turbulence model is implemented as:

$$\frac{\partial\varepsilon}{\partial t} + \nabla{\cdot}(\overline{\mathbf{u}}\varepsilon) - \varepsilon\nabla{\cdot}\overline{\mathbf{u}} - \nabla{\cdot}(\Gamma_{\varepsilon,eff}\nabla\varepsilon) = C_1\frac{\varepsilon^o}{k^o}G + \textcolor{red}{C_2\left(\frac{\varepsilon^o}{k^o}\right)^2 k^n} \textcolor{blue}{-2C_2\frac{\varepsilon^o}{k^o}\varepsilon^n}. \qquad (3.4.21)$$

Additionally, it is important to emphasize that the cross-coupling coefficients S_k^* and S_ε^* need to be eliminated from the block-system in the near-wall cells.

In foam-extend, implementation of $k-\varepsilon$ turbulence in the block-matrix framework is named the `coupledKEpsilon` model.

3.4.2   Linearisation and Implementation of the $k-\omega\,SST$ Turbulence Model in the Block-Matrix Framework

Prior to the implementation of the $k-\omega\,SST$ turbulence model in the block-matrix framework, linearisation of the net source terms in both equations is necessary.

S_k is the (net source term) RHS of Equation (2.3.7) for k. Linearisation of the S_k with respect to both variables is performed according to:

$$S_k^n \approx S_k^o + \left(\frac{\partial S_k}{\partial k}\right)^o (k^n - k^o) + \left(\frac{\partial S_k}{\partial\omega}\right)^o (\omega^n - \omega^o). \qquad (3.4.22)$$

The linearisation products are divided into appropriate groups (see Section 3.3):

$$S_k^n = S_k^+ + S_k^* \omega^n + S_k^- k^n. \tag{3.4.23}$$

For clarity, the linearisation is performed one term at a time. Moreover, the linearisation products which have a contribution to the implicit cross-coupling source S_k^* are coloured blue and products which have a contribution to the implicit sink S_k^- are coloured red.

In Equation (2.3.7), a production limiter is used to prevent the build-up of turbulence in stagnation regions [12], consequently the source term in k equation is calculated as $\min(G, c_1 \beta^* k \omega)$. The linearisation of both arguments needs to be investigated.

G is calculated according to Equation (2.3.12):

$$G = \nu_t S_2, \tag{2.3.12}$$

where ν_t is defined by Equation (2.3.11):

$$\nu_t = \frac{a_1 k}{\max \left[a_1 \omega, b_1 F_{23} \sqrt{2} \left| \frac{1}{2} \left(\nabla \overline{\mathbf{u}} + (\nabla \overline{\mathbf{u}})^T \right) \right| \right]}. \tag{2.3.11}$$

In case when $G < c_1 \beta^* k \omega$ and $a_1 \omega > b_1 F_{23} \sqrt{2} \left| \frac{1}{2} \left(\nabla \overline{\mathbf{u}} + (\nabla \overline{\mathbf{u}})^T \right) \right|$ the source term in k equations is calculated as $S_2 \frac{k}{\omega}$.

$$\left(S_2 \frac{k}{\omega} \right)^n \approx \left(S_2 \frac{k}{\omega} \right)^o + \left(\frac{\partial \left(S_2 \frac{k}{\omega} \right)}{\partial k} \right)^o (k^n - k^o) + \left(\frac{\partial \left(S_2 \frac{k}{\omega} \right)}{\partial \omega} \right)^o (\omega^n - \omega^o), \tag{3.4.24}$$

$$\begin{aligned}
\left(S_2 \frac{k}{\omega} \right)^n &= S_2 \frac{k^o}{\omega^o} + \frac{S_2}{\omega^o} (k^n - k^o) - S_2 \frac{k^o}{(\omega^o)^2} (\omega^n - \omega^o), \\
&= S_2 \frac{k^o}{\omega^o} + \frac{S_2}{\omega^o} k^n + S_2 \frac{k^o}{(\omega^o)^2} \omega^n.
\end{aligned} \tag{3.4.25}$$

None of the linearisation products in Equation (3.4.25) is suitable for treatment as an implicit cross-coupling term nor implicit sink, as both potential candidates have unfavourable signs.

In case $G < c_1 \beta^* k \omega$ and $a_1 \omega < b_1 F_{23} \sqrt{2} \left| \frac{1}{2} \left(\nabla \overline{\mathbf{u}} + (\nabla \overline{\mathbf{u}})^T \right) \right|$ the source term in k equation is calculated as $\frac{a_1 k}{b_1 F_{23} \sqrt{2} \left| \frac{1}{2} \left(\nabla \overline{\mathbf{u}} + (\nabla \overline{\mathbf{u}})^T \right) \right|} S_2$. For easier manipulation of the expression the constant part (in context of k and ω) is substituted with C_G, $\frac{a_1 k}{b_1 F_{23} \sqrt{2} \left| \frac{1}{2} \left(\nabla \overline{\mathbf{u}} + (\nabla \overline{\mathbf{u}})^T \right) \right|} S_2 = C_G \frac{k}{F_{23}}$. If blending

term F_{23} is assumed to be equal to F_2 (rough wall flow treatment is neglected), then F_{23} is calculated according to:

$$F_{23} = F_2 = \tanh\left[(arg_2)^2\right],\tag{3.4.26}$$

where arg_2 is defined by Equation (2.3.21):

$$arg_2 = \min\left[\max\left(\frac{2\sqrt{k}}{\beta^*\omega y},\ \frac{500\nu}{y^2\omega}\right),\ 100\right].\tag{2.3.21}$$

In case $G < c_1\beta^* k\omega$, $a_1\omega < b_1 F_{23}\sqrt{2}\left|\frac{1}{2}\left(\nabla\overline{\mathbf{u}}+(\nabla\overline{\mathbf{u}})^T\right)\right|$ and $\frac{500\nu}{y^2\omega} < \frac{2\sqrt{k}}{\beta^*\omega y} < 100$ the source term in k equation is calculated as:

$$G^b = C_G\frac{k}{\tanh\left[\left(\frac{2\sqrt{k}}{\beta^*\omega y}\right)^2\right]},$$

$$\left(G^b\right)^n \approx \left(G^b\right)^o + \left(\frac{\partial\left(G^b\right)}{\partial k}\right)^o (k^n - k^o) + \left(\frac{\partial\left(G^b\right)}{\partial\omega}\right)^o (\omega^n - \omega^o),\tag{3.4.27}$$

$$\left(\frac{\partial\left(G^b\right)}{\partial k}\right)^o = C_G\coth\left(\frac{4k^o}{(\beta^*)^2(\omega^o)^2 y^2}\right) - \frac{4C_G k^o\operatorname{csch}^2\left(\frac{4k^o}{(\beta^*)^2(\omega^o)^2 y^2}\right)}{(\beta^*)^2(\omega^o)^2 y^2},$$

$$= S_2\frac{a_1}{b_1\sqrt{2}\left|\frac{1}{2}\left(\nabla\overline{\mathbf{u}}+(\nabla\overline{\mathbf{u}})^T\right)\right|}\coth\left(\frac{4k^o}{(\beta^*)^2(\omega^o)^2 y^2}\right)$$

$$- \frac{4S_2\frac{a_1}{b_1\sqrt{2}\left|\frac{1}{2}\left(\nabla\overline{\mathbf{u}}+(\nabla\overline{\mathbf{u}})^T\right)\right|}k^o\operatorname{csch}^2\left(\frac{4k^o}{(\beta^*)^2(\omega^o)^2 y^2}\right)}{(\beta^*)^2(\omega^o)^2 y^2},\tag{3.4.28}$$

$$\left(\frac{\partial\left(G^b\right)}{\partial\omega}\right)^o = \frac{8C_G(k^o)^2\operatorname{csch}^2\left(\frac{4k^o}{\beta^*(\omega^o)^2 y^2}\right)}{(\beta^*)^2(\omega^o)^3 y^2},$$

$$= \frac{8S_2\frac{a_1}{b_1\sqrt{2}\left|\frac{1}{2}\left(\nabla\overline{\mathbf{u}}+(\nabla\overline{\mathbf{u}})^T\right)\right|}(k^o)^2\operatorname{csch}^2\left(\frac{4k^o}{\beta^*(\omega^o)^2 y^2}\right)}{(\beta^*)^2(\omega^o)^3 y^2},\tag{3.4.29}$$

where coth() is the hyperbolic cotangent and csch() is the hyperbolic cosecant function. The linearisation products presented in Equations (3.4.28) and (3.4.29) could eventually even give terms which are suitable for treatment as implicit cross-coupling terms or implicit sinks but their implementation is inapplicable, therefore, blending functions will be treated as constants (and not as functions of k and ω) in the context of linearisation.

In case $G > c_1 \beta^* k \omega$ the source term in k equation is calculated as $c_1 \beta^* k \omega$:

$$(c_1 \beta^* k \omega)^n \approx (c_1 \beta^* k \omega)^o + \left(\frac{\partial (c_1 \beta^* k \omega)}{\partial k}\right)^o (k^n - k^o) + \left(\frac{\partial (c_1 \beta^* k \omega)}{\partial \omega}\right)^o (\omega^n - \omega^o),$$
$$(3.4.30)$$

$$\begin{aligned}
(c_1 \beta^* k \omega)^n &= c_1 \beta^* k^o \omega^o + c_1 \beta^* \omega^o (k^n - k^o) + c_1 \beta^* k^o (\omega^n - \omega^o), \\
&= -c_1 \beta^* k^o \omega^o + c_1 \beta^* \omega^o k^n + c_1 \beta^* k^o \omega^n, \\
&= -c_1 \beta^* k^o \omega^o + c_1 \beta^* \omega^o k^n {\color{blue}+ c_1 \beta^* k^o \omega^n}.
\end{aligned}$$
$$(3.4.31)$$

Equation (3.4.31) gives a suitable term for implicit cross-coupling, but it is only active when $c_1 \beta^* k \omega < G$:

$$(-\beta^* k \omega)^n \approx (-\beta^* k \omega)^o + \left(\frac{\partial (-\beta^* k \omega)}{\partial k}\right)^o (k^n - k^o) + \left(\frac{\partial (-\beta^* k \omega)}{\partial \omega}\right)^o (\omega^n - \omega^o),$$
$$(3.4.32)$$

$$\begin{aligned}
(-\beta^* k \omega)^n &= -\beta^* k^o \omega^o - \beta^* \omega^o (k^n - k^o) - \beta^* k^o (\omega^n - \omega^o), \\
&= \beta^* k^o \omega^o - \beta^* \omega^o k^n - \beta^* k^o \omega^n, \\
&= \beta^* k^o \omega^o {\color{red}- \beta^* \omega^o k^n} - \beta^* k^o \omega^n.
\end{aligned}$$
$$(3.4.33)$$

Equation (3.4.33), i.e. the linearisation of the sink term in k equation, gives a suitable implicit sink term but the cross-coupling term has the unfavourable sign for implicit treatment.

After the linearisation and substitution, the k equation has the following form:

$$\begin{aligned}
\frac{\partial k}{\partial t} + \nabla{\cdot}(\overline{\mathbf{u}} k) - k \nabla{\cdot}\overline{\mathbf{u}} - \nabla{\cdot}(\Gamma_{k,eff} \nabla k) = {}&\min\left(G, -c_1 \beta^* k^o \omega^o + c_1 \beta^* \omega^o k^n {\color{blue}+ c_1 \beta^* k^o \omega^n}\right) \\
&+ \beta^* k^o \omega^o {\color{red}- \beta^* \omega^o k^n} - \beta^* k^o \omega^n.
\end{aligned}$$
$$(3.4.34)$$

The k equation for the $k - \omega\,SST$ turbulence model is implemented as:

$$\frac{\partial k}{\partial t} + \nabla{\cdot}(\overline{\mathbf{u}} k) - k \nabla{\cdot}\overline{\mathbf{u}} - \nabla{\cdot}(\Gamma_{k,eff} \nabla k) = \min\left(G, {\color{blue}c_1 \beta^* k^o \omega^n}\right) {\color{red}- \beta^* \omega^o k^n}. \qquad (3.4.35)$$

After the implementation of the k equation, the ω equation is investigated. S_ω is the (net source term) RHS of Equation (2.3.9). Linearisation of the S_ω in respect with both variables is performed according to:

$$S_\omega^n \approx S_\omega^o + \left(\frac{\partial S_\omega}{\partial k}\right)^o (k^n - k^o) + \left(\frac{\partial S_\omega}{\partial \omega}\right)^o (\omega^n - \omega^o). \tag{3.4.36}$$

The linearisation products are divided into appropriate groups see (Section 3.3):

$$S_\omega^n = S_\omega^+ + S_\omega^* k^n + S_\omega^- \omega^n. \tag{3.4.37}$$

Again, the linearisation is performed one term at a time and the linearisation products which have a contribution to the implicit cross-coupling source S_ω^* are coloured blue products which have a contribution to the implicit sink S_ω^- are coloured red.

In case $S_2 > \frac{c_1}{a_1}\beta^*\omega \max\left(a_1\omega, b_1 F_{23}\sqrt{S_2}\right)$ and $a_1\omega > b_1 F_{23}\sqrt{S_2}$ the source term in ω equation is calculated as $\gamma c_1 \beta^* \omega^2$:

$$\left(\gamma c_1 \beta^* \omega^2\right)^n \approx \left(\gamma c_1 \beta^* \omega^2\right)^o + \left(\frac{\partial \left(\gamma c_1 \beta^* \omega^2\right)}{\partial \omega}\right)^o (\omega^n - \omega^o), \tag{3.4.38}$$

$$\begin{aligned}
\left(\gamma c_1 \beta^* \omega^2\right)^n &= \gamma c_1 \beta^* (\omega^o)^2 + 2\gamma c_1 \beta^* \omega^o (\omega^n - \omega^o), \\
&= -\gamma c_1 \beta^* (\omega^o)^2 + 2\gamma c_1 \beta^* \omega^o \omega^n.
\end{aligned} \tag{3.4.39}$$

Linearisation products in Equation (3.4.39) are not suitable for treatment as implicit cross-coupling term nor as implicit sink.

$$\left(-\beta\omega^2\right)^n \approx \left(-\beta\omega^2\right)^o + \left(\frac{\partial \left(-\beta\omega^2\right)}{\partial \omega}\right)^o (\omega^n - \omega^o), \tag{3.4.40}$$

$$\begin{aligned}
\left(-\beta\omega^2\right)^n &= -\beta (\omega^o)^2 - 2\beta\omega^o (\omega^n - \omega^o), \\
&= \beta (\omega^o)^2 - 2\beta\omega^o \omega^n, \\
&= \beta (\omega^o)^2 {\color{red}- 2\beta\omega^o \omega^n}.
\end{aligned} \tag{3.4.41}$$

Equation (3.4.41), the linearisation of the sink term in ω equation, gives a suitable implicit sink but the implicit cross-coupling is not present.

After the linearisation and substitution, the ω equation has the following form:

$$\begin{aligned}
\frac{\partial \omega}{\partial t} + \nabla_\bullet(\overline{\mathbf{u}}\omega) - \omega\nabla_\bullet\overline{\mathbf{u}} - \nabla_\bullet(\Gamma_{\omega,eff}\nabla\omega) = \\
\gamma\min\left[S_2, \frac{c_1}{a_1}\beta^*\omega^o \max\left(a_1\omega^o, b_1 F_{23}\sqrt{S_2}\right)\right] \\
+ \beta (\omega^o)^2 {\color{red}- 2\beta\omega^o \omega^n} + (1 - F_1)CD_{k\omega}.
\end{aligned} \tag{3.4.42}$$

Equation (3.4.41) does not have implicit cross-coupling terms, therefore modifications are introduced in order to obtain additional implicit cross-coupling of k and ω equations. The ω equation for the $k - \omega \, SST$ turbulence model is implemented as:

$$
\frac{\partial \omega}{\partial t} + \nabla\bullet(\overline{\mathbf{u}}\omega) - \omega\nabla\bullet\overline{\mathbf{u}} - \nabla\bullet(\Gamma_{\omega,eff}\nabla\omega) =
$$
$$
\gamma\min\left[S_2, \frac{c_1}{a_1}\beta^*\omega^o\max\left(a_1\omega^o, b_1F_{23}\sqrt{S_2}\right)\right] \qquad (3.4.43)
$$
$$
+ \beta\,(\omega^o)^2 - 2\beta\,\omega^o\,\omega^n + (1-F_1)\,CD_{k\omega}\,,
$$

where $(1-F_1)\,CD_{k\omega}$ term is defined as:

$$
(1-F_1)\,CD_{k\omega} =
\begin{cases}
(1-F_1)\,CD_{k\omega} = \frac{(1-F_1)CD_{k\omega}}{k^o}k^n & CD_{k\omega} > 0, \\[2mm]
(1-F_1)\,CD_{k\omega} = \frac{(1-F_1)CD_{k\omega}}{\omega^o}\omega^n & CD_{k\omega} < 0.
\end{cases}
\qquad (3.4.44)
$$

Additionally, it is important to emphasize that the cross-coupling coefficients S_k^* and S_ω^* need to be eliminated from the block-system in the cells adjacent to the wall, where wall functions are used.

In foam-extend, implementation of $k - \omega \, SST$ turbulence in the block-matrix framework is named `coupledKOmegaSST`.

3.4.3   Linearisation of the Wall Functions for $k - \varepsilon$ Turbulence Model

For evaluation of the implicit coupling potential of wall functions for $k - \varepsilon$ turbulence model, the linearisation is necessary.

As described in Section 2.4.1, for wall function cells the value ε is obtained by solving the algebraic Equation (2.4.2) and not the ε equation. The value of k is obtained from Equation (2.3.1), but the generation term G is modified according to Equation (2.4.3). Considering that $G_{vis} = 0$, only the expression for G_{log} is linearised:

$$
G_{log}^n \approx G_{log}^o + \left(\frac{\partial G_{log}}{\partial k}\right)^o (k^n - k^o)\,, \qquad (3.4.45)
$$

$$
\begin{aligned}
G_{log}^n &= \frac{((\nu_t + \nu)\,|\nabla\overline{\mathbf{u}}|)^2}{\kappa C_\mu^{1/4}\,(k^o)^{1/2}\,y} - \frac{1}{2}\frac{((\nu_t + \nu)\,|\nabla\overline{\mathbf{u}}|)^2}{\kappa C_\mu^{1/4}\,(k^o)^{3/2}\,y}(k^n - k^o)\,, \\[2mm]
&= \frac{3}{2}\frac{((\nu_t + \nu)\,|\nabla\overline{\mathbf{u}}|)^2}{\kappa C_\mu^{1/4}\,(k^o)^{1/2}\,y} - \frac{1}{2}\frac{((\nu_t + \nu)\,|\nabla\overline{\mathbf{u}}|)^2}{\kappa C_\mu^{1/4}\,(k^o)^{3/2}\,y}k^n\,.
\end{aligned}
\qquad (3.4.46)
$$

Since ε equation is not solved for wall function cells, the G term is only present in the k equation, therefore the Equation (3.4.46), in which G_{log} is a function only of k, does not represent a cross-coupling term, but it could be implemented as an implicit sink term because the coefficient of k^n is negative on the RHS of the k equation.

If ν_t in Equation (2.4.5) is substituted with Equation (2.3.5), G_{log} becomes a function of both k and ε:

$$
\begin{aligned}
G_{log} &= \frac{((\nu_t + \nu)\,|\nabla\overline{\mathbf{u}}|)^2}{\kappa C_\mu^{1/4} k^{1/2} y} = \frac{\left(\nu_t^2 + 2\nu_t\nu + \nu^2\right)|\nabla\overline{\mathbf{u}}|^2}{\kappa C_\mu^{1/4} k^{1/2} y}, \\[2mm]
&= \frac{|\nabla\overline{\mathbf{u}}|^2}{\kappa C_\mu^{1/4} k^{1/2} y}\left(\frac{C_\mu^2 k^4}{\varepsilon^2} + \frac{2C_\mu\nu k^2}{\varepsilon} + \nu^2\right), \\[2mm]
&= \frac{|\nabla\overline{\mathbf{u}}|^2}{\kappa C_\mu^{1/4} y}\left(\frac{C_\mu^2 k^{7/2}}{\varepsilon^2} + \frac{2C_\mu\nu k^{3/2}}{\varepsilon} + \frac{\nu^2}{k^{1/2}}\right),
\end{aligned}
\tag{3.4.47}
$$

and after linearisation as a multi-variable function, the expression has the following form:

$$
G_{log}^n \approx G_{log}^o + \left(\frac{\partial G_{log}}{\partial k}\right)^o (k^n - k^o) + \left(\frac{\partial G_{log}}{\partial \varepsilon}\right)^o (\varepsilon^n - \varepsilon^o),
\tag{3.4.48}
$$

$$
\begin{aligned}
G_{log}^n &= \frac{|\nabla\overline{\mathbf{u}}|^2}{\kappa C_\mu^{1/4} y}\left(\frac{C_\mu^2 (k^o)^{7/2}}{(\varepsilon^o)^2} + \frac{2C_\mu\nu (k^o)^{3/2}}{\varepsilon^o} + \frac{\nu^2}{(k^o)^{1/2}}\right) \\[2mm]
&+ \frac{|\nabla\overline{\mathbf{u}}|^2}{\kappa C_\mu^{1/4} y}\left(\frac{7}{2}\frac{C_\mu^2 (k^o)^{5/2}}{(\varepsilon^o)^2} + \frac{3C_\mu\nu (k^o)^{1/2}}{\varepsilon^o} - \frac{1}{2}\frac{\nu^2}{(k^o)^{3/2}}\right)(k^n - k^o) \\[2mm]
&+ \frac{|\nabla\overline{\mathbf{u}}|^2}{\kappa C_\mu^{1/4} y}\left(-\frac{2C_\mu^2 (k^o)^{7/2}}{(\varepsilon^o)^3} - \frac{2C_\mu\nu (k^o)^{3/2}}{(\varepsilon^o)^2}\right)(\varepsilon^n - \varepsilon^o), \\[2mm]
&= \frac{|\nabla\overline{\mathbf{u}}|^2}{\kappa C_\mu^{1/4} y}\left(-\frac{1}{2}\frac{C_\mu^2 (k^o)^{7/2}}{(\varepsilon^o)^2} + \frac{C_\mu\nu (k^o)^{3/2}}{\varepsilon^o} + \frac{3}{2}\frac{\nu^2}{(k^o)^{1/2}}\right) \\[2mm]
&+ \frac{|\nabla\overline{\mathbf{u}}|^2}{\kappa C_\mu^{1/4} y}\left(\frac{7}{2}\frac{C_\mu^2 (k^o)^{5/2}}{(\varepsilon^o)^2} + \frac{3C_\mu\nu (k^o)^{1/2}}{\varepsilon^o} - \frac{1}{2}\frac{\nu^2}{(k^o)^{3/2}}\right)k^n \\[2mm]
&- \frac{|\nabla\overline{\mathbf{u}}|^2}{\kappa C_\mu^{1/4} y}\left(\frac{2C_\mu^2 (k^o)^{7/2}}{(\varepsilon^o)^3} + \frac{2C_\mu\nu (k^o)^{3/2}}{(\varepsilon^o)^2}\right)\varepsilon^n.
\end{aligned}
\tag{3.4.49}
$$

According to the guidelines for proper source treatment presented in Section 3.3, the potential cross-coupling term with implicit ε^n has the unfavourable sign for implementation as an implicit cross-coupling term.

Moreover, the linearisation and implicit cross-coupling potential of Equation (2.4.2) is in-

vestigated:

$$\varepsilon^n \approx \varepsilon^o + \left(\frac{\partial \varepsilon}{\partial k}\right)^o (k^n - k^o), \tag{3.4.50}$$

$$
\begin{aligned}
\varepsilon^n &= \frac{C_\mu^{3/4}(k^o)^{3/2}}{\kappa y} + \frac{3}{2}\frac{C_\mu^{3/4}(k^o)^{1/2}}{\kappa y}(k^n - k^o), \\
&= -\frac{1}{2}\frac{C_\mu^{3/4}(k^o)^{3/2}}{\kappa y} + \frac{3}{2}\frac{C_\mu^{3/4}(k^o)^{1/2}}{\kappa y}k^n.
\end{aligned}
\tag{3.4.51}
$$

Equation (3.4.51) is suitable for implicit cross-coupling, because the coefficient of the k^n term is positive on the RHS.

Overall implicit cross-coupling potential of the standard wall functions for the $k - \varepsilon$ turbulence model is partial. Linearisation of the modified production term G for the wall function cell does not give adequate terms for implicit treatment but the linearisation of the algebraic expression, which replaces the ε equation in the wall function cells, gives a suitable implicit cross-coupling term. This thesis does not present implementation of the implicit wall functions for the $k - \varepsilon$ turbulence model.

3.4.4 Linearisation of the Wall Functions for $k - \omega\, SST$ Turbulence Model

For evaluation of the implicit coupling potential of wall functions for $k - \omega\, SST$ turbulence model, the linearisation is necessary.

As described in Section 2.4.2, for wall function cells the value ω is obtained by solving the algebraic Equation (2.4.7) and not the ω equation. The value of k is obtained from Equation (2.3.7), but the generation term G is modified according to Equation (2.4.10). Considering that $G_{vis} = 0$, only the expression for G_{log} is linearised:

$$G_{log}^n \approx G_{log}^o + \left(\frac{\partial G_{log}}{\partial k}\right)^o (k^n - k^o), \tag{3.4.52}$$

$$
\begin{aligned}
G_{log}^n &= \frac{C_\mu^{1/4}(k^o)^{1/2}(\nu_t + \nu)|\nabla\bar{\mathbf{u}}|}{\kappa y} + \frac{C_\mu^{1/4}(\nu_t + \nu)|\nabla\bar{\mathbf{u}}|}{2\kappa y(k^o)^{1/2}}(k^n - k^o), \\
&= \frac{C_\mu^{1/4}(k^o)^{1/2}(\nu_t + \nu)|\nabla\bar{\mathbf{u}}|}{2\kappa y} + \frac{C_\mu^{1/4}(\nu_t + \nu)|\nabla\bar{\mathbf{u}}|}{2\kappa y(k^o)^{1/2}}k^n.
\end{aligned}
\tag{3.4.53}
$$

The production term G is only present in the k equation, therefore the Equation (3.4.53), in which G_{log} is function only of k, does not represent a cross-coupling term nor could it be

implemented as an implicit sink term because the coefficient of k^n is positive on the RHS of Equation (2.3.1).

If ν_t in Equation (2.4.12) is substituted with Equation (2.3.11), G_{log} becomes function of both k and ω, but only in case when $a_1 \omega > b_1 F_{23} \sqrt{2} \left| \frac{1}{2} \left(\nabla \overline{\mathbf{u}} + (\nabla \overline{\mathbf{u}})^T \right) \right|$. Since the other cases do not contain ω, because the blending functions are treated as constants in context of linearisation (see Section 3.4.2).

$$
\begin{aligned}
G_{log} &= \frac{C_\mu^{1/4} |\nabla \overline{\mathbf{u}}|}{\kappa y} k^{1/2} \left(\nu_t + \nu \right) \\
&= \frac{C_\mu^{1/4} |\nabla \overline{\mathbf{u}}|}{\kappa y} k^{1/2} \left(\frac{k}{\omega} + \nu \right) \\
&= \frac{C_\mu^{1/4} |\nabla \overline{\mathbf{u}}|}{\kappa y} \left(\frac{k^{3/2}}{\omega} + \nu k^{1/2} \right).
\end{aligned}
\tag{3.4.54}
$$

After linearisation as a multi variable function, the expression has the following form:

$$
G_{log}^n \approx G_{log}^o + \left(\frac{\partial G_{log}}{\partial k} \right)^o (k^n - k^o) + \left(\frac{\partial G_{log}}{\partial \omega} \right)^o (\omega^n - \omega^o),
\tag{3.4.55}
$$

$$
\begin{aligned}
G_{log}^n &= \frac{C_\mu^{1/4} |\nabla \overline{\mathbf{u}}|}{\kappa y} \left(\frac{(k^o)^{3/2}}{\omega^o} + \nu (k^o)^{1/2} \right) \\
&\quad + \frac{C_\mu^{1/4} |\nabla \overline{\mathbf{u}}|}{\kappa y} \left(\frac{3}{2} \frac{(k^o)^{1/2}}{\omega^o} + \frac{1}{2} \frac{\nu}{(k^o)^{1/2}} \right) (k^n - k^o) \\
&\quad + \frac{C_\mu^{1/4} |\nabla \overline{\mathbf{u}}|}{\kappa y} \left(-\frac{(k^o)^{3/2}}{(\omega^o)^2} \right) (\omega^n - \omega^o), \\
&= \frac{C_\mu^{1/4} |\nabla \overline{\mathbf{u}}|}{\kappa y} \left(\frac{1}{2} \frac{(k^o)^{3/2}}{\omega^o} + \frac{1}{2} \nu (k^o)^{1/2} \right) \\
&\quad + \frac{C_\mu^{1/4} |\nabla \overline{\mathbf{u}}|}{\kappa y} \left(\frac{3}{2} \frac{(k^o)^{1/2}}{\omega^o} + \frac{1}{2} \frac{\nu}{(k^o)^{1/2}} \right) k^n \\
&\quad - \frac{C_\mu^{1/4} |\nabla \overline{\mathbf{u}}|}{\kappa y} \left(\frac{(k^o)^{3/2}}{(\omega^o)^2} \right) \omega^n.
\end{aligned}
\tag{3.4.56}
$$

According to the guidelines for proper source treatment presented in Section 3.3, both terms with implicit values, k^n and ω^n, in Equation (3.4.56) have unfavourable signs for implementation as implicit sink and implicit cross-coupling terms.

Furthermore, the linearisation and implicit cross-coupling potential of Equation (2.4.7) is

investigated:

$$\omega^n \approx \omega^o + \left(\frac{\partial \omega}{\partial k}\right)^o (k^n - k^o),$$ (3.4.57)

$$
\omega^n = \sqrt{\left(\frac{6\nu}{\beta_1 y^2}\right)^2 + \left(\frac{(k^o)^{1/2}}{\kappa C_\mu^{1/4} y}\right)^2}
$$
$$
+ \frac{1}{2C_\mu^{1/2}\kappa^2 y^2 \sqrt{\dfrac{36\nu^2}{\beta_1^2 y^4} + \dfrac{k^o}{C_\mu^{1/2}\kappa^2 y^2}}} (k^n - k^o),
$$
$$
= \sqrt{\left(\frac{6\nu}{\beta_1 y^2}\right)^2 + \left(\frac{(k^o)^{1/2}}{\kappa C_\mu^{1/4} y}\right)^2}
$$
$$
- \frac{k^o}{2C_\mu^{1/2}\kappa^2 y^2 \sqrt{\dfrac{36\nu^2}{\beta_1^2 y^4} + \dfrac{k^o}{C_\mu^{1/2}\kappa^2 y^2}}}
$$
$$
+ \frac{1}{2C_\mu^{1/2}\kappa^2 y^2 \sqrt{\dfrac{36\nu^2}{\beta_1^2 y^4} + \dfrac{k^o}{C_\mu^{1/2}\kappa^2 y^2}}} k^n.
$$ (3.4.58)

Equation (3.4.58) is suitable for implicit cross-coupling, because the coefficient of the k^n term is positive on the RHS.

Overall implicit cross-coupling potential of the standard wall functions for the $k - \omega SST$ turbulence model is partial. Linearisation of the modified production term G for the wall function cell does not give adequate terms for implicit treatment but the linearisation of the algebraic expression, which replaces the ω equation in the wall function cells, gives a suitable implicit cross-coupling term. This thesis does not present implementation of the implicit wall functions for the $k - \omega SST$ turbulence model.

3.5 Closure

In this chapter, structure of the block-system was presented, furthermore problems regarding the linearisation, stability and boundedness of the model were investigated. Also, the implementation of $k - \varepsilon$ (`coupledKEpsilon`) and $k - \omega SST$ (`coupledKOmegaSST`) turbulence models in the block-matrix framework was described. At the end of the chapter, suggested linearisation of the wall functions for both models were given.

Chapter 4

Validation of Implemented Turbulence Models

In the previous chapter, linearisation and implementation of the $k - \varepsilon$ (`coupledKEpsilon`) and $k - \omega\,SST$ (`coupledKOmegaSST`) turbulence models in the block-matrix framework was described. In this chapter, the validation of implemented `coupledKOmegaSST` and `coupledKEpsilon` turbulence models shall be presented.

In the first section, a separated flow past a NACA 4412 airfoil at maximum lift is investigated. In this case a low Reynolds turbulence modelling approach is adopted, therefore only the `coupledKOmegaSST` is taken into account.

In the second section, an incompressible turbulent flow over a backward facing step is investigated. In this case a high Reynolds turbulence modelling approach is adopted, therefore both the `coupledKOmegaSST` and the `coupledKEpsilon` are taken into account.

4.1   NACA 4412

The first test case for the validation of the implemented `coupledKOmegaSST` is the separated flow past a NACA 4412 airfoil at maximum lift. The experimental data is available at the *NASA Turbulence Modeling Resource* web-page [30] but the particular data originates from the experiments performed by Coles and Wadcock [31]. Table 4.1.1 presents the selected: Reynolds number (for airfoil chord length), angle of incidence, freestream velocity value, airfoil chord length and the molecular kinematic viscosity.

Re_c $[-]$	α $[°]$	U_{inf} $[m/s]$	c $[m]$	ν $[m^2/s]$
1.52×10^6	13.87	27.13	0.9012	1.61×10^{-5}

Table 4.1.1: Geometry and flow parameters for the NACA 4412 case according to [31, 30].

4.1.1 Case set-up

The grid used in the simulation is available at the *CFD support* page [32] and was scaled to the chosen chord length. The domain size and the grid density are shown in Figure 4.1.1. The simulation is set up as a steady-state two-dimensional simulation, however OpenFOAM always operates in three dimensions, therefore, an `empty` boundary condition needs to be specified on the boundaries normal to the third dimension. In this thesis, these boundaries (patches) are named *FrontAndBack*. The names of the solution domain boundaries are shown in Figure 4.1.2.

The presented problem was solved using the `pUCoupledFoam` [33] solver and the `coupledKOmegaSST` turbulence model with the following boundary conditions and numerical schemes.
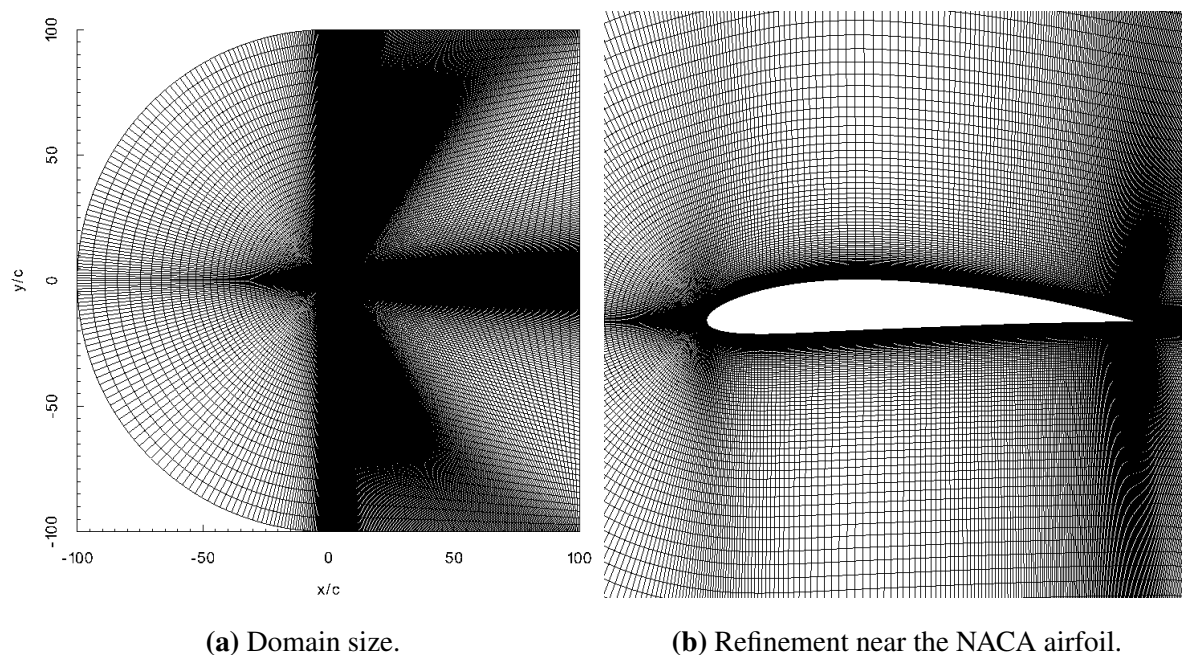

(a) Domain size.   (b) Refinement near the NACA airfoil.

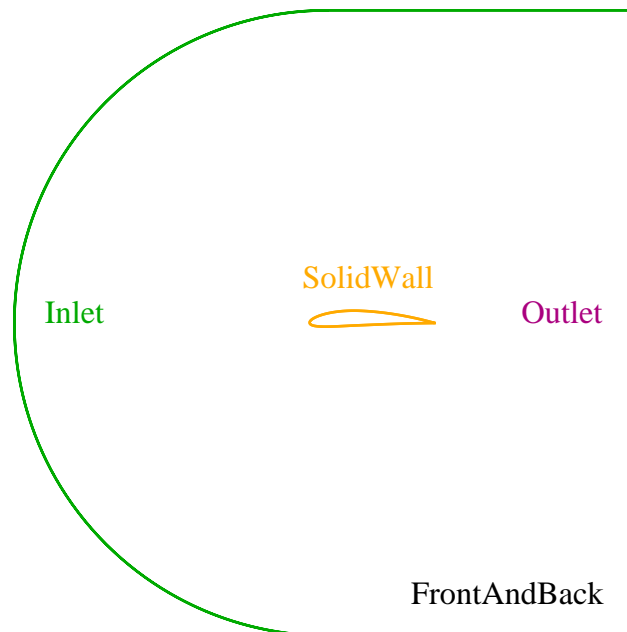**Figure 4.1.1:** NACA 4412: Computational domain.

Figure 4.1.2: NACA 4412: Patch names.

Boundary and initial conditions

- **Inlet**

    - *Velocity*: `inletOutlet` with `inletValue` `uniform (26.34 6.50 0)`

    - *Pressure*: `zeroGradient`

    - *Turbulence kinetic energy*: `inletOutlet` with `inletValue` `uniform 0.00082`

    - *Turbulence dissipation*: `inletOutlet` with `inletValue` `uniform 33.81`

- **Outlet**

    - *Velocity*: `inletOutlet` with `inletValue` `uniform (0 0 0)`

    - *Pressure*: `fixedValue` with `value` `uniform 0`

    - *Turbulence kinetic energy*: `inletOutlet` with `inletValue` `uniform 0.00082`

    - *Turbulence dissipation*: `inletOutlet` with `inletValue` `uniform 33.81`

- **SolidWall**

    – *Velocity*: `fixedValue` with value `uniform (0 0 0)`

    – *Pressure*: `zeroGradient`

    – *Turbulence kinetic energy*: `kqRWallFunction`

    – *Turbulence dissipation*: `omegaWallFunction`

- **FrontAndBack**: type `empty` for all fields

- **Initialisation**

    – *Velocity*: `uniform (26.34 6.50 0)`

    – *Pressure*: `uniform 0`

    – *Turbulence kinetic energy*: `uniform 0.00082`

    – *Turbulence dissipation*: `uniform 33.81`

The selected numerical schemes are shown in Table 4.1.2.

Detailed overview of the basic numerical schemes is presented in [34] and a comprehensive analysis of the Gamma differencing scheme is presented by Jasak et al. [35].

Additionally, simulations were performed using the following combinations of solvers and turbulence models:

- `pUCoupledFoam` and `coupledkOmegaSST`,

- `pUCoupledFoam` and `kOmegaSST`,

- `simpleFoam` and `coupledKOmegaSST`,

- `simpleFoam` and `kOmegaSST`,

and the results were identical to those shown below.

Time schemes	
default	steadyState

Gradient schemes	
default	Gauss linear

Divergence schemes	
default	Gauss linear
div(phi,U)	Gauss GammaV 1
div(phi,k)	Gauss upwind
div(phi,omega)	Gauss upwind

Laplacian schemes	
default	Gauss midPoint limited 0.5

Interpolation schemes	
default	linear

Surface normal gradient schemes	
default	limited 0.5

Table 4.1.2: NACA 4412: Numerical schemes.

4.1.2 Results

Figure 4.1.3 illustrates the calculated y^+ distribution over of the NACA airfoil, where the values are considerably below 5, hence the assumption of the low Reynolds turbulence modelling approach is applicable.
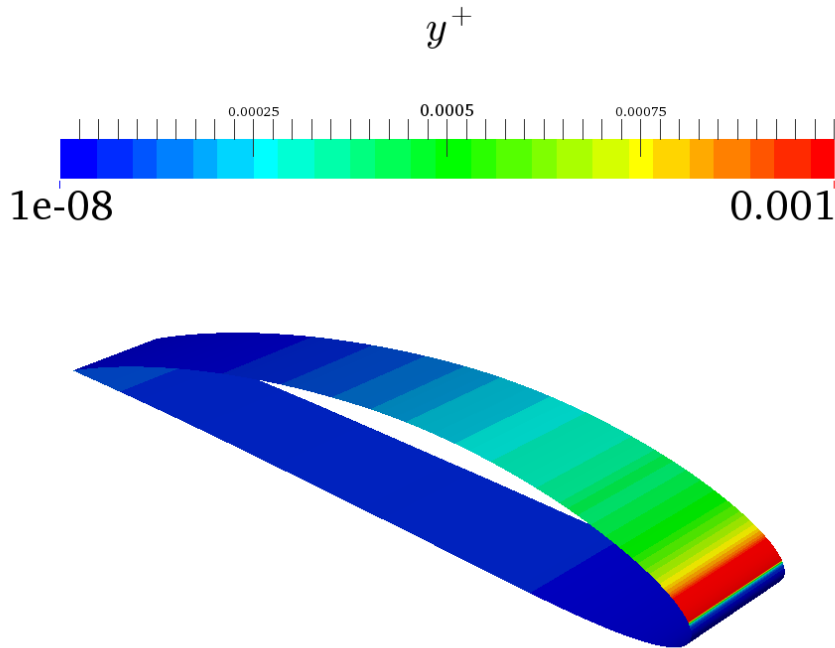

Figure 4.1.3: NACA 4412: Normalised distance to the wall.

The plot of the normalised velocity magnitude is shown in Figure 4.1.4, where the normalisation is carried out with respect to the freestream velocity value U_{inf}. The pressure coefficient plot, which is calculated according to Equation (4.1.1), around the NACA 4412 airfoil is shown in Figure 4.1.5.

$$C_p = \frac{p - p_{inf}}{\frac{1}{2} U_{inf}^2}.$$ (4.1.1)

In Equation (4.1.1), the freestream kinematic pressure value p_{inf} is defined by the pressure boundary condition at the *Outlet* patch.
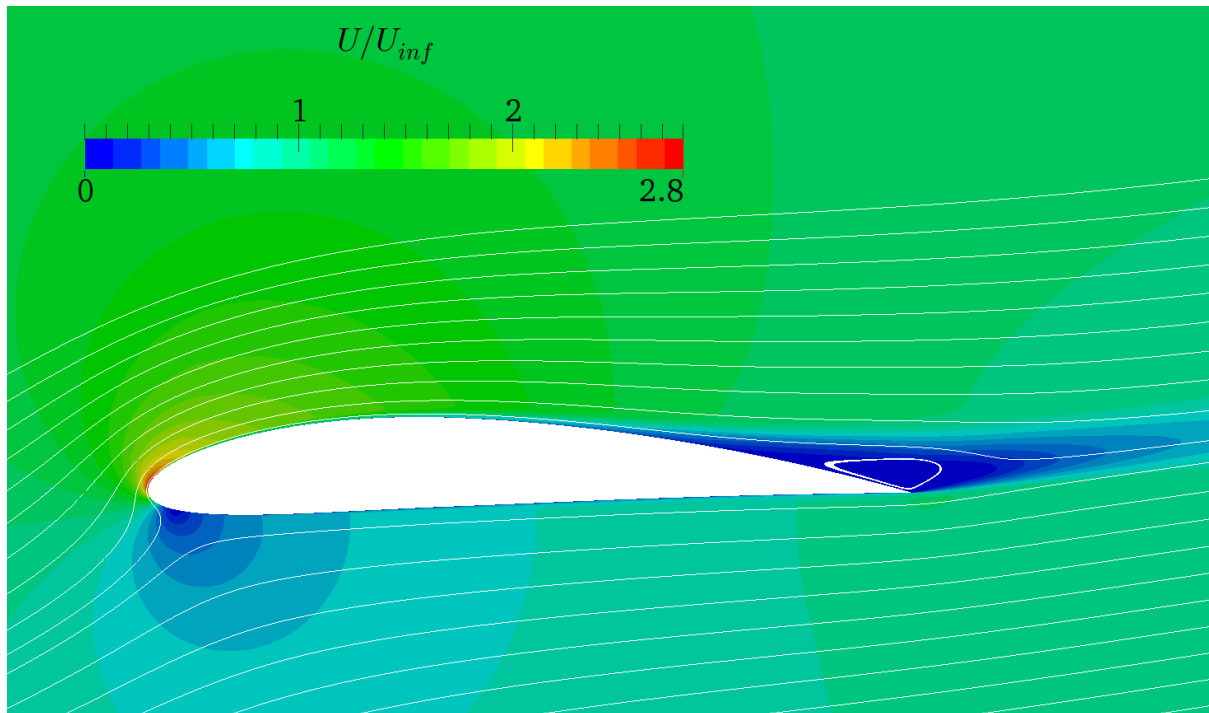
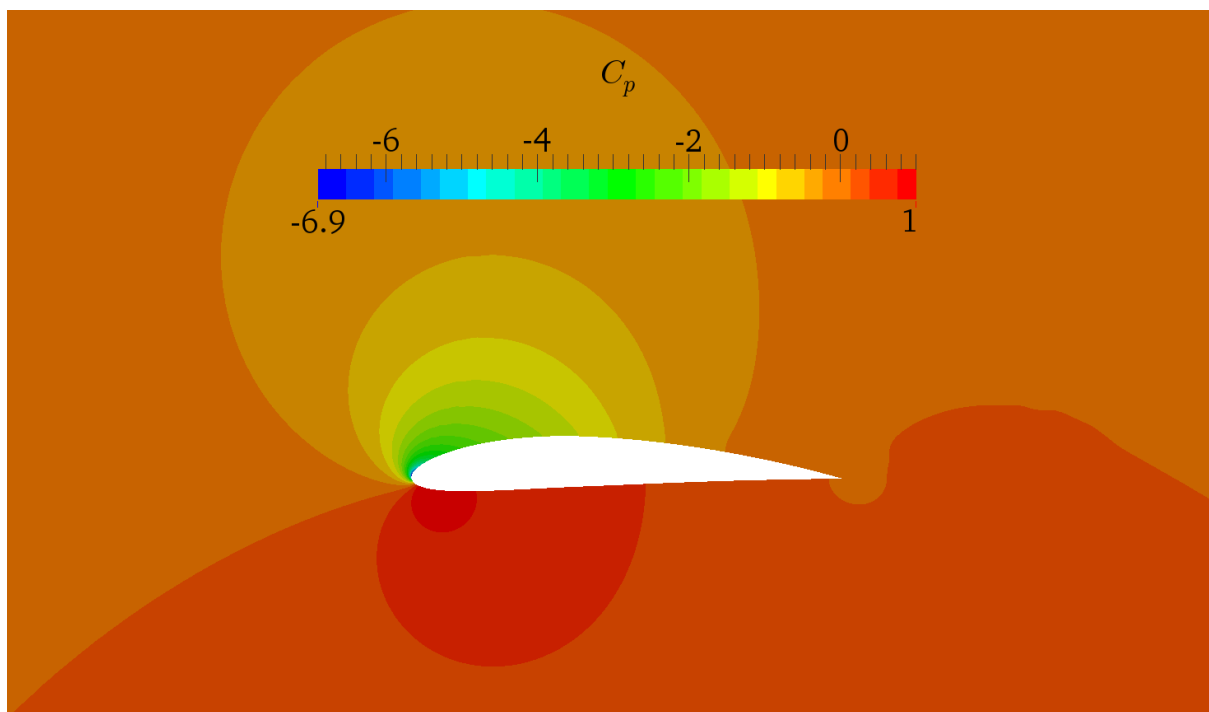**Figure 4.1.4:** NACA 4412: Normalised velocity magnitude plot.

Figure 4.1.5: NACA 4412: Pressure coefficient plot.

The experimental results from [31] are nondimensionalised with respect to a non-traditional velocity value U_{ref}, at a location only about one chord length below and behind the airfoil, which is different from a traditional freestream value. In order to make the traditionally normalised velocity CFD results comparable to the normalised experimental data, the CFD data needs to be divided by 0.93. In case of the chordwise velocity normalisation, the correction looks like:

$$\frac{u}{U_{ref}} = \frac{u}{0.93\,U_{inf}}.$$ (4.1.2)

In Figure 4.1.6 a comparison of constant normalised chordwise velocity contour lines is shown, where the contour lines from the CFD simulation (coloured red) were drawn over the figure from [31].
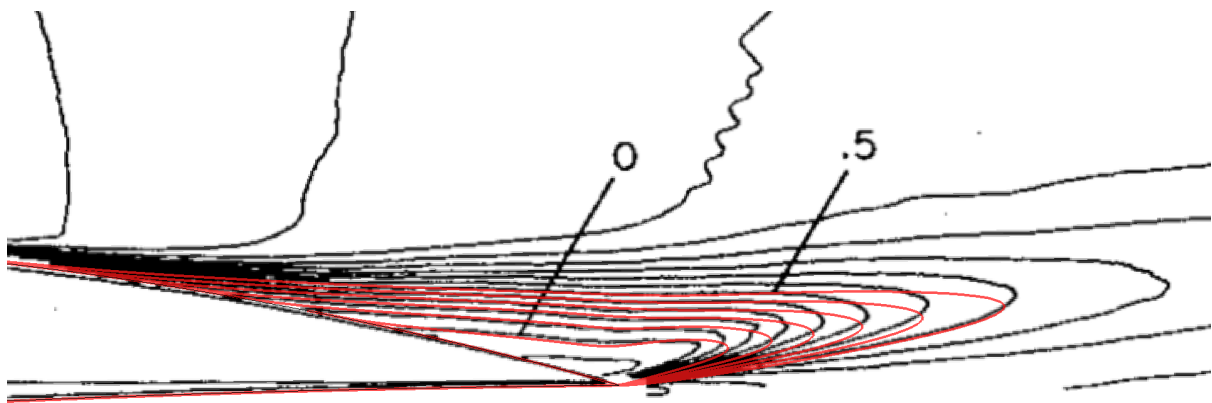

Figure 4.1.6: NACA 4412: Comparison of the constant normalised chordwise velocity contour lines.

The comparison of the surface pressure coefficient distribution, is shown in Figure 4.1.7, but the surface pressure coefficients from the experiment [31] were not corrected, and therefore should only be viewed in a qualitative sense [30]. As the Figure 4.1.7 illustrates, the calculated pressure coefficient distribution trend is in very good agreement with the experiment.

NASA [30] also provides the experimental data [31] for the normalised velocity profiles along the six lines near the trailing edge of the NACA 4412 airfoil, whose locations are shown in Figure 4.1.8. Likewise, the CFD data was interpolated along the same lines for the comparison, which is shown in Figure 4.1.9.
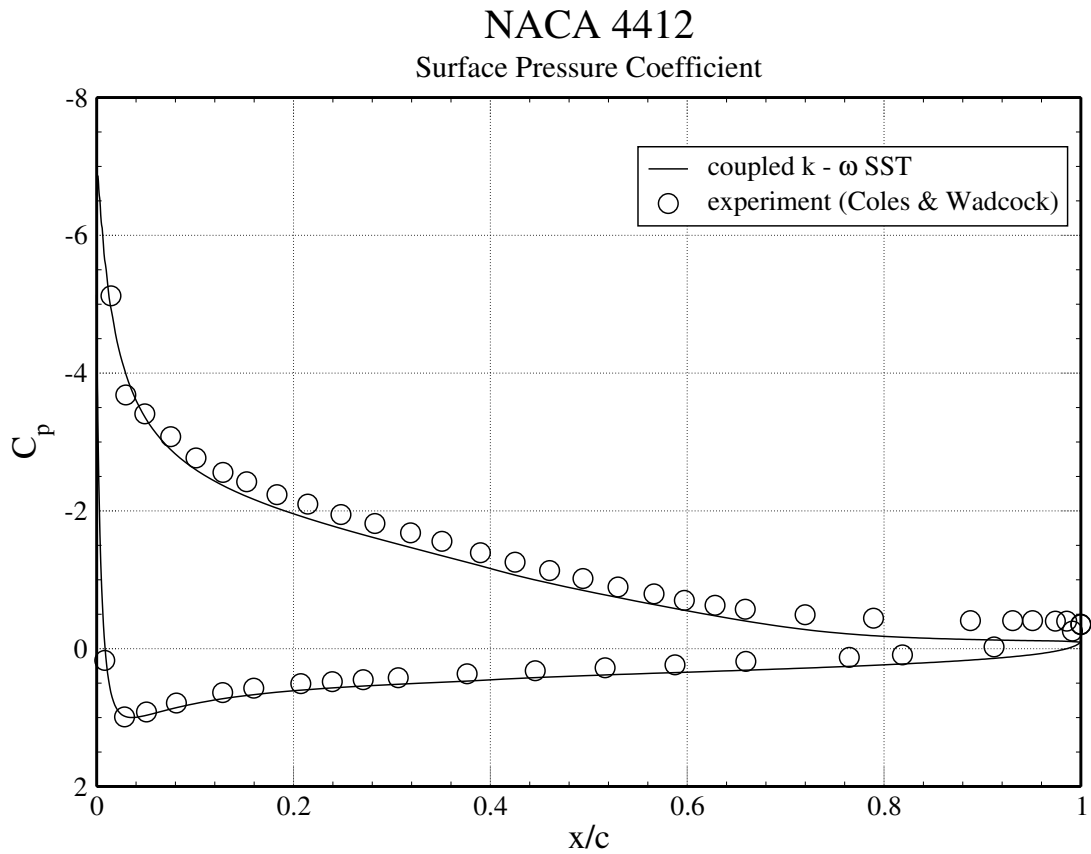
NACA 4412

Surface Pressure Coefficient

Figure 4.1.7: NACA 4412: Comparison of the surface pressure coefficient distribution.
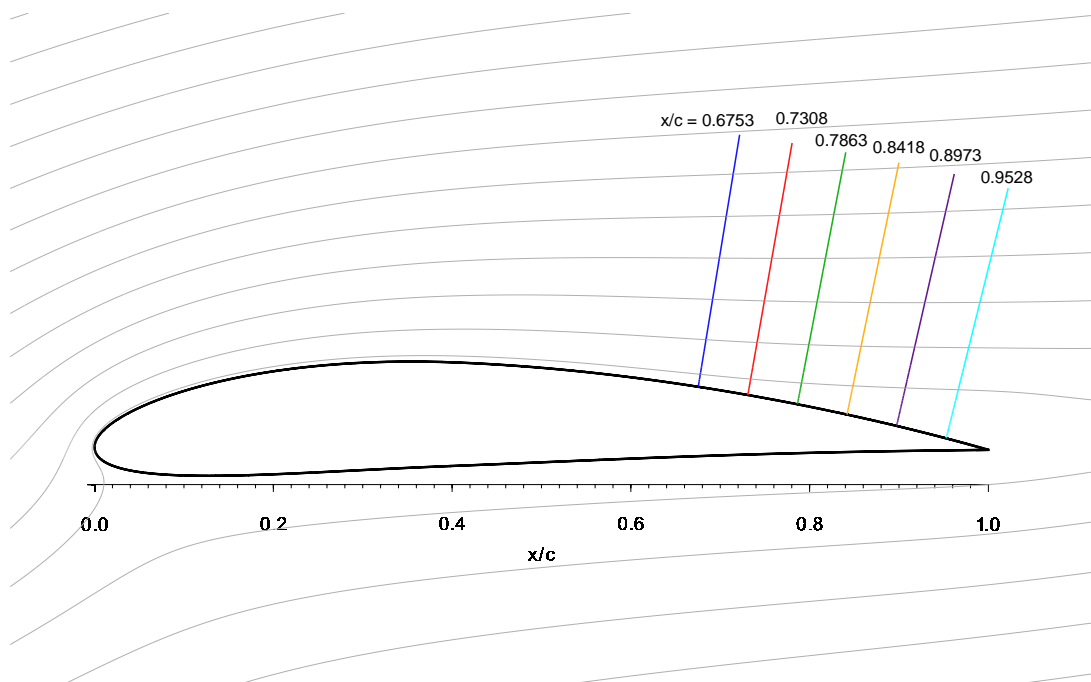
Figure 4.1.8: NACA 4412: Location of the lines along which experimental data was extracted.

(a) x/c = 0.6753,

(b) x/c = 0.7308,

(c) x/c = 0.7863,

(d) x/c = 0.8418,

(e) x/c = 0.8973,
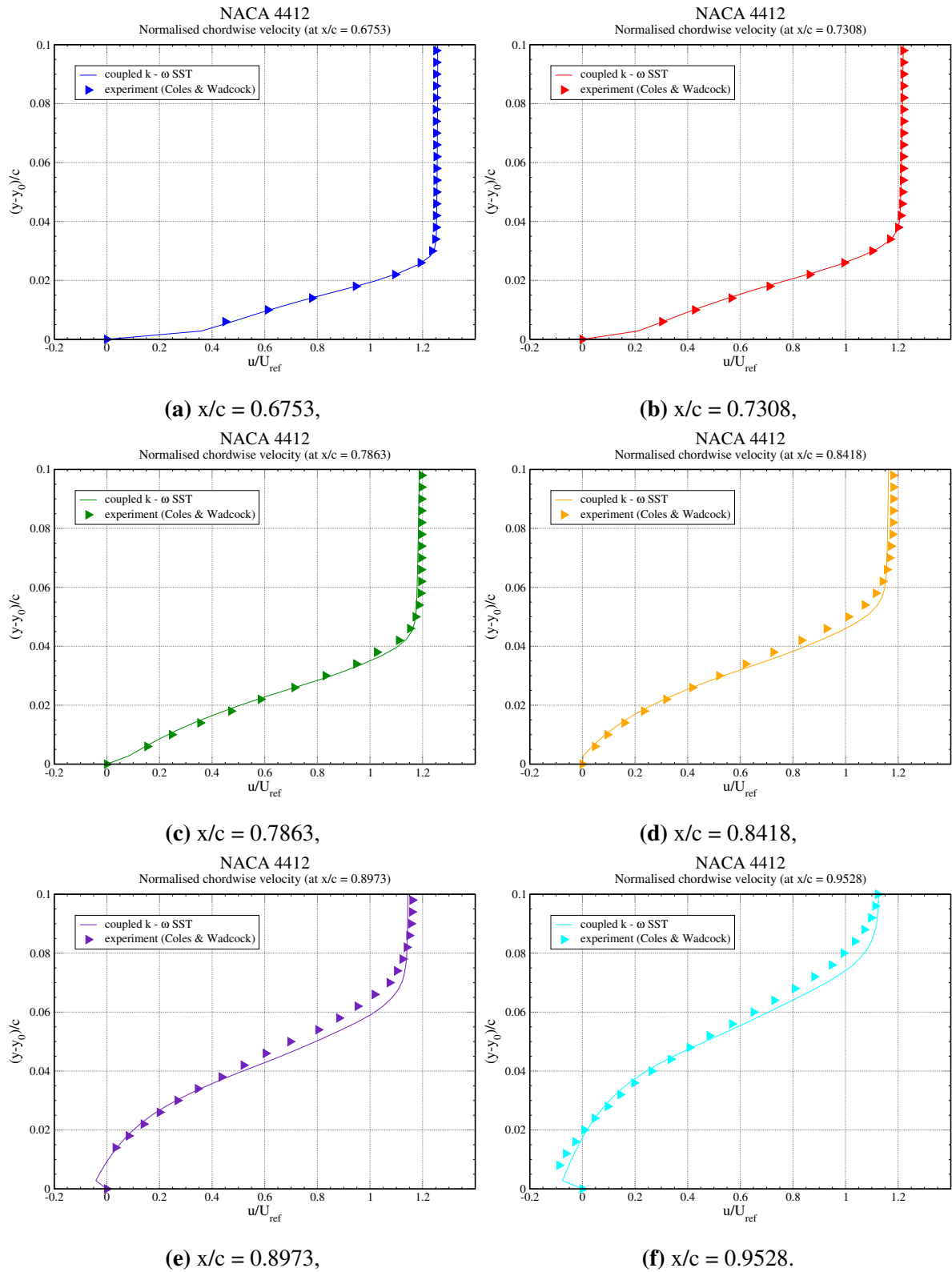
(f) x/c = 0.9528.

Figure 4.1.9: NACA 4412: Comparison of the normalised chordwise velocity profiles.

The comparison given in Figure 4.1.9, shows a very good agreement between the computed normalised chordwise velocity profiles and the experimental data.

4.2 Backward Facing Step

In the second validation test case, an incompressible turbulent flow over a backward facing step is investigated. The experimental data is available at the *NASA Turbulence Modeling Resource* page [36] but the particular data originates from the experiments performed by Driver and Seegmiller [37]. The Reynolds number (based on height of the step), freestream velocity value, step height and molecular kinematic viscosity were chosen according to [38] and are presented in Table 4.2.1.

Re_H $[-]$	U_{inf} $[m/s]$	H $[m]$	ν $\left[m^2/s\right]$
36×10^3	44.32	1	1.23×10^{-3}

Table 4.2.1: Geometry and flow parameters for the BFS case. [38]

4.2.1 Case set-up

The computational grid, which is shown in Figure 4.2.1 is generated using the `blockMesh` utility. The selected near-wall refinement (the height of cells next to the wall were chosen for y^+ values between 30 and 40) is suitable for the high Reynolds turbulence modelling approach, therefore both the `coupledKEpsilon` and the `coupledKOmegaSST` can be validated with this test case. Figure 4.2.1 also illustrates the selected domain size and the near-wall refinement.

The simulation is set up as a steady-state two-dimensional case, where the boundaries normal to the third dimension are named *FrontAndBack* and are specified with the `empty` boundary condition. The names of the solution domain boundaries are shown in Figure 4.2.2. The presented problem was solved using the `simpleFoam` solver and both `coupledKEpsilon` and `coupledKOmegaSST` as turbulence models with the following boundary conditions and numerical schemes.
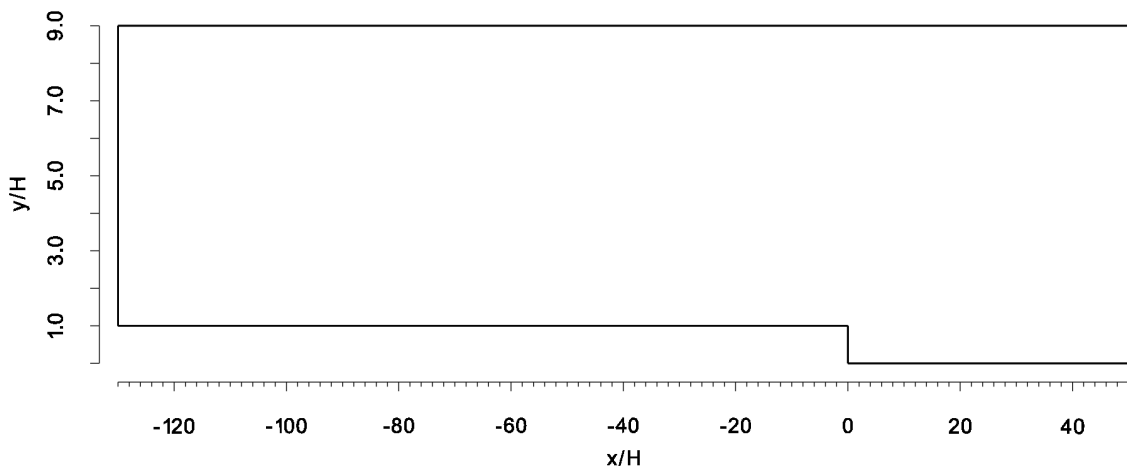
(a) Domain size (not to scale).
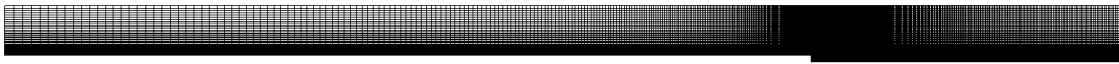
(b) Computational grid.
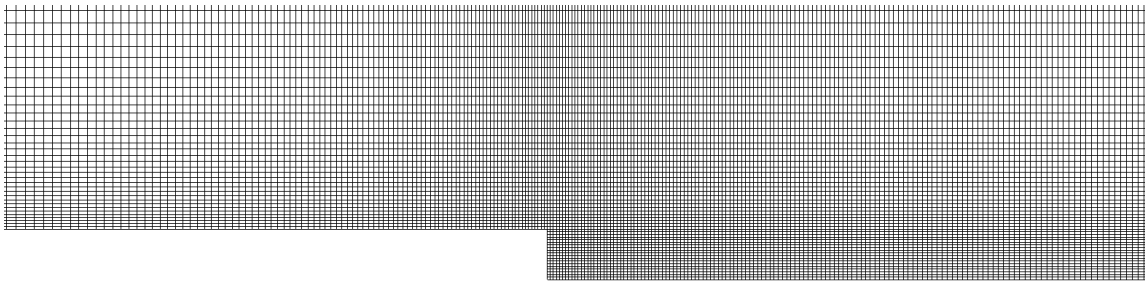
(c) Refinement near the step.

Figure 4.2.1: BFS: Computational domain.

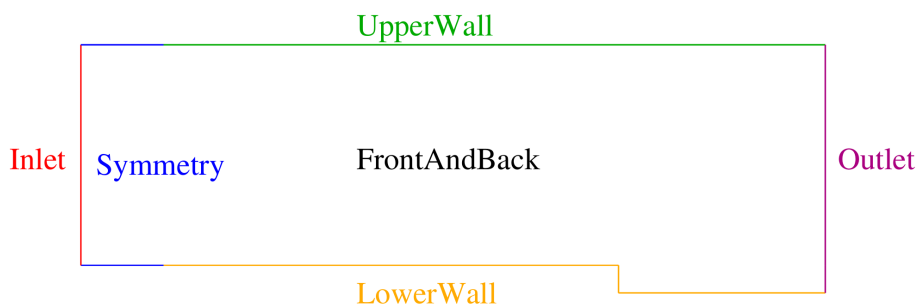

Figure 4.2.2: BFS: Patch names.

Boundary and initial conditions

- **Inlet**

    - *Velocity*: `fixedValue` with value `uniform (44.32 0 0)`

    - *Pressure*: `zeroGradient`

    - *Turbulence kinetic energy*: `fixedValue` with value `uniform 0.295`

    - *Turbulence dissipation*:

        * epsilon: `fixedValue` with value `uniform 0.08`

        * omega: `fixedValue` with value `uniform 97.37`

- **Outlet**

    - *Velocity*: `inletOutlet` with `inletValue uniform (0 0 0)`

    - *Pressure*: `outletInlet` with `outletValue uniform 0`

    - *Turbulence kinetic energy*: `zeroGradient`

    - *Turbulence dissipation*:

        * epsilon: `zeroGradient`

        * omega: `zeroGradient`

- **LowerWall**

    - *Velocity*: `fixedValue` with value `uniform (0 0 0)`

    - *Pressure*: `zeroGradient`

    - *Turbulence kinetic energy*: `kqRWallFunction`

    - *Turbulence dissipation*:

        * epsilon: `epsilonWallFunction`

        * omega: `omegaWallFunction`

- **UpperWall**

    - *Velocity*: `fixedValue` with value `uniform (0 0 0)`

- *Pressure*: `zeroGradient`

- *Turbulence kinetic energy*: `kqRWallFunction`

- *Turbulence dissipation*:

  - ∗ epsilon: `epsilonWallFunction`

  - ∗ omega: `omegaWallFunction`

- **Symmetry**: type `symmetryPlane` for all fields

- **FrontAndBack**: type `empty` for all fields

- **Initialisation**

  - *Velocity*: `uniform (44.32 0 0)`

  - *Pressure*: `uniform 0`

  - *Turbulence kinetic energy*: `uniform 0.295`

  - *Turbulence dissipation*: `uniform 97.37`

    - ∗ epsilon: `uniform 0.08`

    - ∗ omega: `uniform 97.37`

The selected numerical schemes are shown in Table 4.2.2

Time schemes

default	steadyState

Gradient schemes

default	Gauss linear

Divergence schemes

default	Gauss linear
div(phi,U)	Gauss linearUpwind
div(phi,k)	Gauss upwind
div(phi,epsilon)	Gauss upwind
div(phi,omega)	Gauss upwind

Laplacian schemes

default	Gauss linear uncorrected

Interpolation schemes

default	linear

Surface normal gradient schemes

default	uncorrected

Table 4.2.2: BFS: Numerical schemes.

Additionally, simulations were performed using the implemented `coupledKOmegaSST` and `coupledKEpsilon` and the corresponding segregated models, `kOmegaSST` and `kEpsilon`. The implicitly coupled models and their segregated counterparts produced the same results.

4.2.2 Results

Figure 4.2.3 illustrates the calculated y^+ distribution along the *LowerWall*, which is very similar to the desired values, hence the assumption of the high Reynolds turbulence modelling approach is applicable.

The plot of the normalised velocity magnitude, for both turbulence models, is shown in Figure 4.2.4, where the normalisation is carried out with respect to the freestream velocity value U_{inf}.
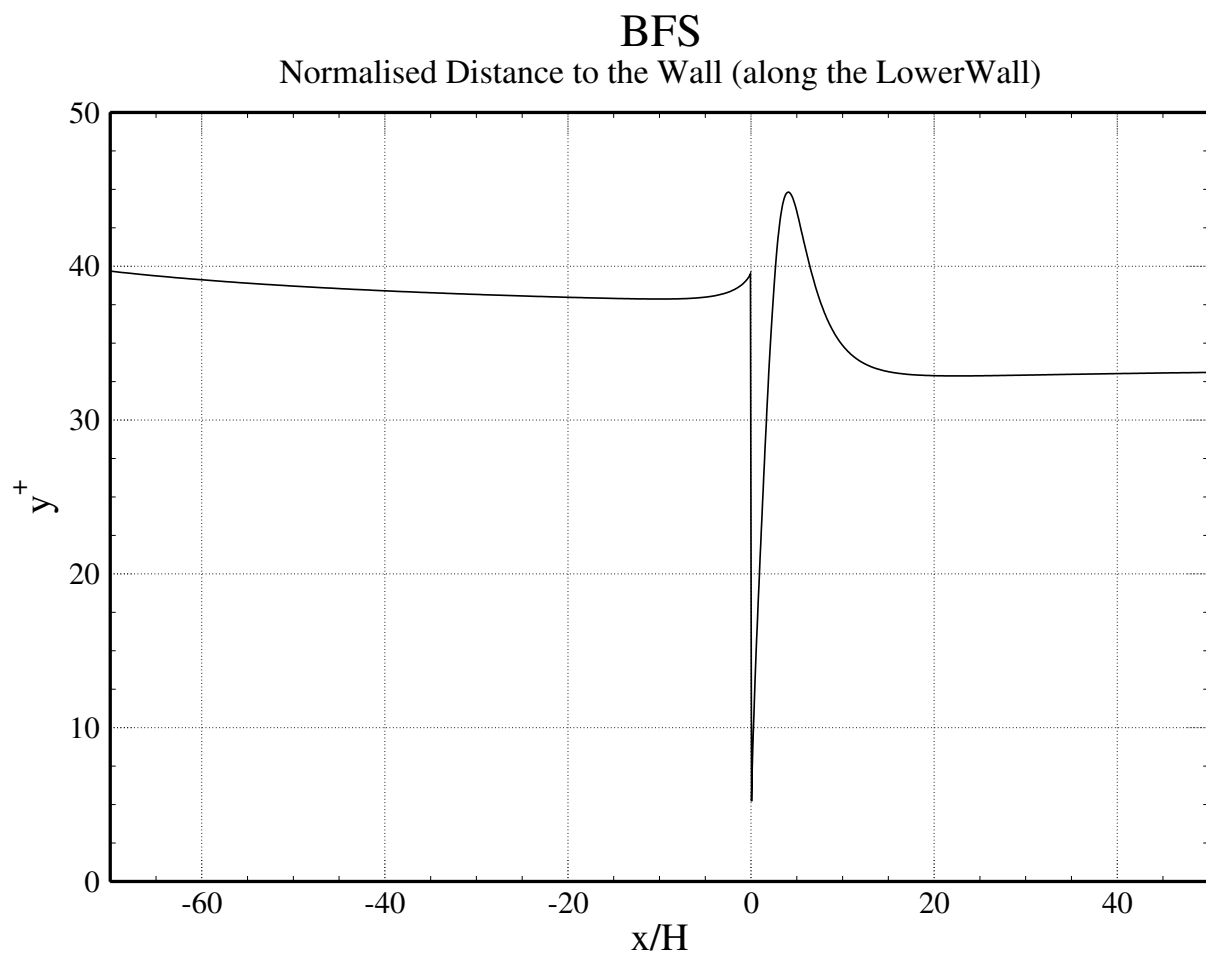

Figure 4.2.3: BFS: Normalised distance to the wall along the *LowerWall*.

$$U/U_{inf}$$

(a) `coupledKOmegaSST`.

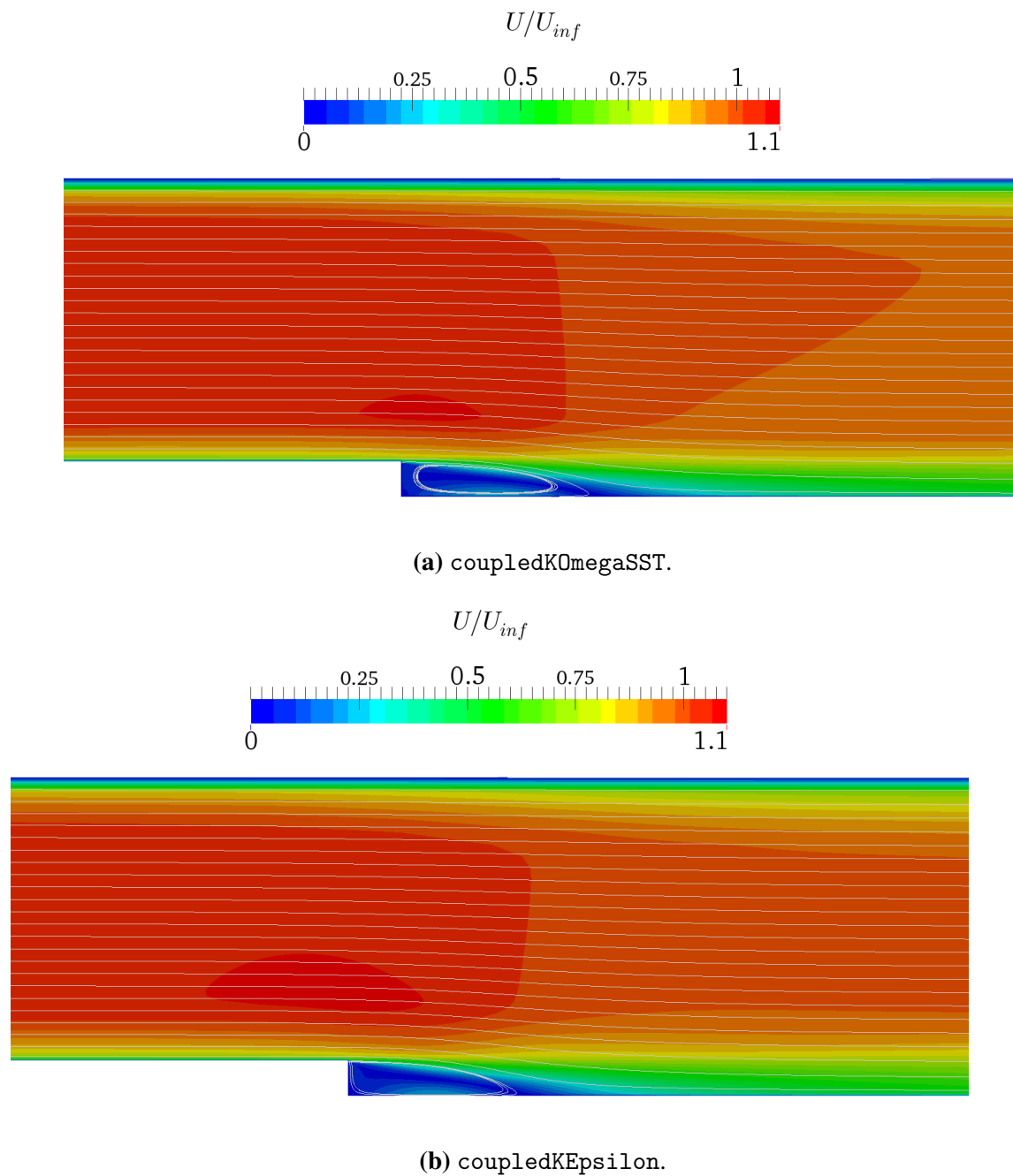$$U/U_{inf}$$

(b) `coupledKEpsilon`.

Figure 4.2.4: BFS: Normalised velocity magnitude plot.

For incompressible flows, the skin friction coefficient is defined by:

$$C_f = \frac{\tau_w}{\frac{1}{2}U_{ref}^2}, \qquad (4.2.1)$$

where τ_w is the wall shear stress and U_{ref} is the reference velocity at the channel centre near

$x/H = -4$ [36]. Similarly, the pressure coefficient is calculated according to Equation (4.2.2):

$$C_p = \frac{p - p_{ref}}{\dfrac{1}{2} U_{ref}^2}, \tag{4.2.2}$$

where p_{ref} is the reference kinematic pressure near the same location. However, NASA [36] mentions that the experimental pressure coefficient data have been shifted uniformly so that C_p has a zero value near the position $x/H = 40$, therefore it can be assumed that $p_{ref} \approx p_{inf}$ which is defined by the pressure boundary condition at the *Outlet* patch. Furthermore, after the comparison of velocity field data, a simple correlation between the U_{ref} and the U_{inf} can be introduced, $U_{ref}/U_{inf} \approx 1.05$.

The comparison of the calculated wall pressure coefficient distribution along the *LowerWall*, for both models with the experimental data, is presented in Figure 4.2.5.

In Figure 4.2.6, a comparison of the wall skin friction coefficient distribution along the *LowerWall* is given.
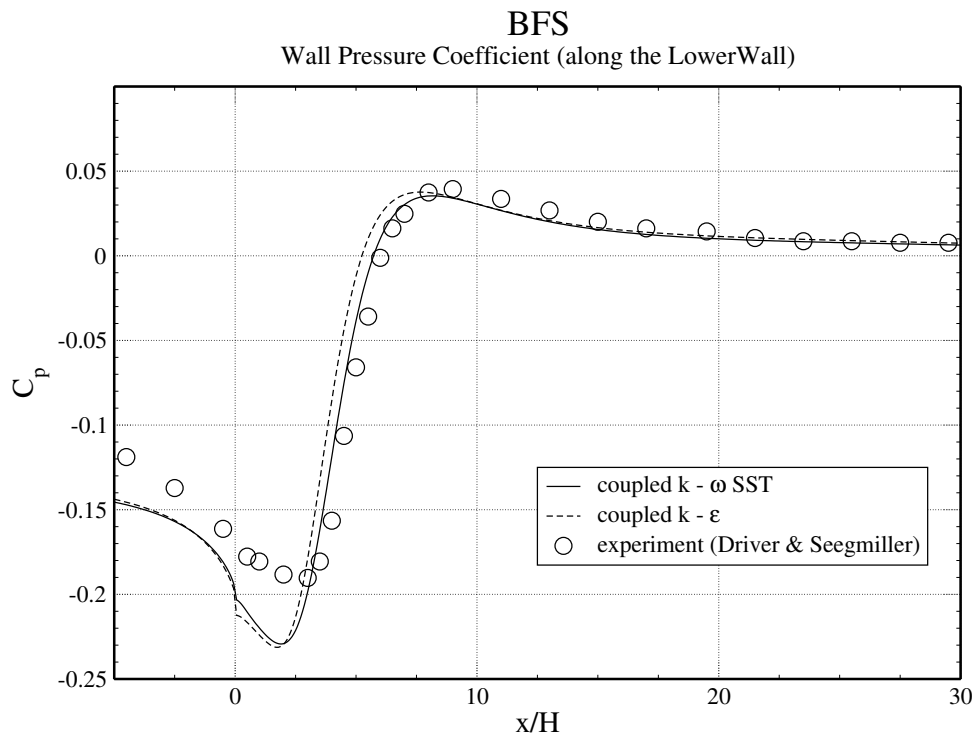

Figure 4.2.5: BFS: Comparison of the wall pressure coefficient distribution along the *LowerWall*.

BFS
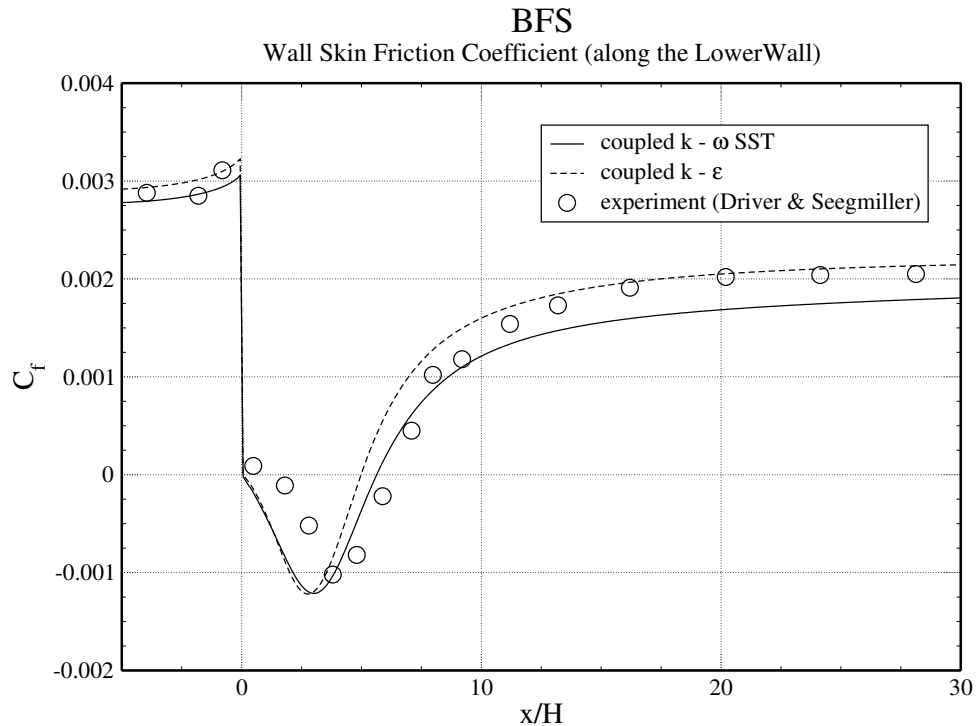Wall Skin Friction Coefficient (along the LowerWall)

Figure 4.2.6: BFS: Comparison of the wall skin friction coefficient distribution along the *LowerWall*.

As shown in Figure 4.2.5, both models give a similar prediction of the pressure distribution which is in fair agreement with the experimental data. A significant pressure value discrepancy is visible in the $0 < x/H < 2$ region, but despite the deviation, the pressure distribution trend is still compatible with the experimental data. Similarly, Figure 4.2.6 also shows fair agreement of the computed skin friction distributions with the experimental data, especially in the upstream region of the step. In the downstream region, both models under predict the reattachment location, but the `coupledKOmegaSST` is slightly more accurate. In both cases, the deviations in the recirculation region are due to inadequate y^+ values, i.e. the first cells next to the wall are in the buffer layer, which can not be adequately modelled by the wall functions.

NASA [36] also provided the experimental data [37] for the normalised velocity profiles along five lines, whose locations are shown in Figure 4.2.7. Likewise, the CFD data was interpolated along the same lines for the comparison, which is shown in Figure 4.2.8.
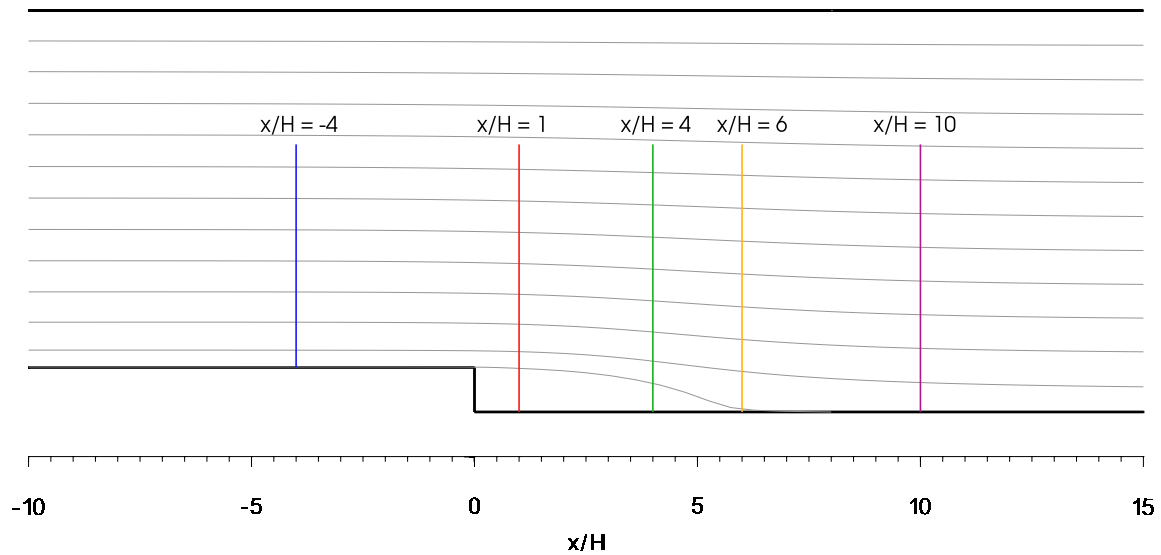

Figure 4.2.7: BFS: Location of the lines along which experimental data was extracted.

(a) x/H = -4,

(b) x/H = 1,

(c) x/H = 4,
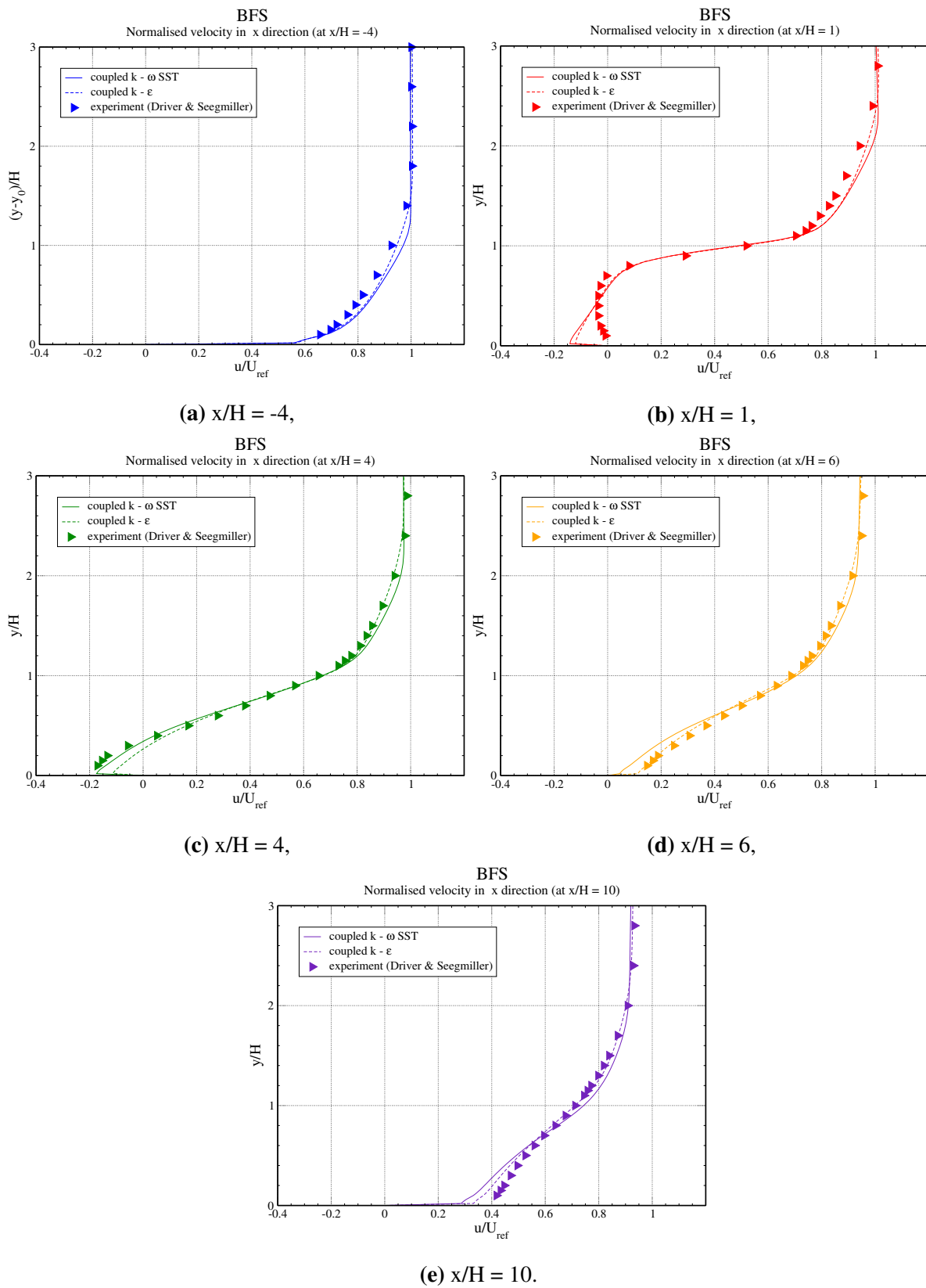
(d) x/H = 6,

(e) x/H = 10.

Figure 4.2.8: BFS: Comparison of the normalised velocities profiles in x direction.

As Figure 4.2.8 illustrates, both models give very similar results to each other, which are consistent with the experimental velocity profiles. The only considerable discrepancy is visible along the line located at $x/H = 1$. As mentioned before, this error is due to inadequate y^+ values is the recirculation region. It is exceptionally hard to achieve desired y^+ values in the whole domain, especially when recirculation or stagnation points are present and when the wall functions are used.

In this chapter, validation of implemented `coupledKOmegaSST` and `coupledKEpsilon` turbulence models were performed. The comparison of the numerical results from both models with the experimental data were presented and described. In the following chapter, benchmarking of the implemented turbulence models will be presented.

Chapter 5

Benchmarking of Coupled vs. Segregated Model Performance

In the previous chapter, validation of implemented `coupledKOmegaSST` and `coupledKEpsilon` turbulence models has been performed. In this chapter, performance of the implemented turbulence models shall be compared with the existing segregated models.

In the first section, benchmarking of both implemented turbulence models on the backward facing step case is presented. In the second section, benchmarking of `coupledKOmegaSST` turbulence model on NACA 4412 case is shown. In all benchmarking cases, `pUCoupledFoam` (with identical linear solver controls) is used for implicit pressure-velocity coupling.

5.1 Backward Facing Step

To qualify the performance improvement of the implemented `coupledKOmegaSST` and `coupledKEpsilon` turbulence models, following items are compared to the existing segregated models:

- Convergence rates for all equations,

- Convergence of field values in specific coordinates,

- Convergence of minimal and maximal field values.

The convergence of field values is monitored with probes whose location in the domain is shown in Figure 5.1.1. The first probe is located at the recirculation boarder, the second is in

the recirculation zone and the third is in the outer zone. Minimal and maximal field values are reported by an existing function object `minMaxField`.
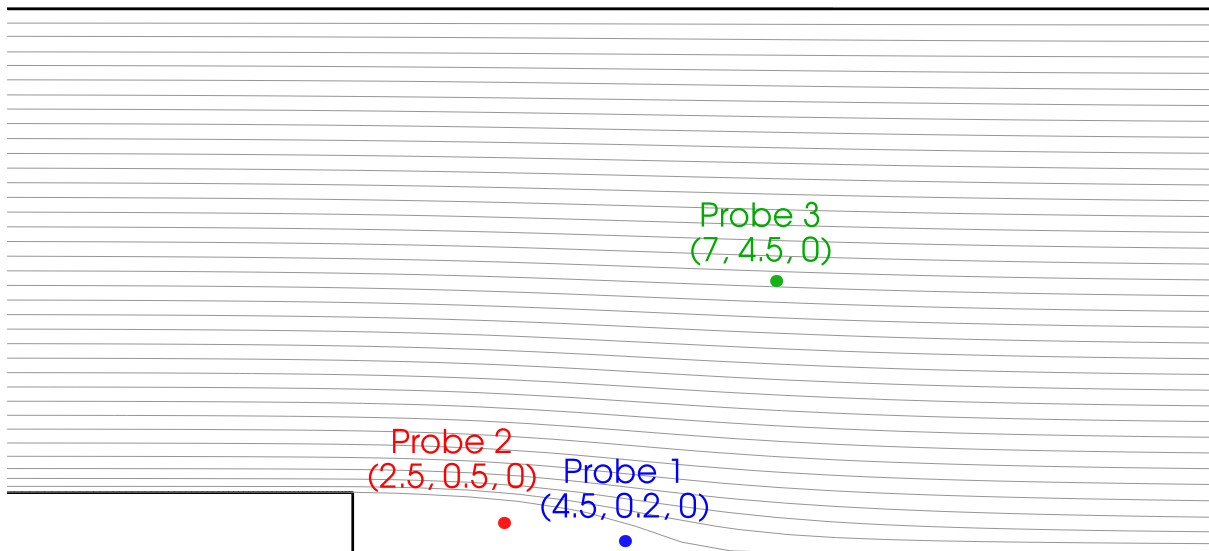

Figure 5.1.1: BFS: Probe locations.

For consistent comparison of residuals, field solutions from the implicitly coupled turbulence models (block-matrices) are placed in the corresponding segregated equations for the evaluation of initial residuals, which are later compared with residuals from the segregated turbulence models.

5.1.1   Solution and algorithm control

Table 5.1.1 specifies linear-solvers that are used for each discretised equation, with corresponding parameters. `kEpsilon` is the solver name for implicitly coupled $k - \varepsilon$ equations, `kOmega` is the solver name for implicitly coupled $k - \omega$ equations, `k` is the solver name for segregated k equation, `epsilon` is the solver name for segregated ε equation and `omega` is the solver name for segregated ω equation.

Solver and parameters	Linear solver control				
	Equation				
	kEpsilon	kOmega	k	epsilon	omega
Solver	BiCGStab	BiCGStab	BiCGStab	BiCGStab	BiCGStab
Preconditioner	Cholesky	Cholesky	DILU	DILU	DILU
Tolerance	1e-09	1e-09	1e-09	1e-09	1e-09
Relative tolerance	0.01	0.01	0.01	0.01	0.01
Minimum number of iterations	1	1	1	1	1
Maximum number of iterations	100	100	100	100	100

Table 5.1.1: BFS: Linear solver controls.

Table 5.1.2 presents the selected under-relaxation parameters.

Solution under-relaxation	
k	0.99 (0.98) *
epsilon	0.99 (0.98) *
omega	0.99

Table 5.1.2: BFS: Solution under-relaxation.

5.1.2 Results

Figure 5.1.2 illustrates the comparison of U_x, U_y, p and ν_t values, obtained by monitoring probes for the coupledKEpsilon and kEpsilon turbulence models. The results show faster convergence of the field values calculated by the coupledKEpsilon in comparison with the kEpsilon model, the enhanced convergence also affects the pressure-velocity system. It is also visible that the implicitly coupled model often prevents overshoots and undershoots of the calculated field values during the calculation. Despite the slightly lower under-relaxation factor, the segregated kEpsilon turbulence model experiences minor instabilities at the beginning of the calculation.

Comparison of the residual convergence profiles are shown in Figure 5.1.3. At first, the coupledKEpsilon model shows a moderate increase in the convergence rates compared to the kEpsilon model. As the iterations advance, convergence rates of the coupledKEpsilon model decrease below the kEpsilon model.

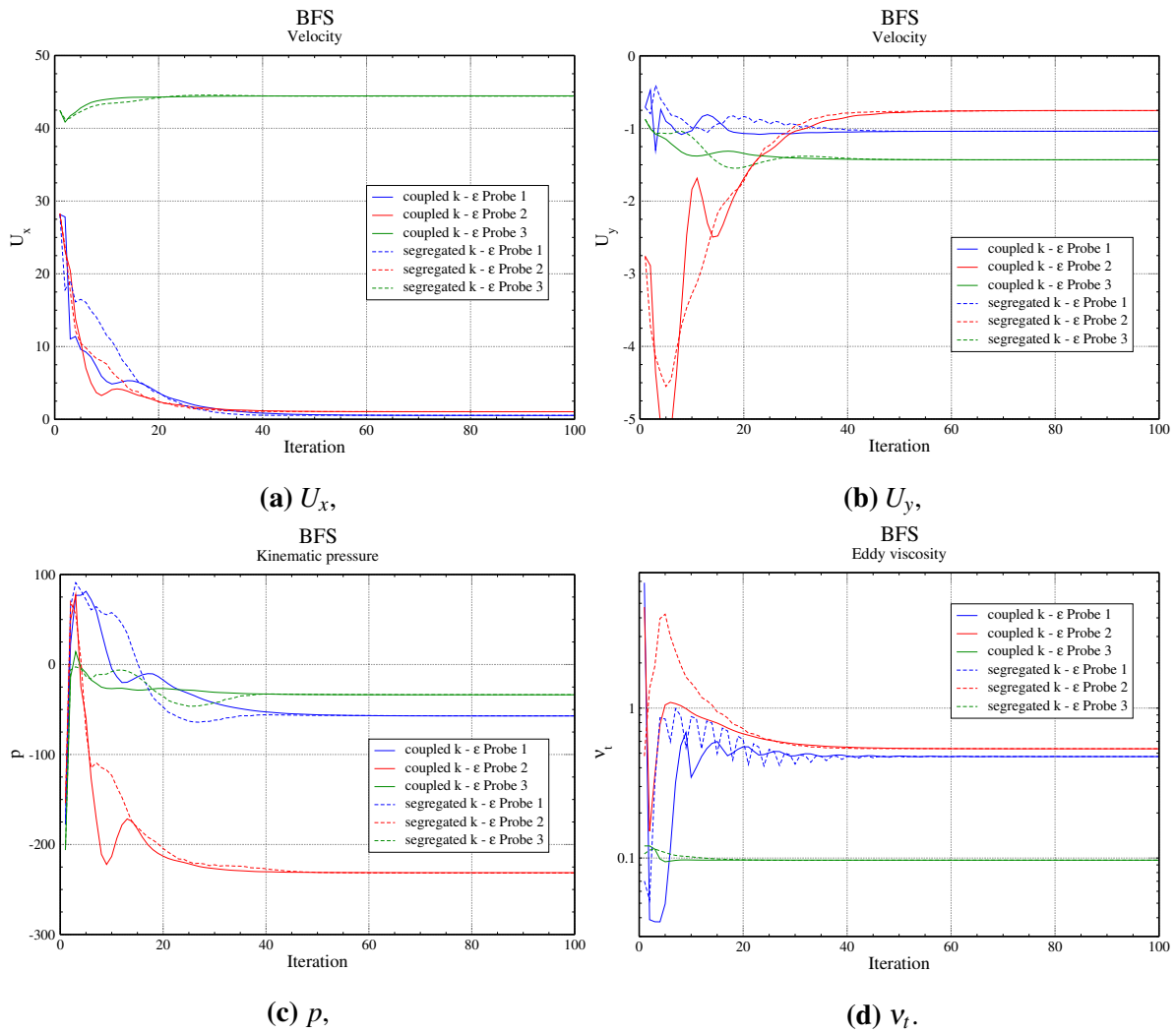* under-relaxation factor 0.98 is used for kEpsilon turbulence model, since it was not stable with 0.99

(a) U_x,

(b) U_y,

(c) p,

(d) ν_t.

Figure 5.1.2: BFS: Field value convergence for coupled and segregated $k - \varepsilon$ turbulence models.

(a) U_x residuals,

(b) U_y residuals,

(c) p residuals,

(d) k residuals,
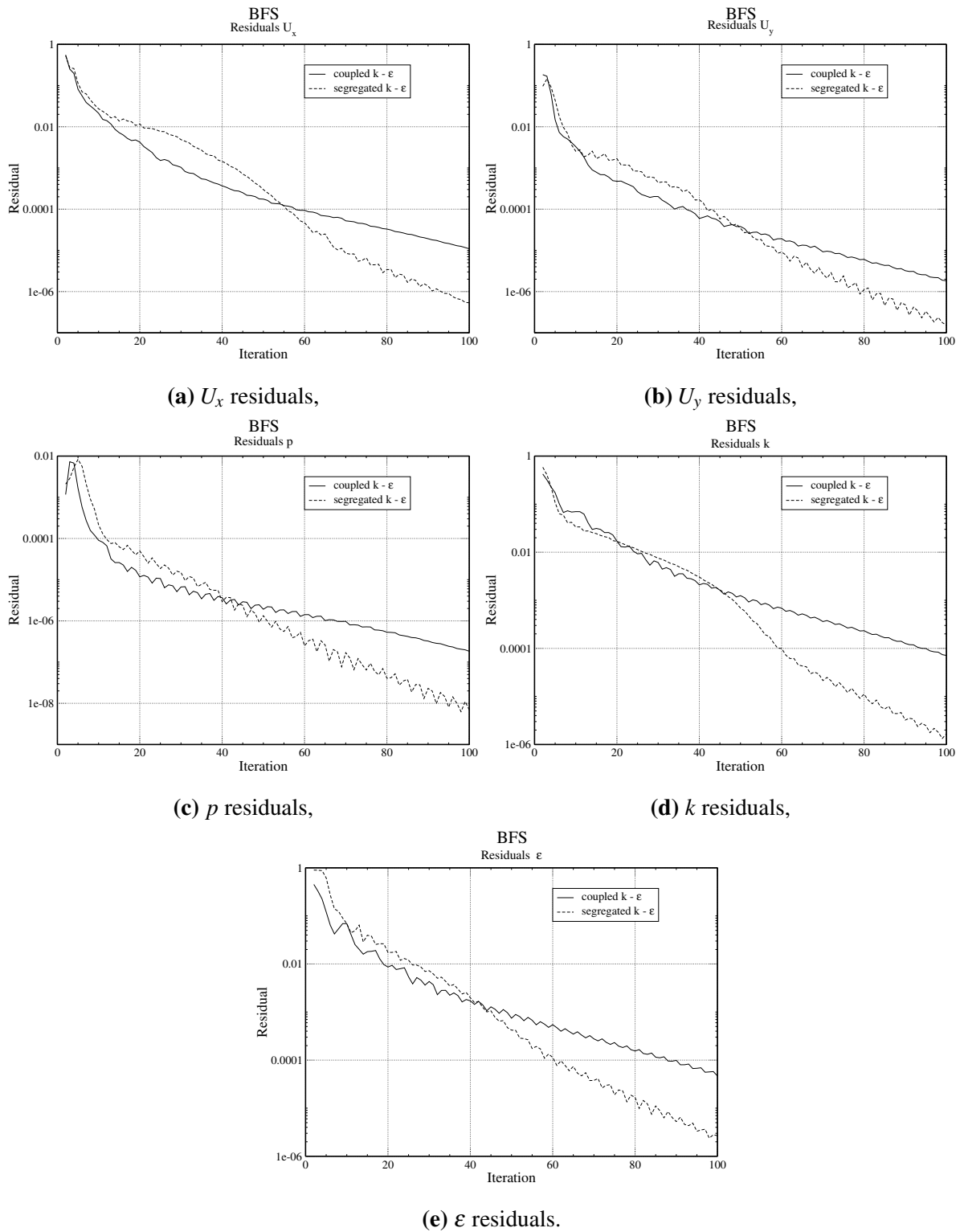

(e) ε residuals.

Figure 5.1.3: BFS: Convergence of residuals for coupled and segregated $k - \varepsilon$ turbulence models.

In Figure 5.1.4 the convergence of the filed values of 3 probes for the `coupledKOmegaSST` and the `kOmegaSST` turbulence models is shown. The results show slightly faster convergence of all (including the pressure-velocity system) field values calculated by the `coupledKOmegaSST` in comparison with the `kOmegaSST` model. It is also visible that the implicitly coupled model often prevents overshoots and undershoots of the calculated field values during the simulation.

Comparison of the residual convergence profiles are shown in Figure 5.1.5. The implicitly coupled model shows a moderate increase in the convergence rates compared to the `kOmegaSST` model.
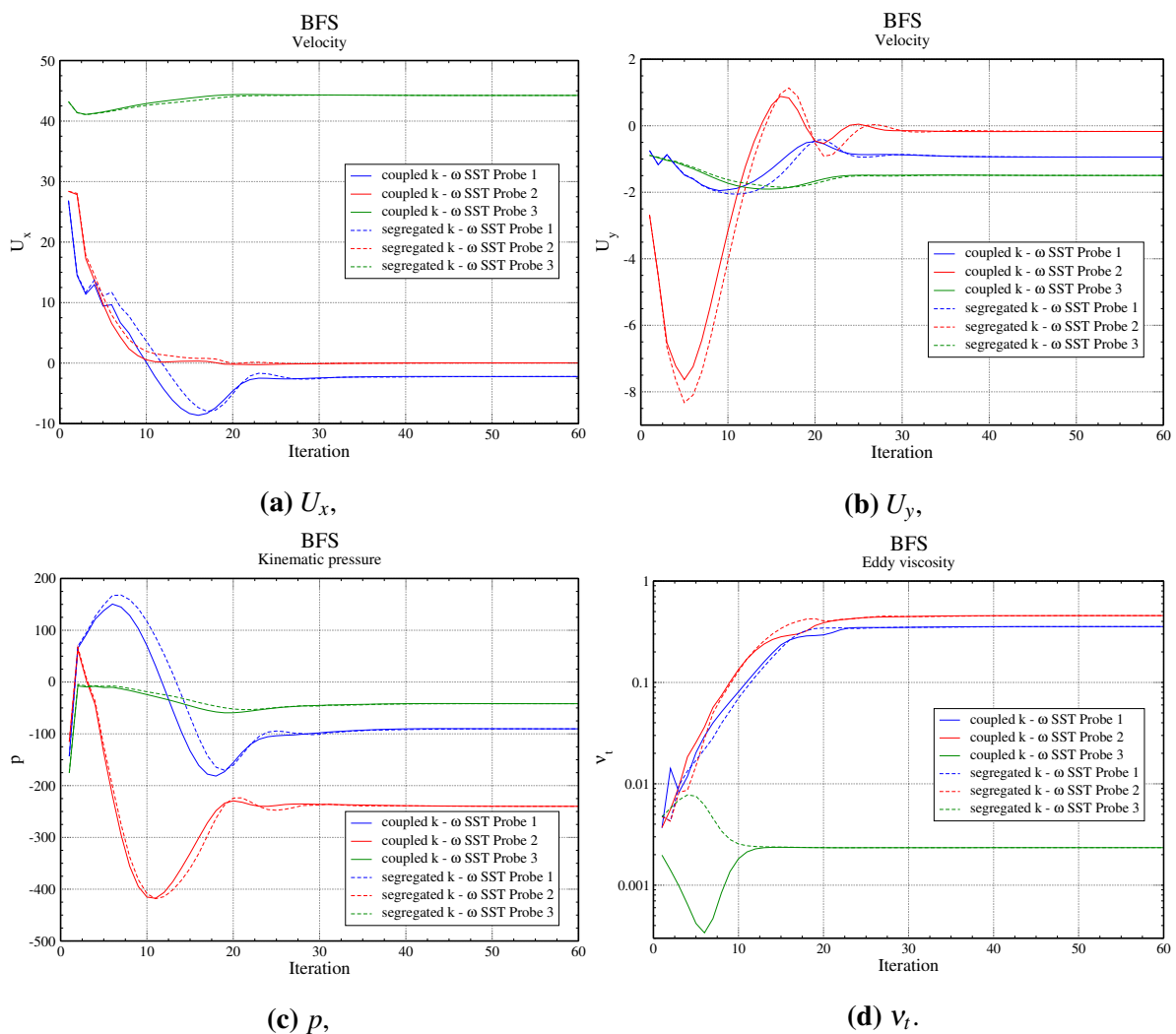

Figure 5.1.4: BFS: Field value convergence for $k - \omega\,SST$ turbulence models.

(a) U_x residuals,

(b) U_y residuals,

(c) p residuals,

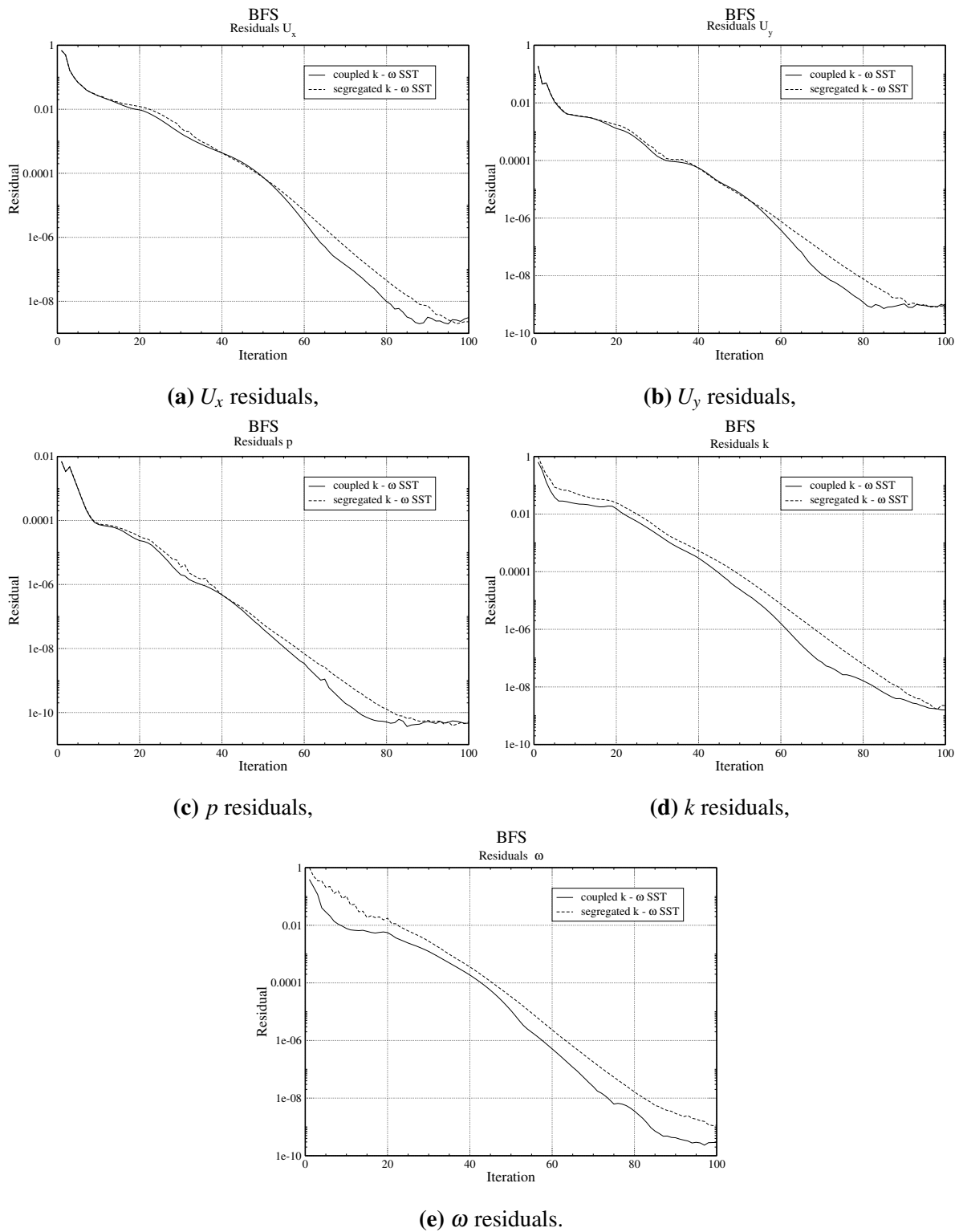**(d)** k residuals,

(e) ω residuals.

Figure 5.1.5: BFS: Convergence of residuals for coupled and segregated $k - \omega \, SST$ turbulence models.

Figure 5.1.6 illustrates the convergence of minimal and maximal field values for both implicit turbulence models and their corresponding segregated versions. As mentioned before, implicitly coupled turbulence models show faster convergence of the minimal and maximal field values and often prevent overshoots and undershoots of the calculated field values in comparison with the segregated versions.
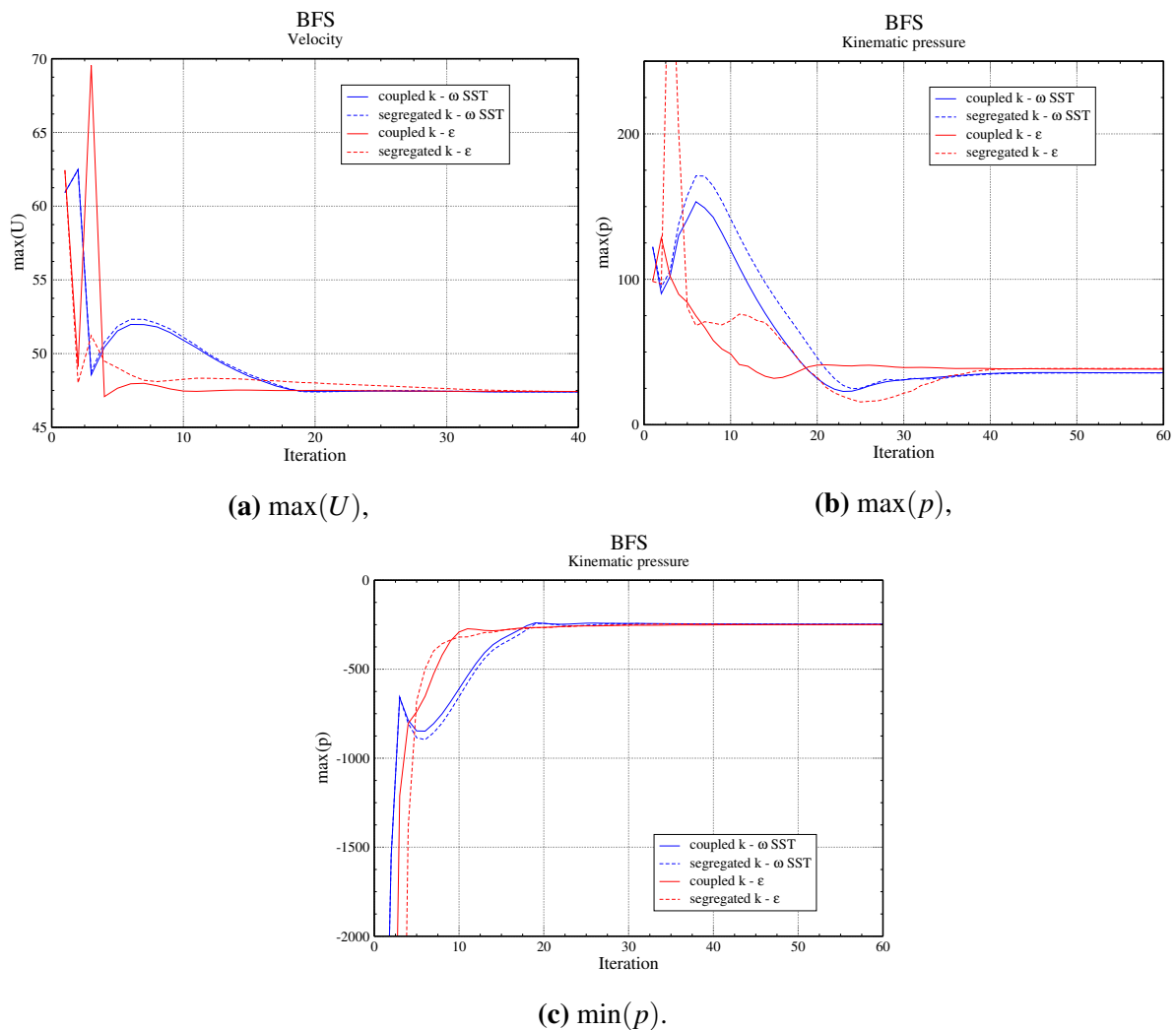

(a) $\max(U)$,

(b) $\max(p)$,

(c) $\min(p)$.

Figure 5.1.6: BFS: Maximum/minimum field value comparison.

5.2 NACA 4412

To qualify the performance improvement of the implemented `coupledKOmegaSST` turbulence models as a low Reynolds model, following items are compared to the existing segregated model:

- Convergence rates for all equations,

- Convergence of force coefficients (drag C_d and lift C_l),

- Convergence of minimal and maximal field values.

Note that the simulation presented in this section uses a coarser grid in comparison with the grid used in the Section 4.1.

Minimal and maximal field values are monitored with the `minMaxField` function object and the convergence of force coefficients is monitored with `forceCoeffs` function object.

5.2.1 Solution and algorithm control

Table 5.2.1 presents the selected linear-solvers with corresponding parameters, while Table 5.2.2 introduces the selected under-relaxation parameters.

Linear solver control			
		Equation	
Solver and parameters	kOmega	k	omega
Solver	BiCGStab	BiCGStab	BiCGStab
Preconditioner	Cholesky	DILU	DILU
Tolerance	1e-09	1e-09	1e-09
Relative tolerance	0.01	0.01	0.01
Minimum number of iterations	1	1	1
Maximum number of iterations	100	100	100

Table 5.2.1: NACA 4412: Linear solver controls.

Solution under-relaxation	
k	0.99
omega	0.99

Table 5.2.2: NACA 4412: Solution under-relaxation.

5.2.2   Results

Figure 5.2.1 illustrates the convergence of drag C_d and lift C_l coefficient throughout the iterations. The results show faster convergence of the force coefficient values calculated by the `coupledKOmegaSST` in comparison with the `kOmegaSST` model. It is also visible that the segregated model experiences larger amplitudes and oscillations during the simulation.

Comparison of the residual convergence profiles are shown in Figure 5.2.2. The implemented `coupledKOmegaSST` model shows a moderate increase in the convergence rates compared to the `kOmegaSST` model, where the improved convergence also influences the pressure-velocity system.

Furthermore, the implicitly coupled model is superior in preserving the boundedness of the turbulence variables than the segregated version.
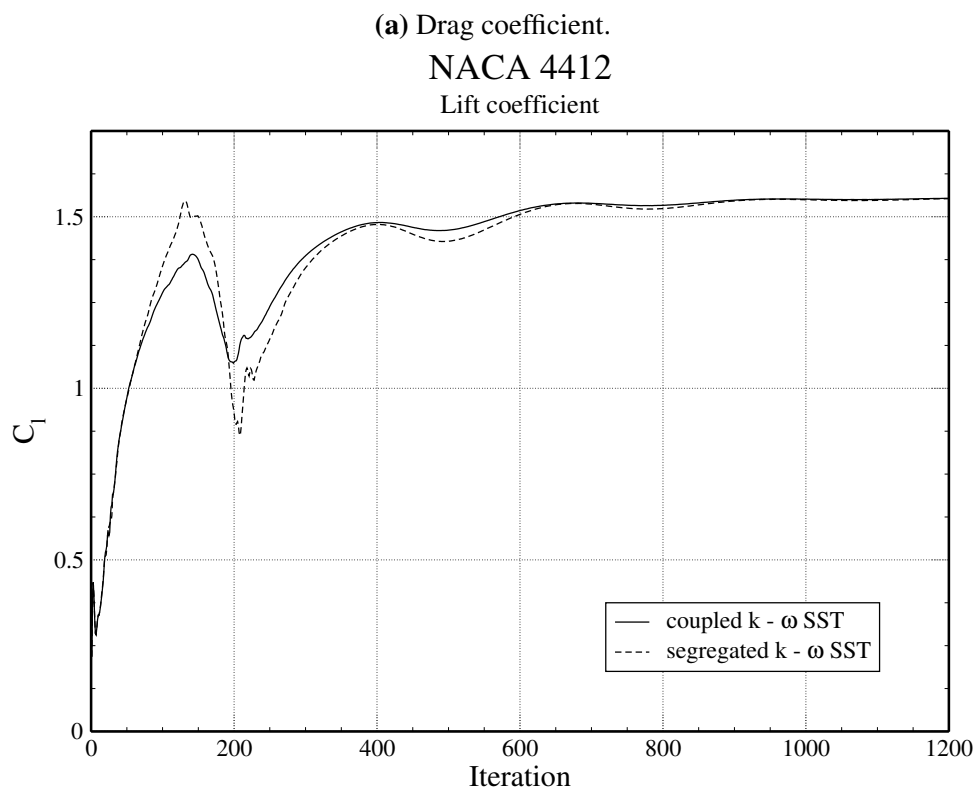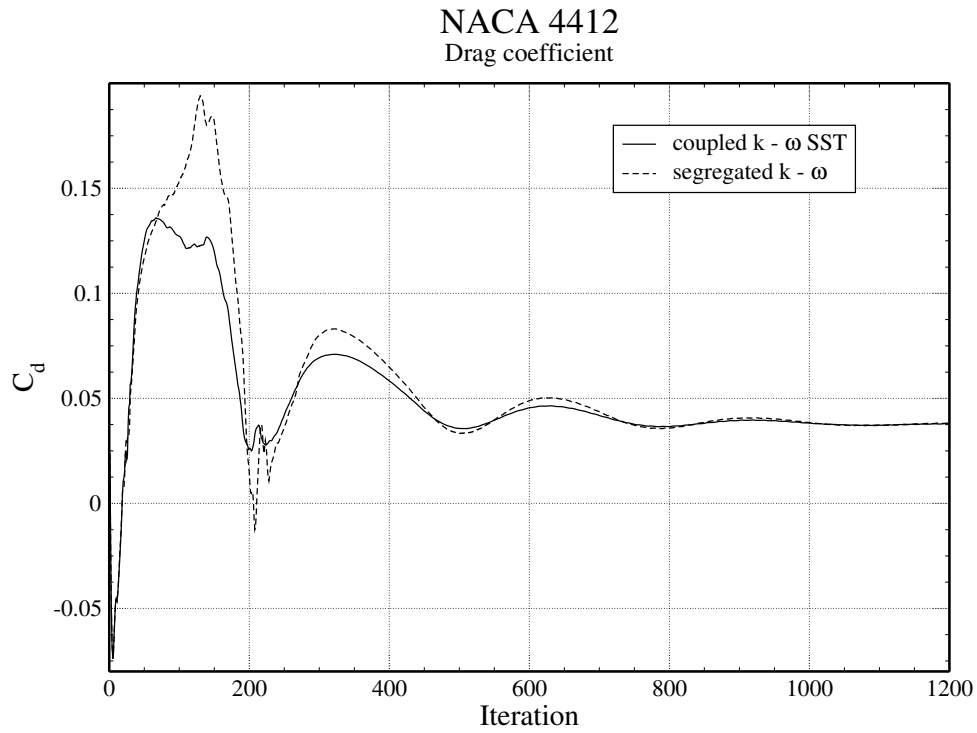
NACA 4412
Drag coefficient

(a) Drag coefficient.

NACA 4412
Lift coefficient

(b) Lift coefficient.

Figure 5.2.1: NACA: Force coefficients convergence per iteration.

(a) U_x residuals,

(b) U_y residuals,

(c) p residuals,

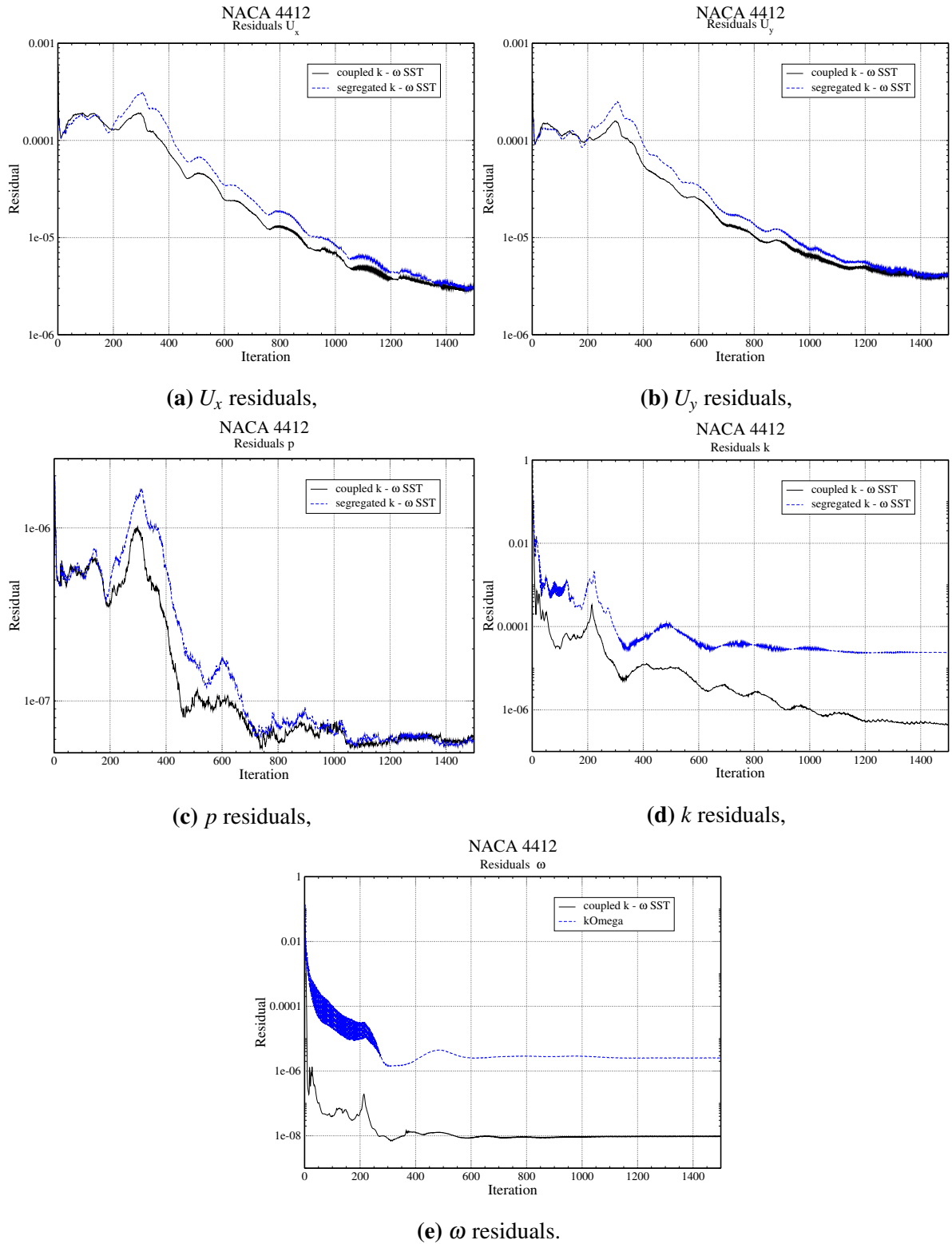**(d)** k residuals,

(e) ω residuals.

Figure 5.2.2: NACA: Convergence of residuals for coupled and segregated $k - \omega\,SST$ turbulence models.

Figure 5.2.3 illustrates the comparison of minimal and maximal field values convergence for the `coupledKOmegaSST` and `kOmegaSST` turbulence models. As mentioned earlier, the implicitly coupled turbulence model shows faster and smoother convergence of the minimal and maximal field values and often prevent overshoots and undershoots of the calculated field values in comparison with the segregated version.
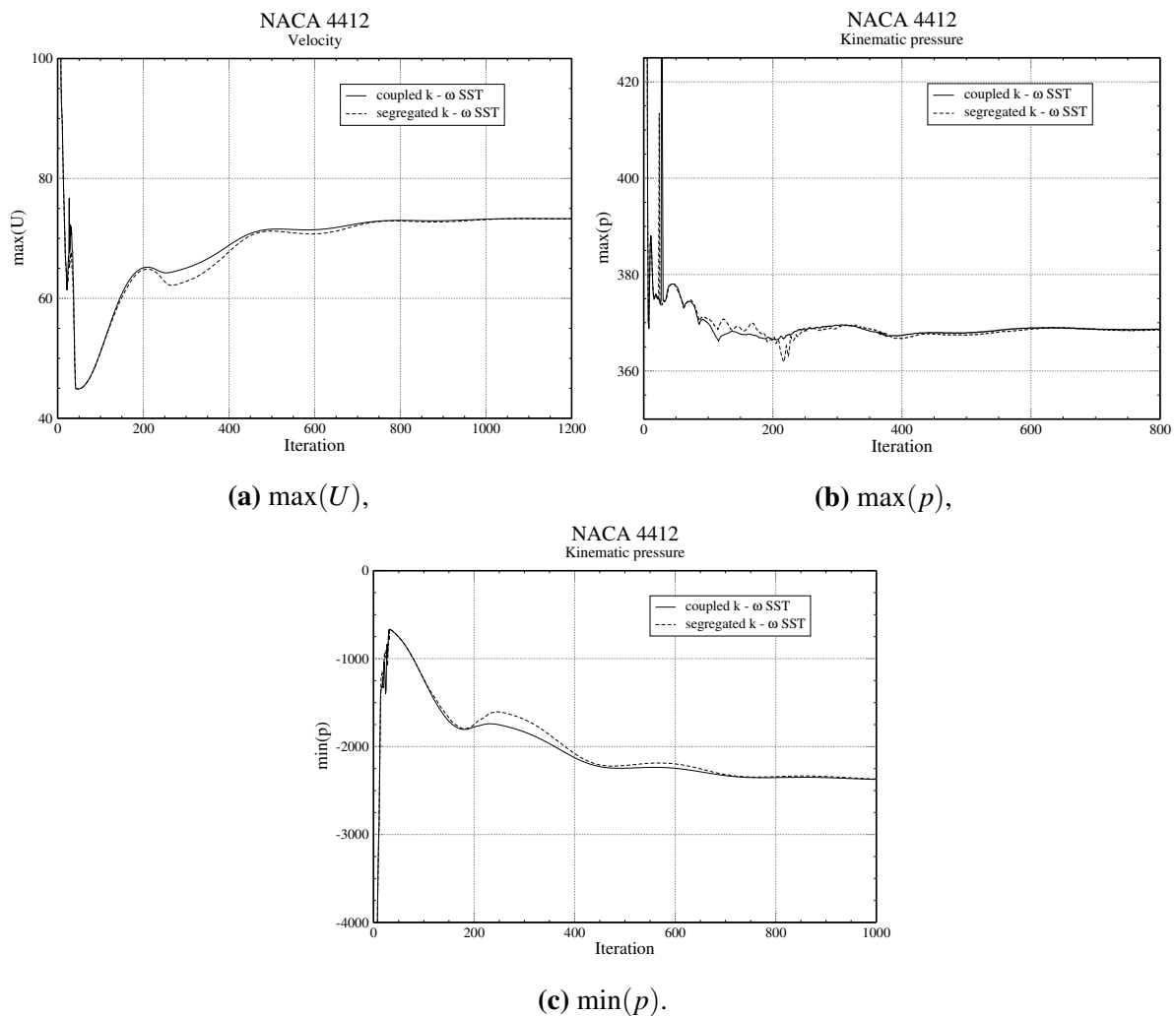

(a) max(U),   **(b)** max(p),

(c) min(p).

Figure 5.2.3: NACA: Maximum/minimum field value comparison.

Figure 5.2.4 presents the comparison of the force coefficient convergence per elapsed CPU time. The implicitly coupled model `coupledKOmegaSST` achieved convergence of the force coefficients in approximately 20% less CPU time, furthermore, the convergence process of the coupled model is significantly more damped than the segregated.
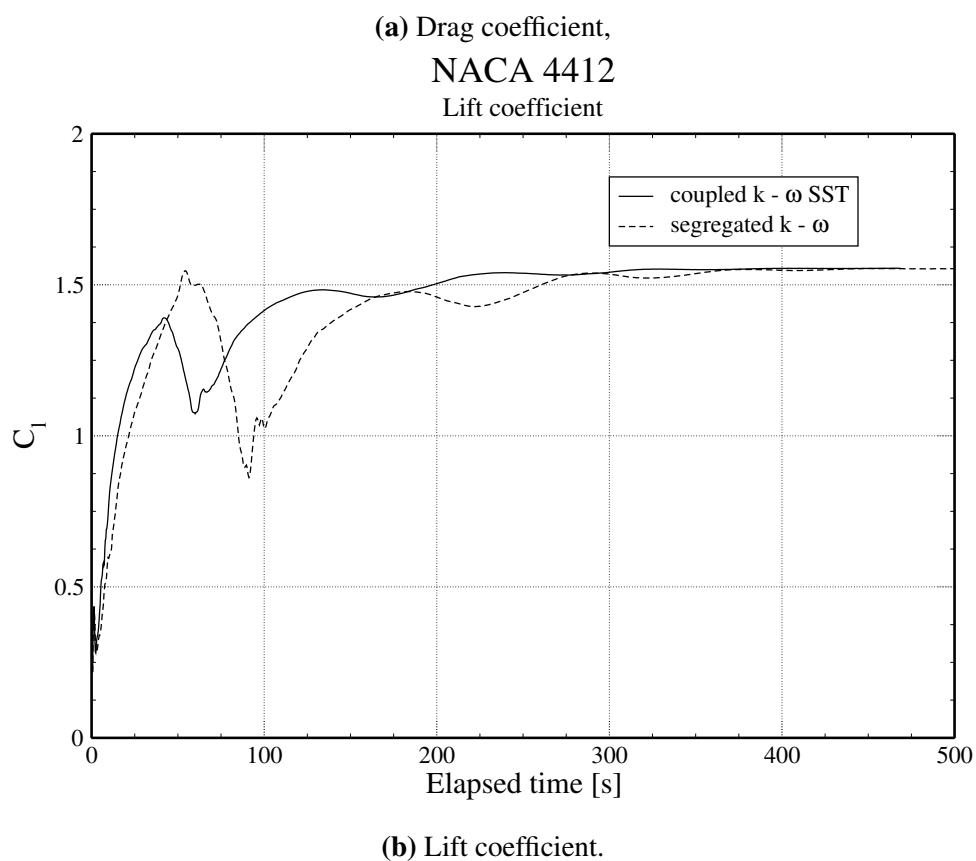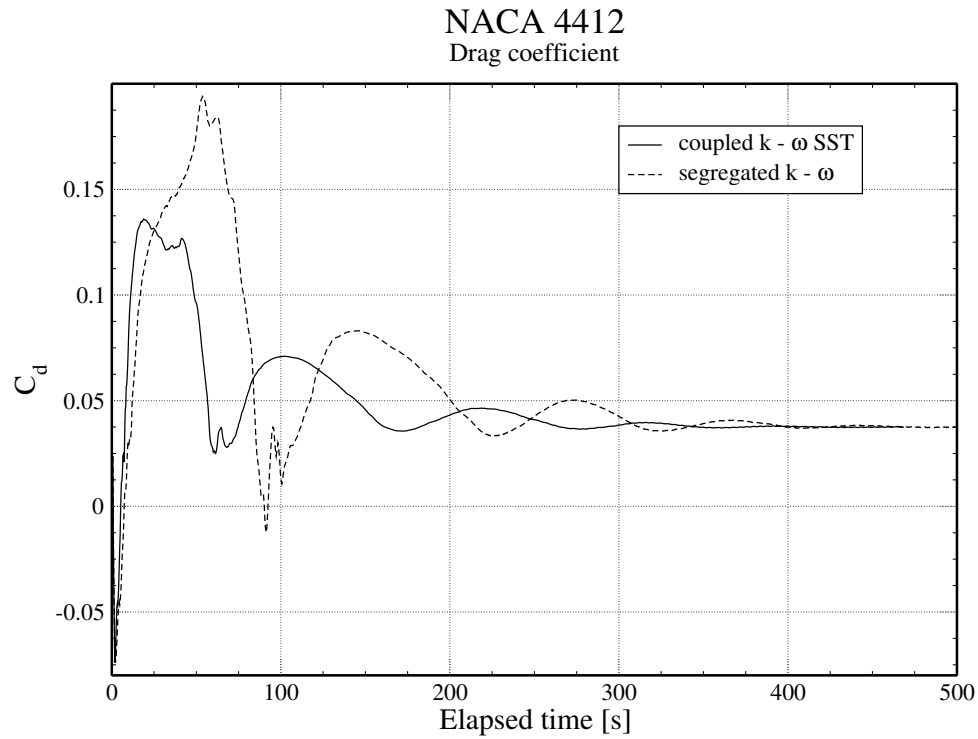
NACA 4412
Drag coefficient

(a) Drag coefficient,

NACA 4412
Lift coefficient

(b) Lift coefficient.

Figure 5.2.4: NACA: Force coefficients convergence per CPU time.

Chapter 6

Conclusion

Block-coupled solution algorithms for incompressible two-equation turbulence models, $k - \varepsilon$ and $k - \omega \, SST$, are presented in this thesis.

Prior to implementation of the turbulence models in the block-matrix framework, linearisation of the non-linear source terms was investigated in detail. Furthermore, investigation of the stability and boundedness of the linearised model was performed. The derived implicitly coupled turbulence models, `coupledKEpsilon` and `coupledKOmegaSST`, were implemented in foam-extend (the community-driven fork of the OpenFOAM) software.

Two validation cases were presented, a separated flow past a NACA 4412 airfoil at maximum lift and an incompressible turbulent flow over a backward facing step (BFS). The NACA 4412 case was set up for the validation of turbulence models with low Reynolds approach and the BFS case was intended for the validation of high Reynolds models. The $k - \varepsilon$ turbulence model is implemented only as a high Reynolds version, therefore, validation was performed only for the BFS case. The $k - \omega \, SST$ turbulence model can blend between the high and low Reynolds formulation consequently, validation was performed for both cases. In the NACA 4412 validation case, the numerical results from the implemented `coupledKOmegaSST` turbulence model were compared with the experimental data and an overall good agreement was obtained. In the BFS case, the numerical results from both implemented turbulence models were compared with the experimental data and an overall good agreement was obtained as well.

Furthermore, performance of the implemented turbulence models was compared with the existing segregated models. Benchmarking was performed on the two validation cases, where

`pUCoupledFoam` was the selected incompressible pressure-velocity solver. Similarly as for the validation, both implemented turbulence models were benchmarked on the BFS case and only `coupledKOmegaSST` was benchmarked on the NACA 4412 case. Overall, implicit cross-coupling of two-equation turbulence models accelerates convergence of field values, exhibits smoother convergence compared to segregated turbulence models and often prevents over-shoots and undershoots of the calculated field values during the simulation. The implemented `coupledKOmegaSST` model achieved convergence of the force coefficients in approximately 20% less CPU time than the segregated model. Additionally, the implicitly coupled models are found to be superior in preserving the boundedness of the turbulence variables than the segregated versions.

Bibliography

[1] M. Darwish, I. Sraj, and F. Moukalled, "A coupled finite volume solver for the solution of incompressible flows on unstructured grids," *Journal of Computational Physics*, vol. 228, no. 1, pp. 180 – 201, 2009.

[2] Z.-N. Wu and S. Fu, "Positivity of $k - \varepsilon$ Turbulence Models for Incompressible Flow," *Mathematical Models and Methods in Applied Sciences*, vol. 12, no. 03, pp. 393–406, 2002.

[3] F. Ilinca and D. Pelletier, "Positivity preservation and adaptive solution of two-equation models of turbulence," *International Journal of Thermal Sciences*, vol. 38, no. 7, pp. 560 – 571, 1999.

[4] L. Ignat, D. Pelletier, and F. Ilinca, "A universal formulation of two-equation models for adaptive computation of turbulent flows," *Computer Methods in Applied Mechanics and Engineering*, vol. 189, no. 4, pp. 1119 – 1139, 2000. Adaptive Methods for Compressible CFD.

[5] T. Du and Z.-N. Wu, "Mixed analytical/numerical method applied to the high Reynolds number $k - \varepsilon$ turbulence model," *Computers and Fluids*, vol. 34, 2005.

[6] M. Wasserman, Y. Mor-Yossef, I. Yavneh, and J. Greenberg, "A robust implicit multigrid method for RANS equations with two-equation turbulence models," *Journal of Computational Physics*, vol. 229, no. 16, pp. 5820 – 5842, 2010.

[7] Y. Moryossef and Y. Levy, "Unconditionally positive implicit procedure for two-equation turbulence models: Application to $k - \omega$ turbulence models," *Journal of Computational Physics*, vol. 220, no. 1, pp. 88 – 108, 2006.

[8] Y. Mor-Yossef and Y. Levy, "The unconditionally positive-convergent implicit time integration scheme for two-equation turbulence models: Revisited ," *Computers & Fluids*, vol. 38, no. 10, pp. 1984 – 1994, 2009.

[9] D. Wilcox, *Turbulence Modeling for CFD*. DCW Industries Incorporated, 1994.

[10] J. H. Ferziger and M. Peric, *Computational Methods for Fluid Dynamics*. Berlin, Germany: Springer-Verlag Berlin Heidelberg, 1996.

[11] H. Jasak, *Course Slides: Turbulence Modelling for CFD*. FAMENA, University of Zagreb, Croatia.

[12] F. R. Menter, M. Kuntz, and R. Langtry, "Ten years of industrial experience with the SST turbulence model," *Heat and Mass Transfer*, vol. 4, pp. 625 – 632, 2003.

[13] OpenCFD Ltd., "OpenFOAM The open source CFD toolbox." `http://www.openfoam.com/`.

[14] H. Jasak, "The OpenFOAM Extend Project (Community-driven Releases of Open-FOAM)." `http://www.extend-project.de/`.

[15] W. Jones and B. Launder, "The prediction of laminarization with a two-equation model of turbulence," *International Journal of Heat and Mass Transfer*, vol. 15, no. 2, pp. 301 – 314, 1972.

[16] F. Menter and T. Esch, "Elements of industrial heat transfer prediction," 16th Brazilian Congress of Mechanical Engineering (COBEM), 2001.

[17] NASA Turbulence Modeling Resource, "The Menter Shear Stress Transport Turbulence Model." `http://turbmodels.larc.nasa.gov/sst.html`.

[18] A. Hellsten, ch. Some improvements in Menter's k-omega SST turbulence model. Fluid Dynamics and Co-located Conferences, American Institute of Aeronautics and Astronautics, 1998.

[19] F. R. Menter, "Two-equation eddy-viscosity turbulence models for engineering applications," *AIAA Journal*, vol. 32, 08 1994.

[20] CFD Online, "Introduction to turbulence / Wall bounded turbulent flows." `http://www.cfd-online.com/Wiki/Introduction_to_turbulence`.

[21] Aokomoriuta, "Wikipedia - Law of the wall." `https://en.wikipedia.org/wiki/Law_of_the_wall`.

[22] CFD Online, "Two equation turbulence models / Near-wall treatments." `http://www.cfd-online.com/Wiki/Two_equation_models`.

[23] E. D. Huckaby and O. A. Marzouk, "Effects of turbulence modeling and parcel approach on dispersed two-phase swirling flow," vol. 2, (San Francisco, USA), 2009.

[24] ANSYS Fluent, "FLUENT 6.3 User's Guide - 12.10.2 Standard Wall Functions." `http://aerojet.engr.ucdavis.edu/`.

[25] V. Vukcevic. Private communication.

[26] S. Patankar, *Numerical Heat Transfer and Fluid Flow*. Series in computational methods in mechanics and thermal sciences, Taylor & Francis, 1980.

[27] F. Ilinca, D. Pelletier, and A. Garon, "Positivity preserving formulations for adaptive solution of two-equation models of turbulence," American Institute of Aeronautics and Astronautics Fluid Dynamics Conference, 1996.

[28] F. Ilinca and D. Pelletier, "Positivity Preservation and Adaptive Solution for the $k - \varepsilon$ Model of Turbulence," *AIAA Journal*, vol. 36, 01 1998.

[29] D. Pelletier and F. Ilinca, "Adaptive Remeshing for the $k - \varepsilon$ Model of Turbulence," *AIAA Journal*, vol. 35, 04 1997.

[30] NASA Turbulence Modeling Resource, "2D NACA 4412 Airfoil Trailing Edge Separation." `http://turbmodels.larc.nasa.gov/`.

[31] D. Coles and A. J. Wadcock, "Flying-Hot-Wire Study of Flow Past an NACA 4412 Airfoil at Maximum Lift," *AIAA Journal*, vol. 17, 04 1979.

[32] CFD support, "NACA4412 Airfoil Case." `http://www.cfdsupport.com/`.

[33] K. Jareteg, V. Vukcevic, and H. Jasak, "pUCoupledFoam - an open source coupled incompressible pressure-velocity solver based on foam-extend," 9th OpenFOAM Workshop, 2014.

[34] H. Jasak, *Error Analysis and Estimation for the Finite Volume Method with Applications to Fluid Flows*. PhD thesis, Department of Mechanical Engineering, Imperial College of Science, Technology and Medicine, 1996.

[35] H. Jasak, H. Weller, and A. Gosman, "High resolution NVD differencing scheme for arbitrarily unstructured meshes," *International Journal for Numerical Methods in Fluids*, vol. 31, 1999.

[36] NASA Turbulence Modeling Resource, "2DBFS: 2D Backward Facing Step." `http://turbmodels.larc.nasa.gov/`.

[37] D. M. Driver and H. L. Seegmiller, "Features of a reattaching turbulent shear layer in divergent channelflow," *AIAA Journal*, vol. 23, 02 1985.

[38] Caelus, "Two-dimensional Backward Facing Step." `http://www.caelus-cml.com/`.